Quarterly Reviews of Biophysics **44**, 1 (2011), pp. 1–93. © Cambridge University Press 2010
doi:10.1017/S0033583510000181 Printed in the United States of America

Nucleases: diversity of structure, function and mechanism

Wei Yang*

Laboratory of Molecular Biology, National Institute of Diabetes and Digestive and Kidney Diseases, National Institutes of Health, 9000 Rockville Pike, Bldg. 5, Rm B1-03, Bethesda, MD 20892, USA

Abstract. Nucleases cleave the phosphodiester bonds of nucleic acids and may be endo or exo, DNase or RNase, topoisomerases, recombinases, ribozymes, or RNA splicing enzymes. In this review, I survey nuclease activities with known structures and catalytic machinery and classify them by reaction mechanism and metal-ion dependence and by their biological function ranging from DNA replication, recombination, repair, RNA maturation, processing, interference, to defense, nutrient regeneration or cell death. Several general principles emerge from this analysis. There is little correlation between catalytic mechanism and biological function. A single catalytic mechanism can be adapted in a variety of reactions and biological pathways. Conversely, a single biological process can often be accomplished by multiple tertiary and quaternary folds and by more than one catalytic mechanism. Two-metal-ion-dependent nucleases comprise the largest number of different tertiary folds and mediate the most diverse set of biological functions. Metal-ion-dependent cleavage is exclusively associated with exonucleases producing mononucleotides and endonucleases that cleave double- or single-stranded substrates in helical and base-stacked conformations. All metal-ion-independent RNases generate 2′,3′-cyclic phosphate products, and all metal-ion-independent DNases form phospho-protein intermediates. I also find several previously unnoted relationships between different nucleases and shared catalytic configurations.

1. Introduction 4

2. Nucleolytic reactions 5
2.1. Basic chemistry 5
2.2. Nucleophiles 5
2.3. Double- *versus* single-stranded substrate 8
2.4. Products of 5′ or 3′ phosphate 9

3. Diversity and classification of nucleases 9
3.1. The lack of correlation in structure, mechanism and biological function 12
3.2. Different catalytic mechanisms of ribozymes 12
3.3. Different catalytic mechanisms of topoisomerases 12
3.4. A two-way approach of categorization in this review 13

4. Basic properties of Mg^{2+} and divalent cations 13

* Author for correspondence: W. Yang, Laboratory of Molecular Biology, National Institute of Diabetes and Digestive and Kidney Diseases, National Institutes of Health, 9000 Rockville Pike, Bldg. 5, Rm B1-03, Bethesda, MD 20892, USA.
Email: wei.yang@nih.gov

https://doi.org/10.1017/S0033583510000181 Published online by Cambridge University Press

5. Three major classes divided by metal-ion dependence 14
5.1. Two-metal-ion catalysis 14
5.2. One-metal-ion catalysis 16
5.3. Metal-independent catalysis 17

6. Two-metal-ion-dependent nuclease superfamilies 17
6.1. DnaQ-like 3′–5′ exonucleases with the DEDD motif 17
6.1.1. DnaQ 18
6.1.2. *E. coli* ExoI and ExoX 19
6.1.3. TREX1 and TREX2 19
6.1.4. WRN exonuclease 19
6.1.5. RNase T and Orn 19
6.1.6. RNase D and Rrp6 20
6.1.7. Poly A-specific ribonuclease (PARN), Pan2 and Pop2 20
6.1.8. ERI-1, 3′hExo and CRN-4 exonucleases 20
6.2. RNase H-like endonucleases 21
6.2.1. RNase H1 21
6.2.2. Transposase and retroviral integrase with the DDE motif 21
6.2.3. RNase H2 23
6.2.4. Argonaute and PIWI 23
6.2.5. RuvC and Ydc2 23
6.2.6. UvrC (C-terminal domain) 23
6.2.7. Structural roles and the ATPase catalytic core of Hsp70 24
6.3. The major REase fold with the D-(D/E)XK motif 24
6.3.1. Restriction endonucleases (BamHI, HincII, MutH, EcoR124I,etc.) 24
6.3.2. Phage λ and RecE 5′–3′exonuclease 25
6.3.3. RecB and AdnAB ssDNA nuclease 25
6.3.4. HJ resolvase: T7 endonuclease I 27
6.3.5. Structure-specific endonuclease: XPF, Hef, Rad1 and Mus81 27
6.3.6. DNA mismatch-repair endonuclease very short-patch repair (Vsr) 27
6.3.7. Rai1/Dom3Z for mRNA degradation and processing 28
6.4. FEN1-like 5′ exo- and endo-nucleases 28
6.4.1. 5′ FENs: T4 RNase H, yeast Rad27 and human FEN1 28
6.4.2. XPG and HJ resolvases Gen1 and Yen1 29
6.4.3. Human and yeast 5′ exonuclease 1 (Exo1) 30
6.4.4. 5′ exoribonuclease Rat1 (XRN2) and XRN1 30
6.4.5. PIN domain RNA exonuclease 30
6.5. RecJ and DHH family 30
6.6. TOPRIM nucleases: RNase M5 31
6.7. DNase I-like endo and 3′ exonucleases 32
6.7.1. DNase I 32
6.7.2. AP endonuclease Exo III and APE1 33
6.7.3. RNase E and G 34
6.8. β-CASP nucleases with the metallo-β-lactamase fold 34
6.8.1. RNase Z for tRNA maturation 35
6.8.2. CPSF-73 and RNase J1 35
6.8.3. Artemis, Snm1 and Pso2 36
6.9. Mre11 and protein phosphatase 2B fold 36
6.10. LAGLIDADG homing endonucleases 37
6.11. RNase II and Rrp44 37
6.12. RNase III and Dicer 37

https://doi.org/10.1017/S0033583510000181 Published online by Cambridge University Press

6.13. RNase PH, PNPase and exosome 39
6.14. RusA 41
6.15. Ribozymes 41
6.15.1. Group I intron 41
6.15.2. Group II intron 43
6.15.3. RNase P 43
6.16. Three-Zn^{2+}-dependent nucleases 43
6.16.1. *E. coli* Endo IV (AP endonuclease) 43
6.16.2. Nuclease P1 and S1 45
6.17. Nucleases that may use two metal ions for catalysis 45
6.17.1. Staphylococcal nuclease 45
6.17.2. MutL 45
6.17.3. Cas1 47
6.17.4. Cas2 47

7. One-metal-ion-dependent nuclease superfamilies 47
7.1. The $\beta\beta\alpha$-Me superfamily 47
7.1.1. HNH and His-Cys homing endonucleases 49
7.1.2. HJ resolvase: phage T4 endonuclease VII 49
7.1.3. Type-II restriction endonucleases 49
7.1.4. Sugar-non-specific endonucleases 50
7.1.4.1. Serratia, NucA and Endo G 50
7.1.4.2. Vvn and periplasmic nucleases 50
7.1.4.3. Colicins E7 and E9 51
7.1.4.4. Cell death and caspase-activated DNase (CAD) 51
7.2. GIY-YIG endonucleases 51
7.3. The HUH superfamily 52
7.3.1. Rep nucleases 52
7.3.2. Mob nucleases (TraI and TrwC) 53
7.3.3. TnpA DNA transposase of IS200/IS605 family 54

8. TOPRIM topoisomerase and Ser recombinase: partial metal-ion dependence 54
8.1. TOPRIM topoisomerases 54
8.1.1. Type-II topoisomerases 55
8.1.2. Type-IA topoisomerases 55
8.2. Ser recombinases 57

9. Metal-independent RNase 59
9.1. RNase T1, Barnase and microbial RNases 59
9.1.1. Barnase 60
9.1.2. RNase T1 61
9.1.3. Restrictocin 61
9.1.4. Colicin E3, E4 and E6 61
9.2. Colicin D and E5 62
9.3. RNase A 62
9.4. RNase T2 64
9.5. tRNA-splicing endonuclease 64
9.6. Ferredoxin-fold Cas6 65
9.7. XendoU 65
9.8. Ire1 and RNase L 65
9.9. Hammerhead, hairpin, glmS, HDV and VS ribozymes 67

https://doi.org/10.1017/S0033583510000181 Published online by Cambridge University Press

10. Metal-ion-independent DNase 67
10.1. DNase with PLD fold 67
10.1.1. Nuc and DNase II 69
10.1.2. BfiI restriction endonuclease 70
10.2. TopIB and Tyr recombinase 70
10.2.1. TopIBs 70
10.2.2. Tyr recombinases: Cre, Flp, Xer and Phage integrase 71
10.3. Halfpipe restriction endonuclease 72

11. Concluding remarks and future directions 72
11.1. Metal ions and nucleases 72
11.2. Diversity and convergence 73
11.2.1. Diversity of nucleases in a similar cleavage reaction 74
11.2.2. Adaptation of a catalytic motif in various nucleases 74
11.3. Future directions 75

12. Acknowledgment 75

13. References 76

1. Introduction

Nucleases catalyzing DNA and RNA cleavage are indispensable for life (Table 1). Nuclease activities are integral parts of DNA replication; the 5′ to 3′ exo- and endonucleases are needed to remove RNA primers (Kao & Bambara, 2003; Shen *et al.* 2005), and the 3′ to 5′ exonuclease for proofreading (Reha-Krantz, 2010). Two other major DNA metabolic processes, recombination and repair, are initiated by nucleases (Marti & Fleck, 2004; Mimitou & Symington, 2009). Nuclease activity is also required for structural alterations of nucleic acids, for example, topoisomerization (Champoux, 2001; Schoeffler & Berger, 2008; Wang, 2002), site-specific recombination (Grindley *et al.* 2006) and RNA splicing (Patel & Steitz, 2003), during which a phosphodiester bond is temporarily broken and reformed after strand passing or transfer to a new target. In addition, nuclease activities are essential in RNA processing, maturation and RNA interference (RNAi) (Abelson *et al.* 1998; Chu & Rana, 2007; Moore & Proudfoot, 2009; Nowotny & Yang, 2009). RNA and DNA degradation are essential components of microbial defense mechanisms (James *et al.* 1996; Sorek *et al.* 2008; Tock & Dryden, 2005). Nucleases are even essential for programmed cell death (Parrish & Xue, 2006). Defective DNase and RNase activities have been associated with various autoimmune diseases due to an incomplete removal of endogenously produced nucleic acids (Crow & Rehwinkel, 2009; Stephenson, 2008).

RNA and DNA present only two types of phosphodiester bonds for cleavage, 5′ or 3′ of a scissile phosphate (Fig. 1*a*), and the fundamental chemistry is bimolecular nucleophilic substitution or S_N2 in short. Nonetheless, structures and catalytic mechanisms of RNA and DNA nucleases are greatly varied and complex. Nucleases can be protein or RNA and use water, (deoxy)ribose, inorganic phosphate, or the side chains of Ser, Tyr or His as a nucleophile. Catalysis may or may not require metal ions. In addition, nuclease activities are strictly regulated by stringent substrate specificity (Pingoud *et al.* 2005; Stoddard, 2005), confined localization, or by potent inhibitors (Chowdhury *et al.* 2006; Kolade *et al.* 2002; Widlak & Garrard, 2005) to avoid unwanted or uncontrolled degradation of cellular DNA and RNA.

Individual nuclease families or superfamilies, for example, topoisomerases (Schoeffler & Berger, 2008), sequence-specific recombinases (Grindley *et al.* 2006), metal-ion-independent

https://doi.org/10.1017/S0033583510000181 Published online by Cambridge University Press

ribozymes (Cochrane & Strobel, 2008), Holliday junction (HJ) resolvases (Declais & Lilley, 2008) and DNA nucleases (Horton, 2008) have been recently reviewed. This particular review is intended to summarize DNases and RNases with known atomic structures and focus on catalytic mechanisms. The aim is to compare and contrast structural and mechanistic diversity in the context of shared functionality.

2. Nucleolytic reactions

2.1 Basic chemistry

A nuclease is a phosphodiesterase that cleaves one of the two bridging P–O bonds, 3′ or 5′, in a nucleic acid polymer (Fig. 1*a*). Cleavage of phosphodiester bonds is thought to be done by a general acid–base catalysis, where the general base activates the nucleophile by deprotonation and the general acid facilitates product formation by protonating the leaving group. Perhaps because of the stability of nucleic acid phosphodiester bonds, the cleavage reaction is usually of the associative S_N2 type (Gerlt *et al.* 1983). The reaction can be divided into three stages: nucleophilic attack, the formation of a highly negatively charged penta-covalent intermediate and the breakage of the scissile bond. Cleavage of the P–O_3' bond, which generates 5′-phosphate and 3′-OH products, requires a nucleophile to be on the 5′ side poised for the in-line attack (Fig. 1*a*). In the penta-covalent bipyramid intermediate, the O_5' moves to the center plane, which consists of the phosphorus and two non-bridging oxygens, and the attacking nucleophile and O_3' leaving group are opposite each other at the apices of the bipyramid. In the cleaved product, the stereo configuration of the phosphorus is inverted in this one-step reaction. Although phosphate in nucleic acid is achiral, due to two chemically indistinguishable non-bridging oxygen atoms, the stereo inversion is evident when one of the non-bridging oxygen is replaced by a heavy isotope or sulfur (Eckstein, 1985; Gerlt *et al.* 1983). Hence, the two non-bridging oxygens are referred to as pro-Sp and pro-Rp. A double inversion, which returns the phosphorus to its original configuration, requires a two-step reaction and occurs if an enzyme–nucleic acid covalent intermediate forms (Fig. 1*b*). To generate 3′-PO_4 and 5′-OH products, the reaction configuration has to be reversed, and the nucleophile has to attack on the 3′ side of the scissile phosphate (Fig. 1*a*).

2.2 Nucleophiles

Nucleases utilize a variety of nucleophiles to cleave a scissile phosphate bond (Fig. 2*a*). The most common nucleophiles are water molecules deprotonated by a general base for direct hydrolysis. A hydroxyl group of the 3′ end of DNA or RNA can also be the nucleophile as during the RNA splicing, DNA strand transfer or hairpin formation (Doudna & Cech, 2002; van Gent *et al.* 1996) (Fig. 2*b*, *c*). For DNA cleavage, the side chains of Ser, Tyr and His have been observed to serve as nucleophiles to form a covalent DNA phosphoryl-protein intermediate, which is subsequently resolved either by phosphoryl transfer reaction back to DNA during recombination and topoisomerization (Fig. 2*d*) or by hydrolysis in two-step cleavage reactions (Grindley *et al.* 2006; Stuckey & Dixon, 1999).

The 2′ hydroxyls of RNA or free ribonucleotides are additional nucleophiles utilized by RNases. The 2′-OH adjacent to a scissile phosphate often serves as the nucleophile and leads to the formation of a labile 2′,3′-cyclic phosphate (Figs 2*e*, 3*b*, and *c*), which is then hydrolyzed to produce a 3′ phosphate as exemplified by RNase A (Raines, 1998) or occasionally a 2′ phosphate as catalyzed by the yeast RNA ligase during tRNA splicing (Abelson *et al.* 1998). Finally, RNase

https://doi.org/10.1017/S0033583510000181 Published online by Cambridge University Press

https://doi.org/10.1017/S0033583510000181 Published online by Cambridge University Press

Table. 1. *Classification of nucleases by function. DNase and RNase are classified according to biological processes they are involved from DNA replication to cell defense. Each process is further divided into functional pathways. Enzymes of different catalytic mechanisms or different tertiary structures are separated by semi-colons for each pathway or process. Detailed descriptions of each category are referred to specific sections and under subsections.*

Process	Function	Enzyme	Substrate	Section	Nucleophile
DNA replication	Proofreading	3′ Exo and DnaQ	ssDNA	6.1.1	H_2O
	Primer removal	5′ Exo, FEN1; Dna2; RNase H	DNA with a 5′ RNA flap	6.4.1; 6.3.3; 6.2.1	H_2O
Rolling-circle replication	Nicking	Rep endonuclease	ssDNA	7.3.1	Tyr
DNA replication, transcription, recombination	Topoisomerization	Type IA; II; Type IB	DNA	8.1.1; 8.1.2; 10.2.1	Tyr
Site-specific recombination	Retroviral integration and V(D)J recombination transposition	Tn5, Hermes, mariner, RAG and integrase	Transposon, phage DNA and plasmid	6.2.2	H_2O; 3′-OH
	Transposition, gene inversion, phage integration and plasmid segregation	Cre, Flp and Int recombinase	Two DNA-specific sites	10.2.2	Tyr
		Resolvase and invertase	Two DNA-specific sites	8.2	Ser
	ICEs and ssDNA-mediated transposition	TraI, TrwC; IS605 TnpA	ssDNA	7.3.2; 7.3.3	Tyr
	Homing endonuclease	LAGLIDAG	DNA	6.10	H_2O
		HNH and His-Cys	DNA	7.1.1	H_2O
		GIY-YIG	DNA	7.2	H_2O
DNA homologous recombination	Processing broken DNA ends	RecBCD; RecE, λ Exo	DNA ends	6.3.2; 6.3.3	H_2O
	HJ resolution	RuvC; Endo I; Mus81; Gen1; RusA; EndoVII	Four-way DNA junction	6.2.5; 6.3.4; 6.3.5; 6.4.2; 6.14; 7.1.2	H_2O
	Meiosis breaks	Spo11	DNA	8.1.1	Tyr
DNA repair	Incision in base excision repair (BER)	Ape1/Exo III; FEN1; Endo IV	Modified bases	6.7.2; 6.4.1; 6.16.1	H_2O
	Incision in nucleotide excision repair (NER)	UvrC (N&C); XPF; XPG	DNA lesions	6.2.6 & 7.2; 6.3.5; 6.4.2	H_2O
	Incision and removal in mismatch repair (MMR)	3′ ExoI and X; MutH; Vsr; 5′ ExoI; RecJ	Mismatched base pairs	6.1.2; 6.3.1; 6.3.6; 6.4.3; 6.5	H_2O
	Double-strand break repair (DSBR)	Wrn; Mre11; Artemis; Dna2	DNA ends	6.1.4; 6.9; 6.8.3; 6.3	H_2O

https://doi.org/10.1017/S0033583510000181 Published online by Cambridge University Press

RNA processing	tRNA 5′ processing	RNase P	tRNA	6.15.3	H_2O
	tRNA 3′ processing	RNase D; T; Z	tRNA	6.1.5; 6.1.6; 6.8.1	H_2O
	tRNA splicing	Endonuclease	tRNA	9.5	2′-OH
	mRNA splicing	Spliceosome	mRNA	6.15.2	H_2O, 3′-OH
	mRNA end processing and degradation	RNase D (Prp6); PARN; Rai; Rat1; PIN; RNase E/G; II; PH; CPSF-73	RNA	6.1.6; 6.1.7; 6.3.7; 6.4.4; 6.4.5; 6.7.3; 6.11; 6.13; 6.8.2	H_2O; PO_4
	rRNA maturation	RNase T; ERI-1; RNase M5; RNase E/G; J1; group I/II intron	RNA	6.1.5; 6.1.8; 6.6; 6.7.3; 6.8.1, 6.15.1/2	H_2O; 2′ and 3′-OH
RNA interference	Dicer	RNase III	dsRNA	6.12	H_2O
	Slicer	Argonaute	RNA	6.2.4	H_2O
Cell death	DNA decay	NucA, EndoG, CAD; Nuc, DNase II	DNA and ssDNA	7.1.4; 10.1.1	H_2O; His
	RNA decay	TREX1 and TREX2; RNase H2; Crn4	RNA and RNA/DNA hybrid	6.1.3; 6.2.3; 6.1.8	H_2O
Nutrition source	DNA digestion and scavenging	DNase I; nuclease P1/S1; Serratia	ssDNA and dsDNA	6.7.1; 6.16.2; 7.1.4	H_2O
	RNA digestion	RNase T1; A; T2	RNA	9.1; 9.3; 9.4	2′-OH; H_2O;
Defense	Restriction/modification	EcoRI; KpnI; BfiI; halfpipe	DNA	6.3.1; 7.1.3; 10.1.2; 10.3	H_2O; Tyr
	Microbial toxins	Restrictocin; colicin E3/4/6; colicin D/E5	RNA	9.1.3; 9.1.4; 9.2	2′-OH
		Colicin E7-9	DNA	7.1.4.3	H_2O
	CRISPR	Cas1; Cas2; Cas6	DNA and RNA	6.17.2; 6.17.3; 9.6	H_2O

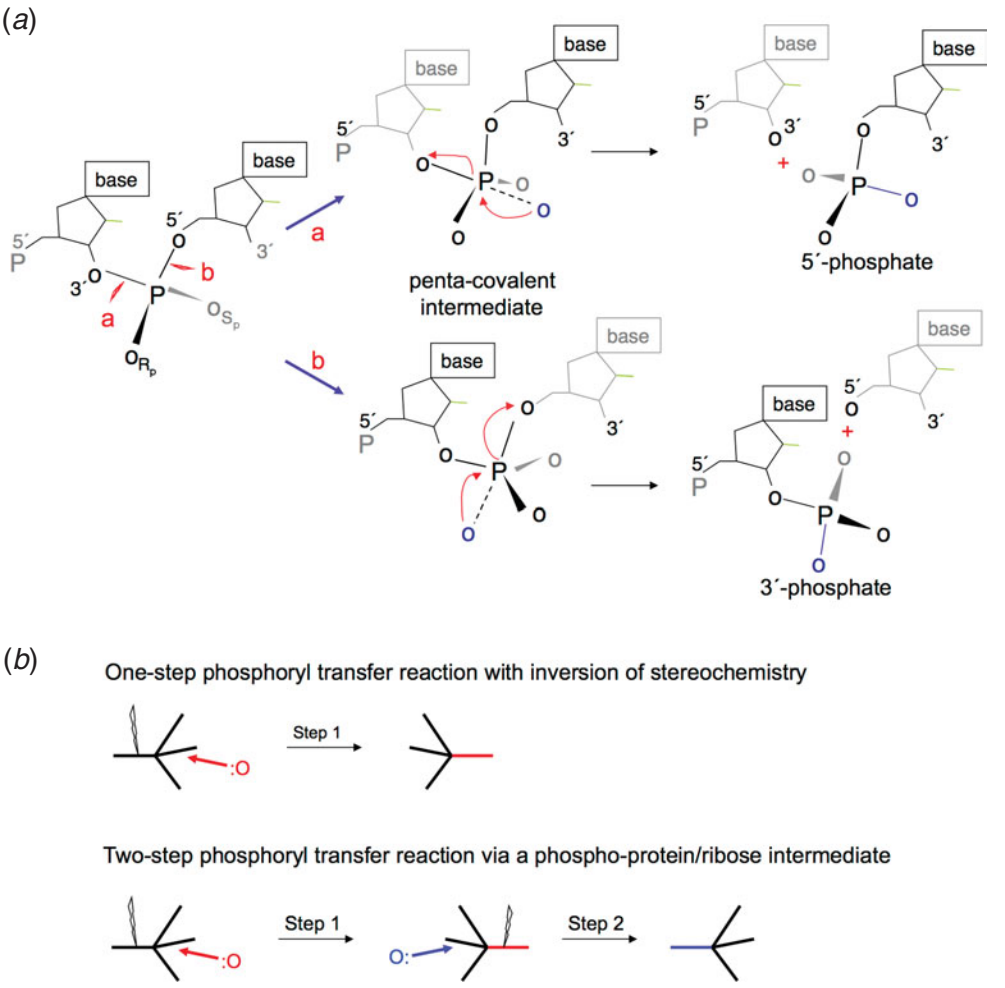


Fig. 1. Adjacent nucleotides in RNA and DNA are linked by 3′ and 5′ O-P phosphodiester bonds. (*a*) Nucleases degrade nucleic acid by breaking either one of these two bonds labeled as 'a' and 'b'. A nucleophile attacking in-line from the 5′ side breaks the 3′ O–P bond and produces 5′-phosphate and 3′-OH. Alternatively, a nucleophile attacking the scissile phosphate from the 3′ side breaks the 5′ O–P bond and produces 3′-phosphate and 5′-OH. Rp stands for pro-Rp and Sp for pro-Sp. (*b*) The S_N2 type associative reaction inverts the stereo configuration of phosphate. A two-step *trans*-esterification reaction can set the stereochemistry back to the original.

PH and polynucleotide phosphorylases (PNPases) use inorganic phosphate as a nucleophile to degrade single-stranded RNA (ssRNA) by phosphorolysis and produce nucleoside 5′-diphosphates (Deutscher *et al.* 1988) (Fig. 2 *f*). The pK_a of these nucleophiles are 6·0 (His), 10·0 (Tyr), 12–14 (2′-OH of ribose), 13 (Ser) and 16 (H_2O) (Saenger, 1984; Voet & Voet, 2004). If water is the nucleophile, a general base is necessary to deprotonate it for efficient cleavage. Similarly, the 2′-OH of ribose also needs deprotonation to be an efficient nucleophile.

2.3 Double- *versus* single-stranded substrate

If the scissile phosphate is in a double helix, the options for placement of an external nucleophile (that is not within the nucleic acid itself) are limited. Looking down the helical axis, a nucleophile

https://doi.org/10.1017/S0033583510000181 Published online by Cambridge University Press

can approach the nucleic acid backbone only from outside the double helix, because the inside is occupied by sugars and bases (Fig. 3*a*). If a nucleic acid is single stranded and bases are unstacked, the approach of a nucleophile is not as restricted. For example, RNA cleavage using the 2′-OH adjacent to a scissile phosphate can only occur with ssRNA, because the reaction coordinate is incompatible with the double helix conformation and requires a distorted backbone phosphate with bases surrounding the scissile phosphate unstacked and splayed (Buckle & Fersht, 1994; Cochrane & Strobel, 2008; Correll *et al.* 2004) (Fig. 3*b* and *c*).

Potential reaction coordinates for nicking double-stranded nucleic acids are far less varied than possibilities for cleaving single-stranded nucleic acids. Most often DNA is in a double helix. Even RNA substrates in pre-mRNA splicing or RNAi-mediated cleavage are often base-paired in a double-helical conformation (Nowotny & Yang, 2009; Patel & Steitz, 2003; Stahley & Strobel, 2006). To date, the nucleases that cleave double-stranded substrates all approach RNA and DNA from the minor groove side, where scissile phosphates are easier to reach than from the major groove side (Fig. 3*a*). Sequence-specific interactions, which usually take place in the major groove, are often accomplished by additional domains attached to catalytic centers (Lee *et al.* 2005).

2.4 Products of 5′ or 3′ phosphate

Nucleolytic cleavage products are most often 5′-phosphates and 3′-OH groups. This type of cleavage is likely to be preferred (over 3′-phosphate and 5′-OH), likely because firstly the 3′-OH can be passed onto other nucleic acid enzymes and be directly used as the nucleophile, e.g. RNA and DNA polymerases, DNA ligases, transposases, spliceosomes, CCA-adding enzymes and aa-tRNA synthetases. Secondly, the 5′-phosphate is a ready substrate for DNA ligation at the end of replication, repair and recombination. The two main exceptions are RNA cleavage via the 2′,3′-cyclic phosphodiester intermediate and DNA cleavage by Tyr-dependent site-specific recombinases and Type IB topoisomerases (TopIBs). For the DNA enzymes, a 3′-phosphotyrosyl bond is a transient intermediate and is reversed back to a phosphodiester bond in the product (Champoux, 2001; Grindley *et al.* 2006). In the RNA cases, either the 3′-phosphate is an end product or these RNA molecules require further hydrolysis and dephosphorylation. For example, the 2′,3′-cyclic phosphodiester formed in the tRNA splicing is hydrolyzed to form 3′-OH and 2′-phosphate (Abelson *et al.* 1998), which require several enzymatic activities to alter the phosphorylation states in a process referred to as healing (Nandakumar *et al.* 2008) before RNA fragments can be ligated.

3. Diversity and classification of nucleases

Nucleases are a very diverse group and include both proteins and catalytic RNA (ribozyes). There is no simple way to classify and divide them. Based on substrate preference, nucleases may be divided into DNase and RNase, yet quite a number of nucleases are sugar non-specific and can cleave both RNA and DNA (Hsia *et al.* 2005; Laskowski, 1985; Rangarajan & Shankar, 2001). Depending on whether a 5′ or 3′ end is required for substrate recognition and whether cleavage products are single or oligo nucleotides, they may be divided into exo- and endonucleases. For instance, all self-cleaving ribozymes found to date only endonucleolytically cleave RNA (Cochrane & Strobel, 2008; Lilley, 2005). Exonucleases, which remove one nucleotide at a time

https://doi.org/10.1017/S0033583510000181 Published online by Cambridge University Press

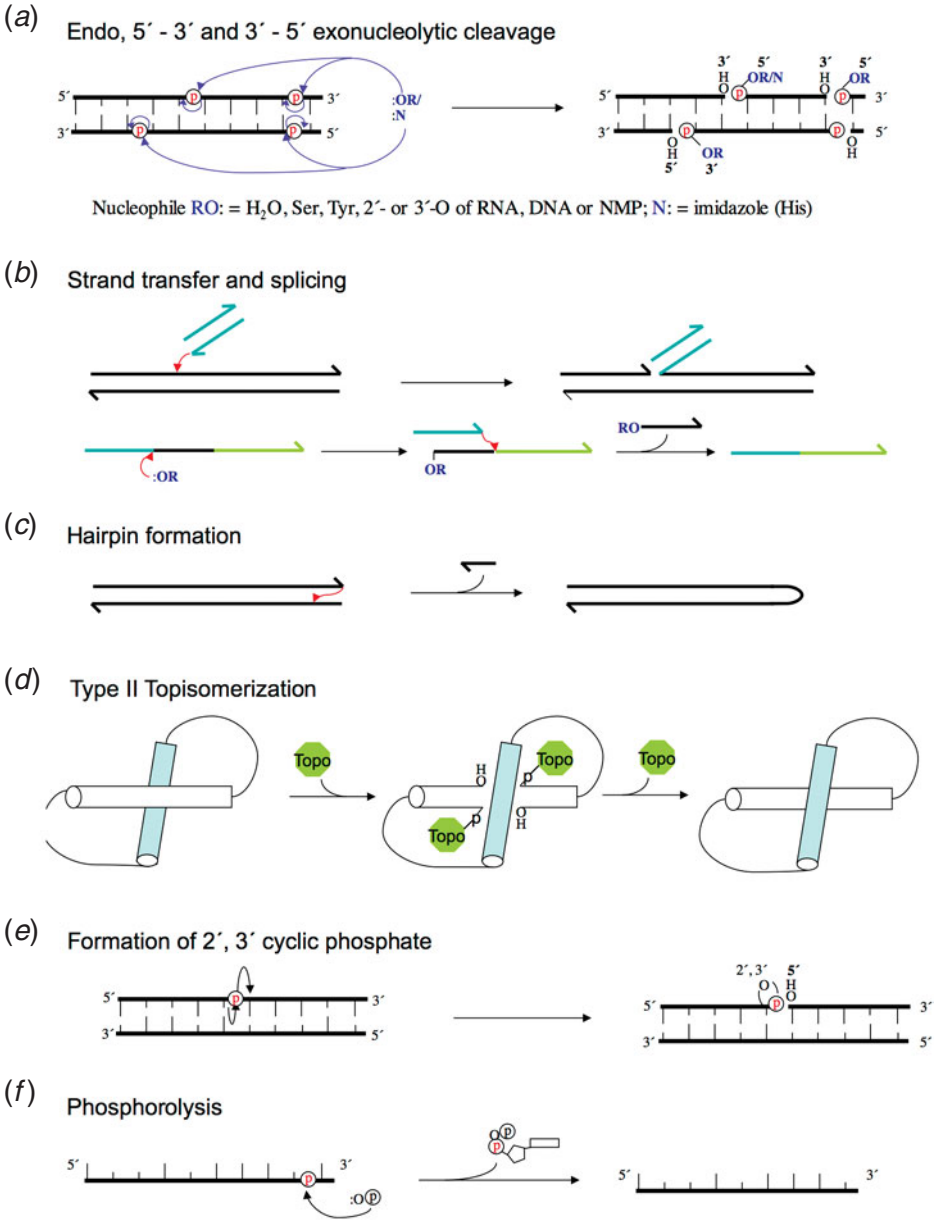


Fig. 2. Phosphodiester bond cleavage. (*a*) Nucleases can attack a scissile phosphate in the middle of nucleic acids (endo) or at the 5′ or 3′ ends (exo). The nucleophiles can be the hydroxyl groups of water molecules, Ser or Tyr side chains, hydroxyls of ribose (2′ or 3′) or deoxyribose (3′) in RNA and DNA, or free nucleophiles. PLD family nucleases use the imidazole of His as the nucleophile. When a protein side chain serves as a nucleophile, the phosphodiester bond to be cleaved is transferred to the protein. Similarly, when the hydroxyl of a nucleotide or nucleic acid serves as the nucleophile, it is transferred to the nucleic acid. Both are indicated as R. (*b*) DNA transposition by the cut-and-paste mechanism. The donor DNA uses its cleaved 3′-OH to attack a phosphate in a target DNA. Thus, the donor DNA is inserted into the target in this strand transfer reaction. RNA splicing is similar. The cleavage of the 5′ exon–intron junction frees the 3′-OH of the first exon. This 3′-OH than attacks the 3′ exon–intron junction and results in a linked two exons and free intron. (*c*) DNA Hairpin formation. When a 3′-OH of a duplex DNA attacks a phosphate of its complementary strand, the two strands of that duplex are linked and become one. (*d*) Type-II

https://doi.org/10.1017/S0033583510000181 Published online by Cambridge University Press

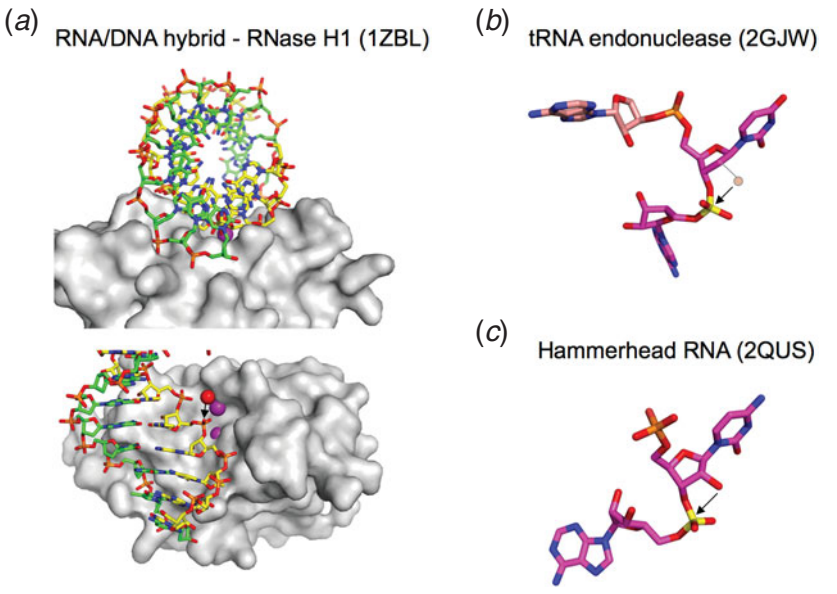


Fig. 3. Double- *versus* single-stranded nucleic acid substrate. (*a*) To cleave a double helix, the nucleophile can attack from outside of the duplex only. Shown here is an RNA/DNA hybrid in a mixed A and B form, which is approached by RNase H1 from the minor groove side. A water molecule is coordinated by the Mg^{2+} ion in the active site to attack the phosphate from the 5′ side and produce a 5′ phosphate and 3′-OH. (*b*) A scissile phosphate in pre-tRNA to be cleaved by tRNA endonuclease using the 2′-OH as the nucleophile. The nucleotides surrounding the scissile phosphate are not base paired and splayed. The phosphate itself is distorted. (*c*) Self-cleaving hammerhead ribozyme distorts the scissile phosphate in a similar way, because the double helix conformation is incompatible with the reaction coordinates of using a 2′-OH to attack the adjacent phosphate. PDB accession codes are shown in parentheses.

from the end of a strand, can be further divided into two groups by the 5′ to 3′ *versus* 3′ to 5′ polarity. However, the fundamental chemistry of endo- and exo-cleavage is the same, and it is not unusual that a single active site may contain both exonuclease and endonuclease activities. For example, members of the Flap endonuclease 1 (FEN1) family have the 5′ to 3′ exonuclease activity in addition to the endonuclease activity (Harrington & Lieber, 1994; Lyamichev *et al.* 1993) and Mre11, which is involved in DNA double-strand break (DSB) repair, has both endo and 3′ to 5′ exonuclease activities (Paull & Gellert, 1998; Usui *et al.* 1998).

According to catalytic mechanism, all nucleases may be divided into three major classes based on whether none, one or two metal ions are involved. However, each of these classes includes many different families and superfamilies. For instance, two-metal-ion-dependent nucleases include both protein enzymes and ribozymes and can be vastly different in the tertiary structure,

topoisomerization. Both strands of one DNA segment are cleaved and form covalent bonds with a dimeric (or tetrameric) topoisomerase. The second DNA segment shown in light blue passes through the cleaved segment thus changing the linking number and topology. The cleaved DNA is then religated and the topoisomerase regenerated. (*e*) The 2′-OH immediate adjacent to a scissile phosphate can serve as a nucleophile and hydrolysis of 5′ O–P bond leads to 2′, 3′ cyclic phosphate and 5′-OH. (*f*) RNase PH and PNPase are 3′ exonucleases. They use inorganic phosphate as nucleophiles and degrade RNA to nucleotide diphosphates.

https://doi.org/10.1017/S0033583510000181 Published online by Cambridge University Press

metal-ion-coordination motif and cellular function. The following are just a few examples of diversity among nucleases.

3.1 The lack of correlation in structure, mechanism and biological function

Similar biological outcomes are often achieved by molecules with unrelated tertiary structures and drastically different mechanisms. For example, sequence-specific restriction of endonucleases encompasses at least five structural families and employ at a minimum four different catalytic mechanisms (Orlowski & Bujnicki, 2008) (Table 1). For an up-to-date complete list of restriction endonucleases, please consult the REBASE database (rebase.neb.com) (Roberts *et al.* 2009). In parallel, HJ resolvases are composed of five different structural and mechanistic families (Declais & Lilley, 2008; Ip *et al.* 2008) (Table 1). Conversely, similar tertiary structures may adopt different catalytic properties. For example, the Cas6 and Cas2 nucleases share the ferredoxin-fold, but their active sites are unrelated (Beloglazova *et al.* 2008; Carte *et al.* 2008). Cas2 is metal-ion dependent and Cas6 is metal independent. Furthermore, structural and mechanistic conservation are not necessarily correlated with identical functions. For example, molecules with the RNase H-like fold that utilizes the two-metal-ion catalysis are involved in RNA processing, DNA cleavage, transposition and HJ resolution (Nowotny *et al.* 2005; Yang & Steitz, 1995b).

3.2 Different catalytic mechanisms of ribozymes

RNA is thought to be the primordial nucleic acid and can function both as a genetic material and a catalytic entity (Chen *et al.* 2007b; Yarus, 2002). It is not surprising that RNases and ribozymes display great mechanistic diversity. Naturally occurring ribozymes can be metal-dependent or -independent (Lilley, 2005). The self-cleaving hammerhead, hairpin, glmS, hepatitis delta virus (HDV) and Varkud satellite (VS) ribozymes cleave the extended ssRNA by a metal-ion-independent mechanism (Cochrane & Strobel, 2008), whereas group I and group II introns cleave exon–intron junctions embedded in double-stranded RNA (dsRNA) by a two-metal-ion mechanism (Stahley & Strobel, 2005; Toor *et al.* 2009). Different catalytic mechanisms lead to the different types of cleavage products. The two-metal-ion-dependent ribozymes generate 5′-phosphate and 3′-OH products, whereas the metal-independent ribozymes use 2′-OH as the nucleophile and generate 2′,3′-cyclic phosphate and 5′-OH products.

3.3 Different catalytic mechanisms of topoisomerases

All topoisomerases cleave DNA using a Tyr side chain as the nucleophile to produce a covalent phosphotyrosyl DNA–enzyme intermediate for strand passing (see reviews by Schoeffler & Berger, 2008; Wang, 2002). Following cleavage and topological change, DNA is religated using the DNA hydroxyl group generated in the cleavage step as the nucleophile to cleave the phosphotyrosyl bond and religate the DNA, which regenerates a free topoisomerase (Fig. 2*d*). In this coupled cleavage-religation scheme, the phosphodiester bond energy is preserved and an external energy source is not necessary. The active site of all topoisomerases consists of an essential Tyr nucleophile. Type IA and type II topoisomerases share a conserved catalytic core and require Mg^{2+} for efficient cleavage and religation, whereas TopIB are different and do not need a

https://doi.org/10.1017/S0033583510000181 Published online by Cambridge University Press

divalent cation. Correlated with the metal ion dependence, type II and IA topoisomerases form 5′-phosphotyrosine and 3′-OH cleavage products, whereas type IB form 3′-phosphotyrosine and 5′-OH products (Schoeffler & Berger, 2008). Type IA and type II topoisomerases further differ in ATP and DNA substrate requirements. Type IA usually requires no ATP and cleaves ssDNA only, whereas type II requires ATP and cleaves dsDNA (Schoeffler & Berger, 2008).

3.4 A two-way approach of categorization in this review

Because of the great diversity of nucleases, their classification cannot be explicitly accomplished using any single criterion. For convenience, I separate nucleases into three major classes based on their metal-ion dependence and catalytic mechanism. In each class, nucleases are further divided into families or superfamilies according to sequence and structure conservation and functional diversity. Because the catalytic mechanisms of some nucleases are yet to be determined, uncertainty in their classification is indicated. To complement the classification by catalytic mechanism, nucleases are also divided using their biological function and summarized in Table 1. Diverse catalytic mechanisms involved in each biological pathway are then cross referenced to the relevant sections and subsections.

Before going into the details of each class and superfamily of nucleases according to this metal-centric classification, the properties of Mg^{2+} and divalent cations and the main characteristics of metal-dependent and -independent catalyses are first summarized.

4. Basic properties of Mg^{2+} and divalent cations

Mg^{2+} and Ca^{2+} are the most abundant divalent cations in living organisms (Cowan, 2002; Lyons & Eide, 2006), and Mg^{2+} is the most abundant divalent cation inside cells (Maguire & Cowan, 2002; Romani & Scarpa, 1992). Other ions like Fe^{2+}, Zn^{2+} and Cu^{2+} are widespread, and Mn^{2+} and Ni^{2+} are essential but found at low concentrations (Lyons & Eide, 2006). The principal quality of these divalent cations is the high density of positive charge, which makes them efficient for charge neutralization of phospholipids and nucleic acids. The second common property is hydration and the specific ligand requirement. According to the atomic or covalent radius Ca^{2+} is the largest (1·9 Å), Mg^{2+} the second (1·6 Å) and the rest are similarly smaller (1·3 Å). However, when hydrated, Mg^{2+} is larger than Ca^{2+}, because Mg^{2+} is associated with multiple shells of ligated water molecules (Maguire & Cowan, 2002). In biological systems, these metal ions never exist without water or ligand. Therefore, ionic (Shannon) radii (Pauling, 1961) are inapplicable. The most common ligand coordination geometry is octahedral or tetrahedral (Harding, 1999) (Fig. 4). Mg^{2+} prefers to have six inner-sphere ligands arranged in an octahedral configuration and so does Fe^{2+} (Harding, 1999). Ca^{2+} and Zn^{2+} can have octahedral coordination, but Zn^{2+} is frequently coordinated by four ligands in a tetrahedron (Christianson, 1991), and Ca^{2+} by seven, eight or even nine ligands (Pidcock & Moore, 2001). The number and length of ligand bonds of metal ions are empirically determined and vary within a very narrow range (Harding, 1999). Metal-ion coordination is far more sensitive to the ligand type and geometry than hydrogen bonds or salt bridges observed in macromolecules.

A variety of divalent cations have been found to be involved in enzymatic catalysis, e.g. Fe^{2+} in non-heme iron enzymes (oxygenases and demethylases) (Lange & Que, 1998), Zn^{2+} in deacetylases and proteases (Hernick & Fierke, 2005; Kim & Mobashery, 2001), Ni^{2+} in urease (Jabri

https://doi.org/10.1017/S0033583510000181 Published online by Cambridge University Press

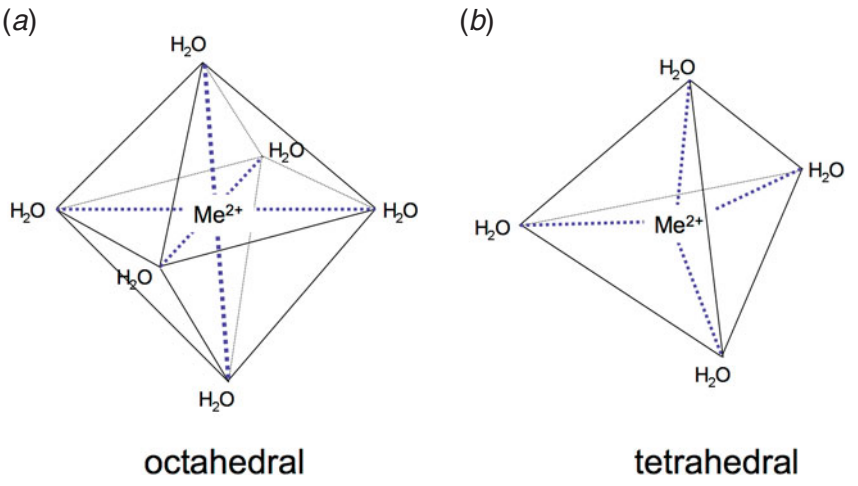


Fig. 4. Metal-dependent nucleases most often use Mg^{2+} and Zn^{2+} to facilitate phosphodiester bond breakage. (*a*) Diagram of octahedral coordination preferred by Mg^{2+} and can also be adopted by Zn^{2+}. (*b*) Tetrahedral coordination favored by Zn^{2+}.

et al. 1995), and the Mg^{2+} ion is most frequently associated with nucleic acid enzymes (Cowan, 2002). This frequent use of Mg^{2+} is perhaps because of its abundance, solubility, redox stability when compared with Mn^{2+}, Fe^{2+} and Cu^{2+}, its small size relative to Ca^{2+}, and its rigid coordination geometry when compared with the transition metals Fe^{2+}, Cu^{2+}, Ni^{2+} and Zn^{2+} (Maguire & Cowan, 2002). The ligand bond of the Mg^{2+} ion is empirically determined to be 2·07 Å (Harding, 1999). The coordination geometry of Mg^{2+} is far more stringent than hydrogen bonds. The unusual hydration property of Mg^{2+} ions may also be a factor for its catalytic role. Mg^{2+} ions exhibit extremely slow exchange rates of inner shell water molecules (Diebler *et al.* 1969; Maguire & Cowan, 2002) and often retain a couple of water ligands when coordinated by organic or macro molecules (Harding, 1999). It is energetically very costly to replace water ligands of Mg^{2+} with macromolecular ligands. The pK_a value of a water molecule is reduced from 16·0 in free solution to 11·4 when associated with Mg^{2+} (Pontius *et al.* 1997).

5. Three major classes divided by metal-ion dependence

An overwhelming majority of nucleases of diverse function and structure belong to one of the three classes, requiring none, one or two metal ions for catalysis. Three Zn^{2+} ions have been found in the active site of two nucleases: nuclease P1 and *Escherichia coli* Endo IV (Garcin *et al.* 2008; Ivanov *et al.* 2007; Romier *et al.* 1998). They are treated as a variation of the two-metal-ion mechanism in this review. The metal-independent RNases and DNases are grouped into different sections, because there is nothing in common.

5.1 Two-metal-ion catalysis

Two-metal-ion catalysis was first proposed after observing two metal ions in the active site of 3′ to 5′ exonuclease (DnaQ-like) active site of the Klenow fragment and alkaline phosphatase (Beese & Steitz, 1991; Freemont *et al.* 1988; Kim & Wyckoff, 1991). It was further suggested to

https://doi.org/10.1017/S0033583510000181 Published online by Cambridge University Press

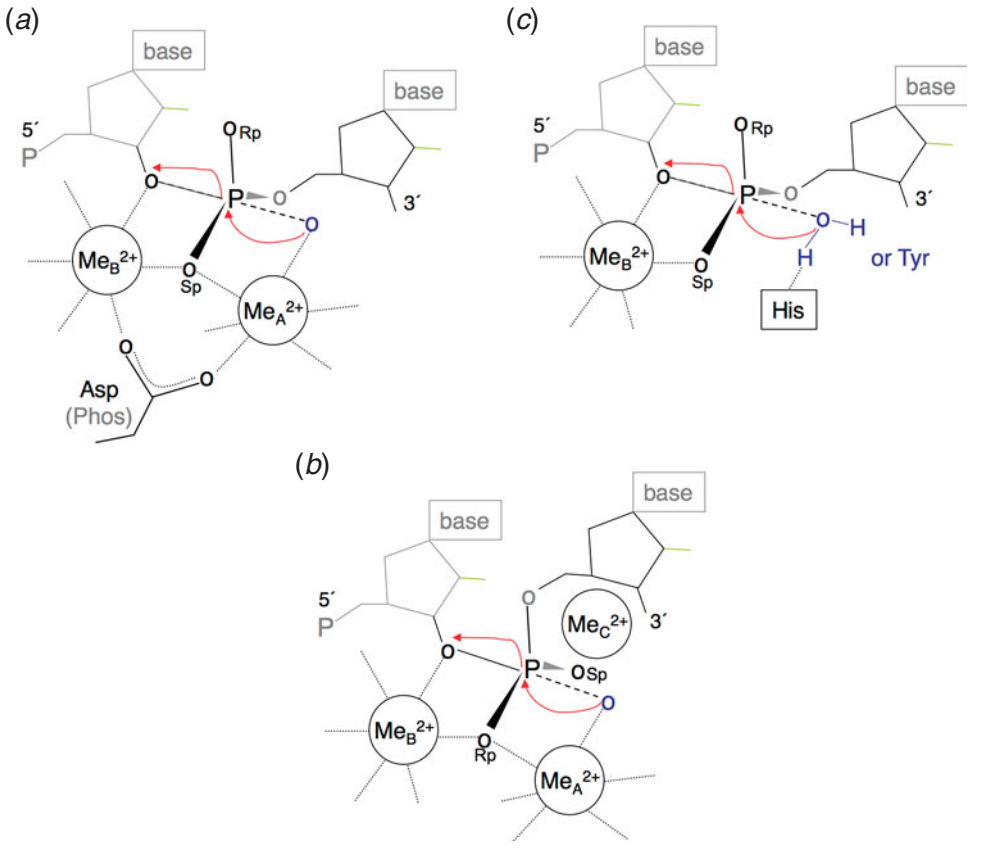


Fig. 5. Metal-ion-dependent catalysis. (*a*) Two-metal-ion mechanism. The pro-Sp oxygen of a scissile phosphate coordinates both metal ions, one on the 5′ side and the other on the 3′ side. The pro-Rp oxygen is exposed to solvent. When labeling, pro-Sp is abbreviated as Sp and pro-Rp as Rp. (*b*) The three-metal-ion mechanism is a variation of the two-metal-ion mechanism. The scissile phosphate is turned and the pro-Rp oxygen coordinates the two catalytic metal ions and, the pro-Sp oxygen is stabilized by the third divalent cation. (*c*) The one-metal-ion mechanism is an alternative to the two-metal-ion mechanism. One metal ion (A) is eliminated and may be replaced by a positively charged protein side chain. In the cases where water is the nucleophile, a conserved His often acts as the general base to deprotonate it for nucleophilic attack. Alternatively, Tyr is the nucleophile as in topoisomerases, relaxases and RCR-related recombinases. In all three metal-ion-dependent mechanisms, the nucleophile is always on the 5′ side, and cleavage results in 5′-phosphate and 3′-OH.

be a general mechanism for ribozymes catalyzing RNA splicing, which have no chemical groups that have pK_a's near neutrality to serve as general base and acid for the phosphoryl transfer reaction (Steitz & Steitz, 1993). Over the years, the two-metal-ion mechanism has been proven to be utilized by all DNA and RNA polymerases (Steitz, 1998) and many nucleases including self-splicing ribozymes (Stahley & Strobel, 2005; Toor *et al.* 2008).

In all cases, the metal-ion-dependent reaction products are 5′-phosphate and 3′-OH groups. The two metal ions (A and B) are ∼4 Å apart in the ground state and coordinated between non-bridging oxygen of the scissile phosphate and an absolutely conserved Asp or a phosphate backbone in the case of ribozymes (Fig. 5*a*). The A metal ion is on the nucleophile side and the B metal ion is on the 3′-O leaving-group side. Additional carboxylates or polar

https://doi.org/10.1017/S0033583510000181 Published online by Cambridge University Press

groups help to coordinate the metal ions and exclude water molecules from metal ion B. Two-metal-ion catalysis is fully compatible with the native double-helix structure and requires no phosphosugar distortion, base unstacking or flipping out. The advantages of incorporating two metal ions into catalysis are high substrate specificity and efficient product release (Yang *et al.* 2006). In addition, two symmetrically placed metal ions in the cut-and-paste recombinases and group I and II introns (ribozymes) allow multiple reactions to be consecutively catalyzed in one active site (Kennedy *et al.* 2000; Steitz & Steitz, 1993).

In most cases, Mg^{2+} is the choice for two-metal-ion catalysis, and Ca^{2+} inhibits phosphoryl transfer (Yang *et al.* 2006). Some enzymes, e.g. Mre11, require Mn^{2+} for *in vitro* nuclease activity (Hopfner *et al.* 2001; Paull & Gellert, 1998). Because of the stringent coordination geometry and charge requirements of Mg^{2+}, a binding of two such metal ions is most often substrate dependent and highly selective. A number of crystal structures have captured metal ions in non-canonical configurations, which can be correlated with mutated metal-ion coordinated ligands and displacement of the scissile phosphate (Devos *et al.* 2007; Horton & Perona, 2004; Nowotny *et al.* 2007). In comparison, Mn^{2+} tends to relax substrate specificity and can rescue defective enzymes (Yang *et al.* 2006 and references therein). This 'relaxing' and broadening of substrate specificity by Mn^{2+} is widely observed in metalloenzymes perhaps due to Mn^{2+} being a transitional element with less stringent coordination requirements than Mg^{2+}. Many enzymes are active in mixed metal ion experiments as long as a trace of Mg^{2+} or Mn^{2+} are present (Brautigam & Steitz, 1998; Pingoud *et al.* 2009). It has been shown that the A site can accept various metal ions but the B site is more selective for Mg^{2+} for catalysis (Brautigam *et al.* 1999).

Although metal ion A was proposed to drive the reaction by deprotonating the nucleophile, a similar pH profile of phosphoryl transfer reaction in the presence of Mg^{2+} or Mn^{2+} (Sam & Perona, 1999), which would result in different pK_a's of their ligands, is inconsistent with the metal ion being the general base and simply deprotonating the nucleophilic water. Hydrolytic reactions may occur without a general base, and the catalytic rate may be reduced by three to five orders of magnitude (Mildvan *et al.* 2005). The current interpretation is that metal ion B is at least as important as metal ion A in two-metal-ion catalysis. In addition to the proposed role of stabilizing the penta-covalent transition state, metal ion B appears to destabilize the ground state of a scissile phosphate for cleavage (Yang *et al.* 2006). Structural studies of an RNase H reaction intermediate and product indicate that the two metal ions are likely to move closer than 3·5 Å and together stabilize the transition state (Nowotny & Yang, 2006).

5.2 One-metal-ion catalysis

An alternative to the two-metal-ion mechanism is one-metal-ion catalysis, in which metal ion B is retained and metal ion A is absent (Yang, 2008) (Fig. 5*b*). Two major classes of endonucleases are confirmed to use one-metal ion for catalysis: $\beta\beta\alpha$-Me and HUH (Friedhoff *et al.* 1999; Koonin & Ilyina, 1993; Kuhlmann *et al.* 1999; Monzingo *et al.* 2007). Although sharing little tertiary structural similarity, both classes of nucleases use at least one His side chain to coordinate the metal ion, and the reaction coordinates (arrangement of the metal ion, scissile phosphate and nucleophile) are nearly superimposable. Like the two-metal-ion mechanism, the active site configuration of $\beta\beta\alpha$-Me and HuH nucleases is compatible with the double-helix structure and produces 5′-phosphate and 3′-OH groups (Fig. 5*b*). The $\beta\beta\alpha$-Me nucleases most often contain a His as a general base to deprotonate and activate a nucleophilic water, whereas the HUH nucleases invariably use Tyr as the nucleophile to cleave DNA substrates (Yang, 2008). Metal ion selection

https://doi.org/10.1017/S0033583510000181 Published online by Cambridge University Press

by one-metal-ion-dependent nucleases is often less stringent, and substrate specificity is concomitantly less discriminating than for two-metal-ion enzymes (Yang, 2008). A number of $\beta\beta\alpha$-Me nucleases are equally capable of hydrolyzing RNA and DNA (sugar non-specific) with little sequence specificity (Hsia *et al.* 2005). Sequence-specific DNases in the $\beta\beta\alpha$-Me family, for example, homing endonuclease I-PpoI and the type-II restriction endonuclease KpnI, depend on additional DNA-binding domains to achieve their specificity (Sokolowska *et al.* 2009; Stoddard, 2005).

5.3 Metal-independent catalysis

Both RNase and DNase can be metal independent. To date, the RNases that do not require metal ions all use a 2′-OH as the nucleophile to generate 2′,3′ cyclic phosphate intermediates. These enzymes therefore require phosphoribose distortion and base unstacking and unpairing surrounding a scissile phosphate for catalysis to proceed (Fig. 3*b* and *c*) (Buckle & Fersht, 1994; Calvin & Li, 2008; Cochrane & Strobel, 2008; Correll *et al.* 2004). The DNases that have been shown to cleave DNA without metal ions form phosphoenzyme covalent intermediates via Tyr, Ser or His side chains (Champoux, 2001; Gottlin *et al.* 1998; Grindley *et al.* 2006; Sasnauskas *et al.* 2007). The active site and mechanisms for metal-ion-independent cleavage by RNases and ribozymes, in particular, have been extensively characterized by X-ray crystallography (Cochrane & Strobel, 2008; Deshpande & Shankar, 2002; Raines, 1998; Xue *et al.* 2006; Yoshida, 2001). The mechanism for DNA cleavage without metal ions has also been revealed by combined biochemical analysis and atomic resolution structures (Grindley *et al.* 2006; Schoeffler & Berger, 2008; Stuckey & Dixon, 1999). Despite variations in structures and active site components, some common features emerge from metal-independent RNases and DNases. Water appears to be excluded from the active site, a 2′-OH of RNA or a protein side chain serves as the nucleophile, and the highly negatively charged penta-covalent intermediate is neutralized by positively charged side chains.

6. Two-metal-ion-dependent nuclease superfamilies

This is by far the largest class of nucleases. It includes protein enzymes and ribozymes, sequence-specific and non-specific nucleases, endo- and exonucleases with the 5′ to 3′ or 3′ to 5′ polarity, RNase and DNase. Based on the tertiary fold and catalytic motifs, they are divided into more than a dozen superfamilies and families as listed below.

6.1 DnaQ-like 3′–5′ exonucleases with the DEDD motif

DnaQ-like nucleases share the absolutely conserved sequence motif of DEDD and all carry out 3′–5′ exonucleolytic degradation of DNA or RNA. The topology of the catalytic core, after removing the non-conservative parts, is β1-β2-β3-αA-β4-αB-β5-αC, of which the five strands form a central mixed β-sheet (54123, ↑↑↑↓↑) (Fig. 6*a*). The first two conserved carboxylates (DE) are one residue apart on the β1 strand, and the remaining two (DD) are located on αB and αC on either side of the β-sheet. The two-metal ions are coordinated between the first Asp of the DEDD motif and the pro-Sp non-bridging oxygen of the scissile phosphate. Each of the remaining three carboxylates coordinates one of the two-metal ions. The nucleophilic water may

https://doi.org/10.1017/S0033583510000181 Published online by Cambridge University Press

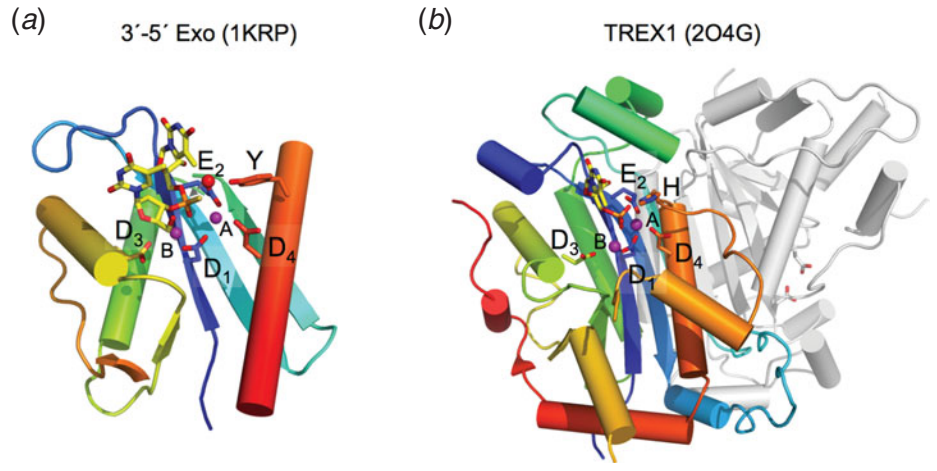


Fig. 6. The DEDD superfamily consists of DnaQ-like 3′–5′ exonucleases. (*a*) The core of the 3′–5′ exonuclease domain of *E. coli* DNA polymerase I (PDB code is shown in parenthesis) represents the DEDDy nucleases. (*b*) Dimeric TREX1 (2O4G) represents the DEDDh exonucleases. Proteins are shown in ribbon diagrams. One subunit of each enzyme is shown in rainbow colors from the blue N- to red C-terminus. Divalent cations are shown as purple spheres and the nucleophile water as a red sphere. The side chains of the conserved DEDDy/h motifs and nucleic acid/nucleotide are shown in sticks with oxygen in red and nitrogen in blue. All DEDD family members use the two-metal-ion mechanism as represented in the enzyme–nucleic acid or nucleotide complex structures.

be oriented and activated by the highly conserved Tyr or His 4 or 5 residues proceeding to the last D of DEDD, which give rise to the name of DEDDy or DEDDh exonucleases. Interestingly, the difference in the sequence motif appears to result in little difference in function. For example, both DEDDy and DEDDh are found in the proofreading exonucleases (see below). Several members of this family form dimers (Fig. 6*b*), but with vastly different dimeric interfaces. Curiously, most dimeric 3′ exonucleases of the DnaQ superfamily have the DEDDh motif (see below).

6.1.1 DnaQ

DnaQ, also known as MutD or epsilon subunit of *E. coli* DNA polymerase III holoenzyme, encodes the 3′–5′ exonuclease (DEDDh) that performs proofreading in DNA replication (McHenry, 1985). The 3′–5′ exonuclease may exist as a domain of DNA polymerase or a separate polypeptide chain in the replisome. As a domain of the Klenow fragment, the 3′–5′ exonuclease (DEDDy) was one of the earliest crystal structures of nucleic acid enzymes determined (Ollis *et al.* 1985) and the structures of Klenow-oligonucleotide complexes led to the proposal of the two-metal-ion mechanism (Beese & Steitz, 1991; Freemont *et al.* 1988). The structure of epsilon subunit is homologous to the 3′–5′ exonuclease domain of Klenow fragment, and only one metal ion was detected in the absence of ssDNA (Hamdan *et al.* 2002). The structure of the Klenow fragment complexed with ssDNA substrate reveals the coordination of two-metal ions (Fig. 6*a*). Although the substrate DNA is single stranded, its conformation is highly similar to a strand in a double helix (Brautigam & Steitz, 1998; Brautigam *et al.* 1999). These observations indicate that proper binding of two metal ions requires the presence of a cognate DNA substrate. The importance of the scissile phosphate in metal ion coordination is revealed by the sulfur

https://doi.org/10.1017/S0033583510000181 Published online by Cambridge University Press

substitution experiments. Replacement of the pro-Sp oxygen with sulfur essentially abolishes the metal-ion binding and the nuclease activity, and replacement of the 3′ bridging oxygen (leaving group) affects the metal-ion binding, particularly in the B site, whereas the replacement of pro-Rp oxygen moderately affects the metal ions, active site configuration and nuclease activity (Brautigam & Steitz, 1998; Brautigam *et al.* 1999).

6.1.2 *E. coli* ExoI and ExoX

The 3′ ExoI is the first deoxyribonuclease purified and characterized from *E. coli* (Lehman & Nussbaum, 1964). It specifically degrades ssDNA from the 3′-end and is implicated in various DNA repair pathways. The crystal structure of ExoI reveals a C-shaped monomer (PDB: 1FXX) (Breyer & Matthews, 2000). The DEDDh catalytic core is followed by a C-terminal SH3-like domain and surrounded by α-helices. The structure suggests a mechanism for processive digestion of ssDNA. *E. coli* ExoX is highly similar to ExoI in the catalytic domain and ssDNA preference. But, without the C-terminal domain, ExoX is about a half of ExoI in size (Viswanathan & Lovett, 1999). Homologs of *E. coli* ExoI and X are widely spread in bacteria.

6.1.3 TREX1 and TREX2

TREX1 and TREX2 are the major mammalian 3′–5′ exonucleases and also prefer ssDNA substrate. They can perform proofreading function for polymerases that lack an intrinsic 3′–5′ exonuclease activity (Shevelev *et al.* 2002). Defective TREX1 (aka DNase III) causes the Aicardi–Goutieres syndrome in humans, a severe neurological disease, and systemic lupus erythematosus probably due to abnormal innate immune responses to the accumulation of intracellular nucleic acids (Crow *et al.* 2006a). Mice lacking TREX1 develop inflammatory myocarditis (Morita *et al.* 2004). It has recently been shown that TREX1 removes DNA of endogenous retroelements and prevents a type I interferon-mediated autoimmune response to self-nucleic acids (Stetson *et al.* 2008). TREX1 is also a part of SET complex and degrades DNA during granzyme A-mediated caspase-independent cell death (Chowdhury *et al.* 2006). Structures of TREX1 and TREX2 have been determined and are highly similar to that of DnaQ (PDB: 2OA8, 2IOC, 2O4I and 1Y97) (Brucet *et al.* 2007; de Silva *et al.* 2007; Perrino *et al.* 2005). TREX1 and TREX2 differ from DnaQ in being obligatory dimers, and the conserved residue in addition to DEDD in the active site is His rather than Tyr (Fig. 6*b*).

6.1.4 WRN exonuclease

Defective WRN protein is responsible for the Werner Syndrome, or premature aging (Muftuoglu *et al.* 2008). WRN contains both a DNA helicase and 3′–5′ exonuclease activity. The isolated WRN exonuclease domain is monomeric and can degrade the 3′-ends of dsDNA with a 5′ overhang (Perry *et al.* 2006a). The structure of the WRN exonuclease domain contains the DEDDy motif and is similar to other members of the DnaQ family. Two divalent ions were found in the active site in the presence of 50 mM metal ions even without DNA substrate (Perry *et al.* 2006a).

6.1.5 RNase T and Orn

Bacterial RNase T and Orn (oligoribonuclease) are homodimeric 3′–5′ exonucleases with the DEDDh motif. Both prefer ssRNA (Zuo *et al.* 2007) (PDB: 2F96, 2IS3, 1YTA, 2IGI, 2GBZ

https://doi.org/10.1017/S0033583510000181 Published online by Cambridge University Press

and 1J9A). RNase T is essential for 5S and 23S rRNA maturation and for processing of precursor tRNA (Deutscher & Li, 2001). Orn can also hydrolyze DNA in the 3′–5′ direction (Fiedler *et al.* 2004). In the absence of Orn, *E. coli* cells grow slowly. Interestingly, the two active sites of the dimeric RNase T and Orn are on opposite surfaces and appear to be independent of each other.

6.1.6 RNase D and Rrp6

RNase D has the DEDDy motif and processes the 3′ end of structured RNA (Zuo *et al.* 2005). It contains two HRDC (helicase RNase D C-terminal) nucleic acid binding domains in addition to the DnaQ-like catalytic domain. The circular substrate-binding tunnel suggests processivity of RNase D (PDB: 1YT3). One Zn^{2+} ion is tightly bound in the active site and the second Zn^{2+} ion has low occupancy (Zuo *et al.* 2005). The yeast homologue of RNase D, Rrp6p, is a component of the nuclear exosome for the degradation of unstable mRNA transcripts and maturation of rRNA, small nuclear RNA (snRNA) and small nucleolar RNAs (snoRNAs) (for review, see Houseley *et al.* 2006). In the presence of 10 mM $MnCl_2$, two-metal ions are also found in the active site of yeast Rrp6 (PDB: 2HBK) (Midtgaard *et al.* 2006).

6.1.7 Poly A-specific ribonuclease (PARN), Pan2 and Pop2

PARN is a dimeric processive 3′-exonuclease with the DEDDh motif. In addition to the DnaQ-like catalytic domain, PARN has RNA-binding domains (PDB: 2A1S) (Wu *et al.* 2005). Related to PARN, Pop2 is a component of the Ccr4–NOT complex and functions in mRNA degradation. Pop2 is likely to participate in mRNA deadenylation both directly with its 3′–5′-exonuclease activity and indirectly by facilitating the Ccr4 nuclease activity (Parker & Song, 2004). Curiously, although the DEDDh motif is replaced by SEDQt, yeast Pop2 (yPop2) still has the RNase activity (Thore *et al.* 2003). It is unknown whether the active site still uses two-metal-ion catalysis. Fission Yeast Pop2p, however, has the normal DEDDh motifs, and its structure has been determined at high resolution and two-metal ions are found in the active site (Andersen *et al.* 2009; Jonstrup *et al.* 2007). Pan2 (poly-A nuclease), which is a component of the third 3′–5′ exoribonuclease complex for mRNA degradation and maturation, is also predicted to have a DnaQ-like exonuclease domain with the DEDDh motif.

6.1.8 ERI-1, 3′hExo and CRN-4 exonucleases

Eukaryotic ERI-1 (stands for exoribonuclease 1), human 3′-Exo (3′hExo) and *C. elegans* CRN-4 nucleaes share the conserved catalytic domain and the DEDDh motif. However, they are not functional orthologs perhaps owing to different additional structural domains. 3′hExo is responsible for histone mRNA degradation (Cheng & Patel, 2004), ERI-1 is implicated in 5·8S rRNA processing and production of small RNA for RNAi (Gabel & Ruvkun, 2008), whereas CRN-4 is implicated in apoptotic DNA degradation (Parrish & Xue, 2006). The crystal structure of the full-length *Caenorhabditis elegans* CRN-4 has been reported (Hsiao *et al.* 2009). It is a dimeric nuclease and cleaves both RNA and DNA. A C-terminal Zn-domain is appended to the catalytic core and may influence CRN-4's preference to exonucleolytically degrade dsDNA over ssDNA.

https://doi.org/10.1017/S0033583510000181 Published online by Cambridge University Press

6.2 RNase H-like endonucleases

The RNase H fold has the same topology as DnaQ and consists of a five-stranded mixed β-sheet (54123, ↑↑↑↓↑) surrounded by α-helices. However, the catalytic residues are different, and instead of exonucleases only endonucleolytic RNase and DNase are found in this superfamily. The catalytic residues are more varied in composition (Asp, Glu or His) and location than those in the DnaQ family. Only the first Asp in β1 is conserved in all members and is likely to coordinate both metal ions (Nowotny *et al.* 2005). The Asp located at the end of adjacent β4 is the second most conserved, but it is replaced by Glu in the HJ resolvase RuvC and Ydc2 (Yang & Steitz, 1995b). This RNase H superfamily has been recently reviewed by M. Nowotny (Nowotny, 2009), and readers are referred to it for in-depth descriptions. The representative families and their characteristic are summarized below.

6.2.1 RNase H1

RNase H1 (also referred to as RNase H) is the founding member of this large eclectic superfamily of endonucleases. It is conserved from bacteria, retroviruses to humans and cleaves an RNA strand when it is hybridized to DNA. Cellular RNase H1 primarily degrades RNA primers in DNA replication and RNAs in random RNA–DNA hybrids (R loops) (Cerritelli & Crouch, 2009; Tadokoro & Kanaya, 2009). RNase H activity is essential for retroviral reverse transcription (Champoux & Schultz, 2009). Although not sequence-specific, RNase H1 requires a minimum of four ribonucleotides forming RNA/DNA hybrid for cleavage to occur (Tadokoro & Kanaya, 2009). Substrate binding and specificity can be further strengthened by one or two RNA/DNA hybrid-binding domains (HBD) found in many cellular RNase H1 and by the DNA polymerase domain in retroviral reverse transcriptase (Champoux & Schultz, 2009; Nowotny *et al.* 2008).

RNase H catalysis by the two-metal-ion mechanism has been established in a series of enzyme–nucleic acid complexes along the reaction pathway by X-ray crystallography (Nowotny *et al.* 2005; Nowotny & Yang, 2006). Four carboxylates (D10, E48, D70 and D134 according to *E. coli* RNase H) form the catalytic core (Fig. 7*a*). The first and third carboxylates coordinate the two metal ions (Fig. 7*b*). The second carboxylate, Glu located on helix αA, is unique to RNase H1 and binds both the 2′-OH of RNA substrate and metal ion B, thereby enhancing the catalysis specificity (Nowotny *et al.* 2005). The fourth carboxylate coordinates metal ion A only. Although its replacement by Asn significantly reduces catalytic activity, it can be restored by the substitution of Mn^{2+} for Mg^{2+} (Nowotny & Yang, 2006; Nowotny *et al.* 2005). In addition, the substrate actively participates in cleavage. The pro-Sp oxygen of the scissile phosphate coordinates both metal ions and the pro-Rp oxygen of the 3′ neighboring phosphate participates in nucleophile formation (Haruki *et al.* 2000; Nowotny *et al.* 2005).

6.2.2 Transposase and retroviral integrase with the DDE motif

When the structure of HIV integrase and bacterial Mu transposase were determined, it was a surprise to find that these DNA endonucleases bear clear similarity to RNase H1 (Dyda *et al.* 1994; Rice & Mizuuchi, 1995). Sequence alignment predicts that many cellular and retroviral enzymes catalyzing cut-and-paste sequence-specific transposition/recombination have the RNase H fold and a DDE motif, which is approximately equivalent to the 1st, 3rd and 4th carboxylates of RNase H1 (Fig. 7*a–c*). They include the human RAG1 and RAG2 proteins

https://doi.org/10.1017/S0033583510000181 Published online by Cambridge University Press

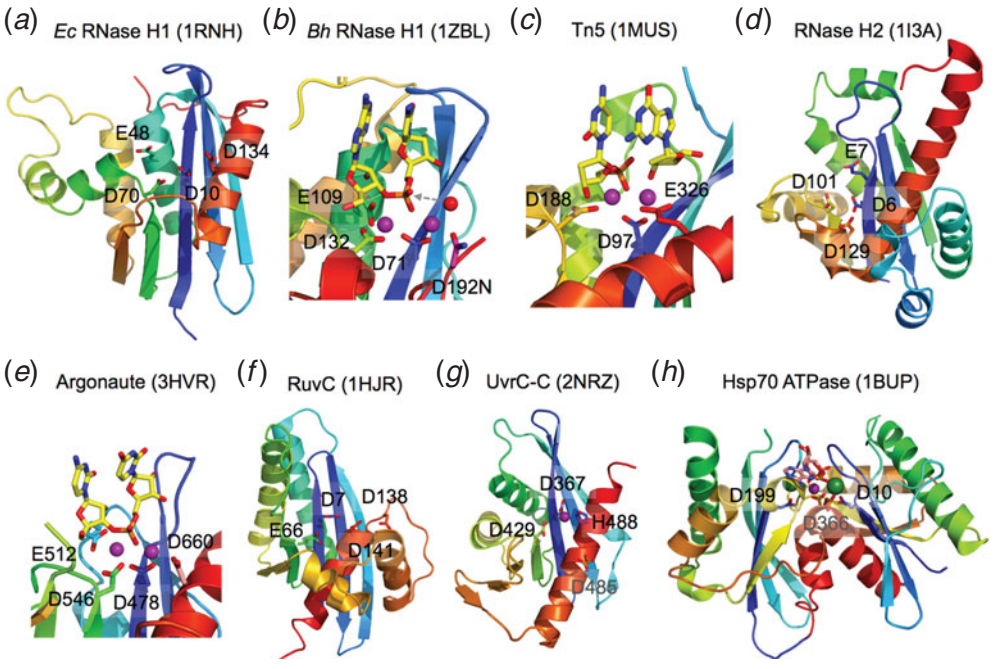


Fig. 7. The RNase H superfamily consists of various endonucleases. (*a*) *E. coli* RNase H1 is the prototype of this superfamily. (*b*) The active site of *Bacillus halodurans* RNase H complexed with an RNA/DNA hybrid substrate. (*c*) Tn5 transposase (complexed with a cleaved DNA product) represents the HIV integrase-like recombinases with the DDE motif. (*d*) RNase H2 has the same topology as RNase H1 but the second and fourth conserved carboxylates are differently located. (*e*) The active site of *Tth* Argonaute, essential for RNAi pathways is similar to that of RNase H1. (*f*) RuvC is a HJ resolvase. (*g*) The C-terminal nuclease domain of UvrC may use two conserved carboxylates and a His for metal-ion coordination and catalysis. (*h*) Monomeric Hsp70 ATPases contain two RNase H-like domains. The duplicated domains are both shown in blue- to red-colored gradients. The Asp residues in the first β-strand (D10 and D199) are conserved throughout the Hsp70 family and essential for the ATPase activity. Proteins, nucleic acids and divalent cations are shown in the same scheme as in Fig. 6. The green spheres represent the K^+ ions.

essential for immunoglobulin gene rearrangement (Kim *et al.* 1999; Landree *et al.* 1999), and eukaryotic Mariner and Hermes transposases (Hickman *et al.* 2005; Richardson *et al.* 2009). Integrases and transposases are at least dimeric when associated with two donor-DNA ends and engaged in recombination. As revealed by the Tn5 transposase–DNA complex structures, the three carboxylates in these integrases and transposases are symmetrically arranged around the two metal ions (Davies *et al.* 2000; Steiniger-White *et al.* 2004). The first Asp coordinates both and the remaining two coordinate one metal ion each (Fig. 7*c*). The recently reported structure of a retroviral integrase complexed with two donor DNA ends, which are nearly perpendicular to each other rather than antiparallel as in the case of Tn5, confirms the active site configuration (Hare *et al.* 2010). The symmetry surrounding the two metal ions has implications for the DNA transposition reaction. These integrase and transposase often catalyze two or more consecutive phosphoryltransfer reactions and the 3′-OH product of the first cleavage reaction can be used as a nucleophile for the second strand transfer reaction (Kennedy *et al.* 2000). It has thus been proposed that the two metal ions switch their roles in coordinating the nucleophile and the leaving group in the two consecutive steps (Nowotny, 2009; Nowotny *et al.* 2005; Steitz & Steitz, 1993).

https://doi.org/10.1017/S0033583510000181 Published online by Cambridge University Press

6.2.3 RNase H2

RNase H2 is the second cellular RNase H found from bacteria to humans (Cerritelli & Crouch, 2009). Eukaryotic RNase H2 consists of two auxiliary subunits, and all three subunits of human RNase H2 have been implicated in the Aicardi–Goutieres syndrome, a heritable autoimmune disease caused by either TREX1 or RNase H2 deficiency due to the accumulation of residual RNA and DNA (Crow & Rehwinkel, 2009; Crow *et al.* 2006b). RNase H2 differs from RNase H1 in that it can cleave a single ribonucleotide embedded in a DNA duplex. Crystal structures of bacterial RNase H2 reveal an RNase H1-like structure with altered locations of catalytic carboxylates (Fig. 7*d*). Only the first and third of the four catalytic carboxylates are superimposable with those of RNase H1. The second carboxylate (E) is immediately located next to the first one (D) instead of 40 residues away. The reaction coordinate is yet to be determined.

6.2.4 Argonaute and PIWI

Argonautes (Ago) and PIWI are the key players in the RNAi pathway and the RNase activity cleaves target mRNA when it forms base pairs with guide RNA (Joshua-Tor, 2006; Nowotny & Yang, 2009). But the catalytic residues are not always conserved, and some Ago and PIWI without catalytic activity function in RNAi pathways by binding complementary guide and target RNA duplexes (Farazi *et al.* 2008; Joshua-Tor, 2006). For those having RNase activity, the three catalytic residues, either DDD or DDH, are approximately equivalent to the DDE in the integrase family and the 1st, 3rd and 4th carboxylates of RNase H1 (Joshua-Tor, 2006). The catalytic mechanism is revealed in a series of elegant crystallographic studies of Ago–nucleic acid complexes (Wang *et al.* 2008, 2009). Similar to transposases, the first carboxylate coordinates the two metal ions and the remaining two coordinate one metal ion each (Fig. 7*e*).

6.2.5 RuvC and Ydc2

Bacterial RuvC and mitochondrial Cce1/Ydc2 are the HJ resolvases that have the RNase H fold (Ariyoshi *et al.* 1994; Ceschini *et al.* 2001; Iwasaki *et al.* 1991; West & Connolly, 1992; White & Lilley, 1997). These proteins are obligatory dimers (Bennett *et al.* 1993). The active site consists of four carboxylates, and the first two appear to be equivalent to the 1st and 3rd carboxylates of RNase H1, but the carboxylate at the end of β4 is Glu instead of Asp (Fig. 7*f*). The last two carboxylates are located on the C-terminal α-helix two residues apart. Based on biochemical analyses, a protein–DNA complex model has been proposed (Fogg *et al.* 2001; Yoshikawa *et al.* 2001). How these carboxylates together with the DNA substrate coordinate the metal ions is yet to be elucidated.

6.2.6 UvrC (C-terminal domain)

UvrC is a bacterial endonuclease involved in nucleotide excision repair. It makes two incisions, one on each side of a lesion (Verhoeven *et al.* 2000). UvrC has two nuclease domains in one polypeptide chain, one for each incision. The C-terminal domain of UvrC, which makes the incision 5′ to a lesion, is homologous to RNase H and shares two catalytic carboxylates with RNase H1 (1st and 3rd) (Karakas *et al.* 2007). But the third catalytic residue in UvrC may be a His that participates in single metal-ion coordination in the absence of DNA substrate

https://doi.org/10.1017/S0033583510000181 Published online by Cambridge University Press

(Fig. 7*g*). Interestingly, replacement of this conserved His with Ala only moderately reduces the enzymatic activity (Karakas *et al.* 2007). How the active site is formed upon substrate binding and whether the conserved Asp adjacent to the His is involved in catalysis awaits future analysis.

6.2.7 Structural roles and the ATPase catalytic core of Hsp70

The RNase H-like fold has been found in many proteins, where it plays a structural role, e.g. in T7 DNA polymerase and mismatch recognition protein MutS (Obmolova *et al.* 2000) and RNase E (Callaghan *et al.* 2005). Intriguingly, it is found in pre-mRNA splicing protein Prp8 (Pena *et al.* 2008; Ritchie *et al.* 2008), where the first carboxylate is conserved and may play an essential structural rather than a catalytic role (Yang *et al.* 2008). Finally, two RNase H-like domains are found in actin and Hsp70 proteins and form the ATPase catalytic core (Flaherty *et al.* 1991). Most interestingly, a conserved Asp is found in the first β-strand of each RNase H domain in Hsp70 (D10 and D199) just as in the nucleases of the RNase H superfamily and both are essential for cation binding (K^+ and Mg^{2+}) and ATPase activity (Johnson & McKay, 1999) (Fig. 7*h*).

6.3 The major REase fold with the D-(D/E)XK motif

Many commonly used type-II restriction endonucleases (REases) share the conserved motif PD-(D/E)XK, or shortened as DEK (Ban & Yang, 1998b; Orlowski & Bujnicki, 2008). The three catalytic residues are located close to each other on an uneven β-hairpin (Fig. 8*a*). The first D is located at the beginning of the first and shorter strand, and the E and K, separated by a hydrophobic residue x, are located in the middle of the second and longer strand. The first D is most conserved and coordinates both metal ions, whereas the second E can be replaced by Q, D, N, H or S, and the third K can be replaced E, Q, D, S, N or T (Lee *et al.* 2005; Orlowski & Bujnicki, 2008). For instance, the third catalytic residue in BamHI is Glu (E113) rather than Lys (Fig. 8*a*). Members of this superfamily have a very diverse primary sequence and thus different structures surrounding the catalytic core. They can be monomeric, dimeric or even tetrameric and are involved in diverse processes, from restriction digestion, DNA repair and homologous recombination to the resolution of the HJ. In addition to endonucleases, members in this superfamily can also be 5′ or 3′ exonucleases. Although not every member with a crystal structure determined is shown to bind two metal ions, the two-metal ion mechanism is consistent with all biochemical and structural observations (Horton & Perona, 2004; Lee *et al.* 2005; Newman *et al.* 1998; Pingoud *et al.* 2005; Viadiu & Aggarwal, 1998, 2000).

6.3.1 Restriction endonucleases (BamHI, HincII, MutH, EcoR124I, etc.)

Nearly 70% REases belong to this superfamily (Orlowski & Bujnicki, 2008). Many REases in this family have a Pro immediately before the conserved Asp making the PD-EXK motif and a conserved N-terminal Glu, which contributes to the metal-ion coordination as observed in EcoRV, BglI, BamHI and MutH of type-II REase family (Horton & Perona, 2004; Lee *et al.* 2005; Newman *et al.* 1998; Viadiu & Aggarwal, 1998; Winkler *et al.* 1993). These REases are most often dimeric (Bitinaite *et al.* 1998), but monomeric REase also exist (Lee *et al.* 2005; Sokolowska *et al.* 2007; Xu *et al.* 2005). By varying dimeric interfaces and thus the relative positions of the two catalytic centers, dimeric REases can cleave DNA to generate blunt ends or staggered ends with

https://doi.org/10.1017/S0033583510000181 Published online by Cambridge University Press

various 5′ or 3′ overhangs (Fig. 8 *b* and *c*) (Ban & Yang, 1998b; Newman *et al.* 1998). The catalytic module invariably approaches DNA from the minor groove side, and the sequence-specific binding is conducted by a separate module/subdomain in the major groove (Fig. 8 *d*). The first two carboxylates of the DEK motif coordinate the metal ions. The third, which usually is hydrogen bonded with both the nucleophilic water and the DNA-binding module in the major groove (Fig. 8 *d*), has been attributed to couple DNA sequence recognition with the cleavage reaction (Lee *et al.* 2005).

Type-I and type-III restriction/modification systems differ from type-II in the requirement of nucleotide triphosphate and DNA translocation (Dryden *et al.* 2001; Murray, 2000), but their endonucleases have a similar active site composed of D and EXK motifs (Niv *et al.* 2007). The crystal structure of EcoR124I of type-I motor-endonuclease subunit shows that the conserved DEK motif indeed forms the catalytic center although the Pro before the first conserved D is absent (Lapkouski *et al.* 2009).

6.3.2 Phage λ and RecE 5′–3′ exonuclease

The active site of the PD-(D/E)XK motif is found among bacterial and phage 5′–3′ exonucleases, which act on dsDNA and produce a protruding 3′ ssDNA for strand annealing or invasion in homologous recombination (Kolodner *et al.* 1994; Stahl *et al.* 1997). RecE together with the ssDNA annealing protein RecT has been exploited for enhanced homologous recombination for *in vivo* gene manipulation (Muyrers *et al.* 2000; Zhang *et al.* 1998). Phage λ exonuclease (aka Red recombinase) and *E. coli* RecE are trimeric and tetrameric, respectively, and both form a toroidal structure, whose central hole is proposed to bind DNA for processive degradation (Kovall & Matthews, 1997; Zhang *et al.* 2009) (Fig. 8 *e*). A conserved Glu precedes the DEK motif in Phage λ exonuclease (Fig. 8 *f*). In RecE, the DEK motif becomes DDK and it is preceeded by a conserved His (Fig. 8 *g*). Whether the multiple active sites in these highly processive exonucleases work sequentially or stochastically is not known yet.

6.3.3 RecB and AdnAB ssDNA nuclease

The nuclease domains of the bacterial motor-nuclease machines RecBCD and AdnAB are closely related to RecE and REases (Singleton *et al.* 2004; Sinha *et al.* 2009). They have both exonuclease and endonuclease activities on ssDNA (Yu *et al.* 1998). Although RecB contains a single nuclease domain, it is one of the three subunits in the helicase/nuclease RecBCD complex. RecBCD forms a cylindrical molecule and DNA threads through the central hole similar to the cases of RecE and phage λ exonuclease. But the DNA becomes unwound by the helicase activity carried by RecB and RecD of RecBCD or by AdnA and AdnB (Unciuleac & Shuman, 2009). The nucleases then nick the ssDNA and ultimately generate 3′ ssDNA overhangs for homologous recombination (Dillingham & Kowalczykowski, 2008; Sinha *et al.* 2009). Deviating from the canonical DEK motif, the Glu is replaced by Asp in RecB as in RecE. RecB does not have the Pro preceding the DDK motif. A conserved His N-terminal to the DDK is likely to participatein catalysis (Fig. 8 *h*).

Dna2 ubiquitous in all eukaryotes has a helicase domain and a RecB-like nuclease domain containing the DEK motif (Budd *et al.* 2000). Dna2 works with ssDNA-binding protein during DNA replication and removes excessively long primers (Kim *et al.* 2006; Masuda-Sasa *et al.* 2006).

https://doi.org/10.1017/S0033583510000181 Published online by Cambridge University Press

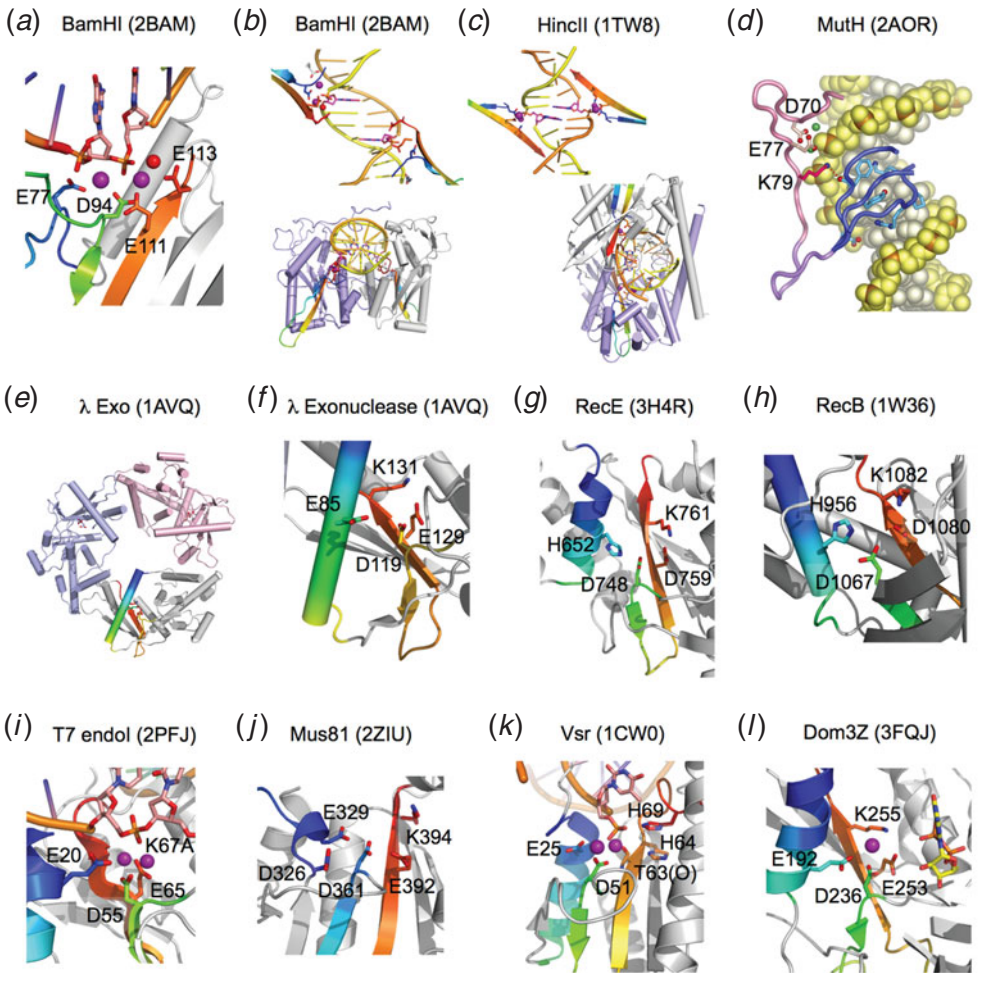


Fig. 8. The DEK superfamily consists of sequence- or structure-specific endonucleases and processive 5′–3′ exonucleases. (*a*) The active site of BamHI contains (E)DEE, a variation of DEK. Except for (*d*), the region containing the catalytic residues is shown in rainbow colored ribbon diagrams. The rest of the protein is colored gray. Divalent cations and the nucleophilic water are shown in purple and red spheres, respectively. (*b*) Orthogonal views of BamHI–DNA interactions. The two BamHI subunits are shown in gray and light purple. The uneven β-hairpins containing the DEK motif are highlighted in the rainbow colors. Only the β-hairpins are shown when looking into the DNA major groove. BamHI cleaves DNA to form 4 nt 5′ overhangs. The nucleotides containing the scissile phosphate are highlighted in pink sticks. (*c*) Orthogonal views of HincII–DNA interactions. HincII cleaves DNA to blunt ends. The dimerization interface of HincII is nearly perpendicular to that of BamHI when looking down the DNA helical axis. (*d*) *E. coli* MutH is a sequence- and methyl-specific endonuclease with the DEK motif. The conserved Lys (K79) bridges the DNA sequence-specific binding in the major groove (shown in blue) and catalytic center approaching the minor groove (shown in pink). The divalent cations (Ca^{2+}) are shown as green spheres. (*e*) The trimeric phage λ exonuclease has a toroidal shape and degrades ssDNA processively. The three subunits are shown in grey, pink and blue ribbon diagrams. The active site region of the grey subunit is highlighted in rainbow colors. (*f*) A zoom-in view of the active site with the (E)DEK motif. (*g*) RecE, which is a processive exonuclease and promotes DNA recombination, is shown in the same color scheme as BamHI. (*h*) The active site of RecB has the DEK motif with a His at its N-terminus like RecE. (*i*) The HJ resolvase T7 endonuclease I has the (E)DEK motif-like MutH and binds two metal ions. (*j*) The structure-specific endonuclease Mus81 and XPF also contain the DEK motif with two conserved carboxylates N-terminal to it. (*k*) Vsr is a sequence-specific endonuclease. The DEK motif may be replaced by DHH,

https://doi.org/10.1017/S0033583510000181 Published online by Cambridge University Press

6.3.4 HJ resolvase: T7 endonuclease I

Phage T7 endonuclease I and archaeal Hjc are HJ resolvases, whose active sites contain the REase-like (E)-PD-EXK motif (Lilley & White, 2001). These HJ resolvases are homodimeric and recognize four-way junctions in a distorted stacked-X form as shown in the crystal structures of enzyme–DNA complexes (PDB: 2PFJ and 2WJ0) (Hadden *et al.* 2007). Recognition and resolution of HJ are recently reviewed (Declais & Lilley, 2008). T7 endonuclease I cleaves DNA by the two-metal-ion mechanism with the two most conserved carboxylates coordinating two metal ions (Hadden *et al.* 2007) (Fig. 8*i*).

6.3.5 Structure-specific endonuclease: XPF, Hef, Rad1 and Mus81

The archaeal and eukaryotic structure-specific nucleases, Hef, Rad1, XPF and Mus81 all share the conserved nuclease domain, known as ERCC4 domain. The catalytic motif of D-ERK is homologous to that of REases (Chang *et al.* 2008; Newman *et al.* 2005; Nishino *et al.* 2003) (Fig. 8*j*). These nucleases are required for DNA repair, processing of a stalled replication fork, and repair-associated recombination (for an in-depth review, read Ciccia *et al.* 2008). In addition to the DEK motif, two conserved carboxylates, Asp and Glu, N-terminal to it are located in the active site (Fig. 8*j*). DNA substrates can vary from a 3′ flap, replication fork, to a HJ, all of which have the common feature of a 3′ flap, and cleavage occurs at the single- and double-strand junction. Although archaeal Hef nuclease is homodimeric, all eukaryotic nucleases in this family, for example, Rad1, XPF and Mus81, form heterodimers (Rad1/Rad10, XPF/ERCC1 and Mus81/Eme1, Mus81/Eme2, or Mus81/Mms4) with only one active subunit. Interestingly, even with homodimeric nucleases it is likely that only one subunit is engaged in catalysis at a given time (Newman *et al.* 2005). Based on the conservation of the active site, two-metal-ion catalysis is predicted.

6.3.6 DNA mismatch-repair endonuclease very short-patch repair (Vsr)

E. coli Vsr endonuclease specifically cleave 5′ to the T of mismatched T:G base pair, which results from the deamination of 5-methyl-cytosine in a specific sequence (Hennecke *et al.* 1991). The crystal structures of Vsr and Vsr complexed with DNA cleavage products reveal the REase fold in spite of the absence of the last two conserved catalytic residues of the DEK motif (Bunting *et al.* 2003; Tsutakawa *et al.* 1999). A conserved Glu preceding the central uneven β-hairpin and two His residues C-terminal to it are in the catalytic center and may be involved in metal-ion coordination and nucleophile activation (Fig. 8*k*). In addition to the absolutely conserved Asp at the beginning of the uneven β-hairpin, a backbone carbonyl oxygen in the second β-strand also contributes to the metal-ion coordination in the Vsr–DNA cleavage product complex (Fig. 8*k*). The presence of two Mg^{2+} ions in the enzyme–product complex structure is highly suggestive of the two-metal-ion mechanism as observed for the other members of this superfamily.

and the two metal ions in the active site are coordinated by the carbonyl oxygen (of T63) in addition to the conserved Asp and scissile phosphate. (*l*) Dom3Z and Rai1 have the conserved DEK motif and can hydrolyze GTP.

https://doi.org/10.1017/S0033583510000181 Published online by Cambridge University Press

6.3.7 Rai1/Dom3Z for mRNA degradation and processing

Human Dom3Z and yeast Rai1 are the newest enzymes found to have the conserved REase fold and the (E)-D-EXK motif (Xiang *et al.* 2009) (Fig. 8*b*). Before the crystal structure of Rat1–Rai1 complex was determined, Rai1 was thought to activate the 5′ to 3′ exoribonuclease Rat1 in the processing of RNA (Xue *et al.* 2000). But the structure reveals a divalent cation-binding site in Rai1. The authors proceed to show that the Rai1 homologue Dom3Z binds GDP, possesses a pyrophosphatase activity and can remove pyrophosphate from a 5′ triphosphorylated RNA. However, the GDP in the crystal structure is too far from the (E)-D-EXK motif to be either a substrate or product (Fig. 8*b*). Whether Rai1 has nuclease activity is yet to be determined.

6.4 FEN1-like 5′ exo- and endo-nucleases

The nucleases in this family share a conserved $\beta\alpha$ Rossmann-like fold consisting of a central parallel five-stranded β-sheet (in the order of 54123) surrounded by α-helices. The catalytic residues are located between the ends of strands (β1, β3 and β4) and the beginning of the following helices. They are almost exclusively Asp and Glu residues, and the number of conserved carboxylates ranges from five to eight, four of which may directly participate in phosphodiester bond cleavage (Fig. 9*a*). Although the crystal structures of *Archaeoglobus fulgidus* FEN1 and T4 RNase H were determined in complex with DNA (Chapados *et al.* 2004; Devos *et al.* 2007), the DNA is either far away from the active site (Fig. 9*c*) or approximately in the active site but with the scissile phosphate displaced in the absence of metal ions (Fig. 9*b*). However, two divalent cations have been observed in several apo-FEN1 structures and biochemical analyses suggest that these nucleases use the two-metal-ion mechanism like other nucleases containing an absolutely conserved Asp (Liu *et al.* 2004; Tomlinson *et al.* 2010 and reference therein). Many members of this superfamily have dual 5′-exo and 5′ flap-endonuclease activities.

6.4.1 5′ FENs: T4 RNase H, yeast Rad27 and human FEN1

The 5′–3′ exonuclease intrinsic to *E. coli* DNA Pol I is the founding member of the superfamily (Klett *et al.* 1968; Setlow & Kornberg, 1972), which includes Phage T4 RNase H, yeast Rad27 and human FEN1. The exonuclease is active on either RNA or DNA and its main function is to remove RNA primers in lagging strand synthesis (Bhagwat *et al.* 1997; Liu *et al.* 2004). These nucleases also contain the structure-specific endonuclease activity and can cleave the 5′ displaced ssDNA flap, such as the displaced primers in lagging strand DNA synthesis. The latter activity gives rise to the name of flap endonuclease, FEN1 (Harrington & Lieber, 1994). In bacteriophages, archaea and mammals, the 5′–3′ exo and FENs can exist as an independent protein, for example, T4 RNase H (a mis-nomenclature; Bhagwat *et al.* 1997). In fact, T4 RNase H has the same activities and structure as the 5′–3′ exonuclease of *E. coli* Pol I (Fig. 9*a*, *b*). To avoid confusion, phage T4 RNase H has been renamed as T4FEN (Tomlinson *et al.* 2010). FEN activity is not only involved in DNA replication but also in long-patch base excision and DSB repair (Shen *et al.* 2005).

To date, crystal structures of several apo-nucleases in this family and phage T4 and archaeal FEN in complex with DNA have been determined (Ceska *et al.* 1996; Chapados *et al.* 2004; Devos *et al.* 2007; Hwang *et al.* 1998; Kim *et al.* 1995). The catalytic center often contains 6–7 highly conserved Asp and Glu residues (Fig. 9*a–c*). The four most conserved carboxylates located after β1, β3 and β4 are reminiscent of the catalytic carboxylates in RNase H (Fig. 7*a*).

https://doi.org/10.1017/S0033583510000181 Published online by Cambridge University Press

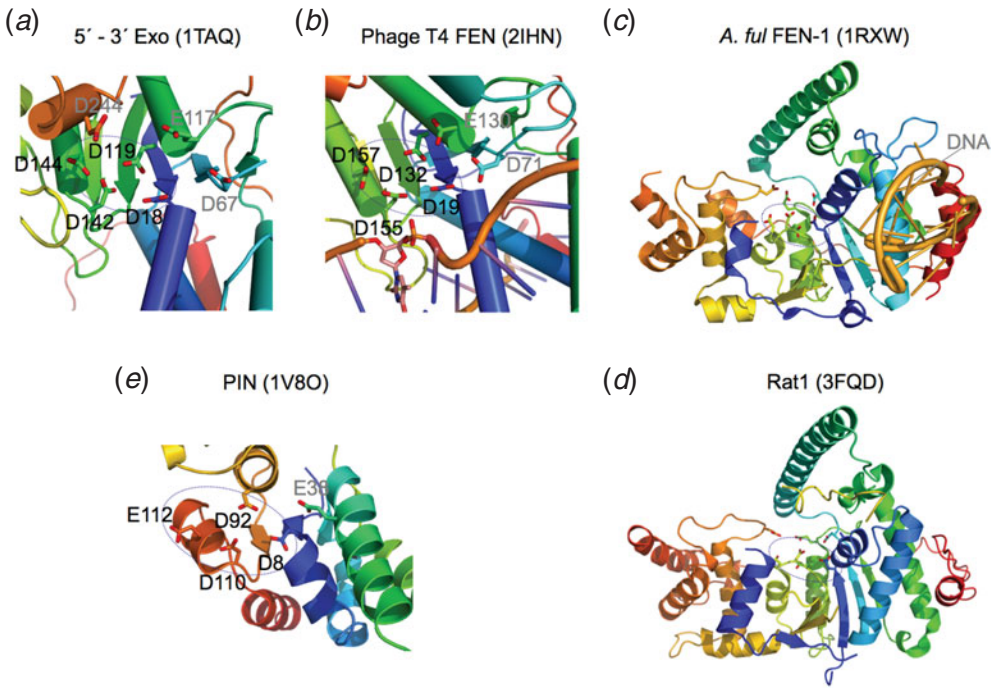


Fig. 9. The FEN1 and 5′–3′ exonuclease superfamily. (*a*) The active site of the 5′–3′ exonuclease domain of Taq DNA polymerase. Four of the seven conserved carboxylates (encircled) are likely to participate in metal-ion binding and catalysis. (*b*) Phage T4 FEN1, previously known as T4 RNase H. The structure was determined in the complex with DNA substrate, but the scissile phosphate is too far away from the catalytic residues in the absence of divalent cations. (*c*) The archaeal FEN1 has the same active site composition as the bacterial and phage orthologs. The bound DNA is far away from the nuclease active site. (*d*) Rat1, which is an RNase, has the same overall structure and conserved active site as archaeal FEN1. (*e*) The PIN domain represents the minimal catalytic core of the nucleases in this superfamily. In all panels, the protein topology is shown in the color gradient from the blue N- to red C-terminus.

The remaining negatively charged residues in the catalytic center is likely to be involved in binding of a third metal ion, which may facilitate substrate binding and thus indirectly contribute to the catalysis (Syson *et al.* 2008). However, in the absence of knowledge of the active site complete with scissile phosphate and metal ions, the reaction coordinates and chemistry for bond breakage remain uncertain.

6.4.2 XPG and HJ resolvases Gen1 and Yen1

XPG is required for nucleotide excision repair to incise at the 3′ side of a lesion and shares sequence homology with FEN1 (Habraken *et al.* 1993; O'Donovan *et al.* 1994; Scherly *et al.* 1993). Recently isolated eukaryotic HJ resolvases Gen1 and Yen1 are also found to be homologous to FEN1 (Ip *et al.* 2008). Interestingly, like FEN1, human XPG and its yeast homolog Rad2 both exhibit 5′-exonuclease activity (Habraken *et al.* 1994). Although no crystal structure has been reported for these endonucleases, the conserved active site residues and functional assay indicate that they all recognize a 5′ flap or branch structure and endonucleolytically cleave DNA at or adjacent to a branch point (including a ss–ds junction), likely by the two-metal-ion mechanism.

https://doi.org/10.1017/S0033583510000181 Published online by Cambridge University Press

6.4.3 Human and yeast 5′ exonuclease I (Exo1)

It is perhaps not surprising to find that human and yeast 5′ exonuclease I, which are implicated in mismatch and DSB repair (Genschel *et al.* 2002; Szankasi & Smith, 1995), are homologous to FEN1 and XPG and share the same conserved active site. Like its homologues, Exo1 also has the FEN activity (Lee & Wilson, 1999; Tran *et al.* 2002). This FEN activity of ExoI is reported to be stimulated by Wrn protein (Sharma *et al.* 2003). Exo1 also uses the two-metal-ion mechanism.

6.4.4 5′ exoribonuclease Rat1 (XRN2) and XRN1

Recently, the structure of mouse Rat1 or XRN2, the 5′ exoribonuclease for RNA processing, has been reported (Xiang *et al.* 2009). Rat1 is highly similar to the structure of archaeal FEN1 with a large N-terminal loop wrapping around the protein and a helical tower (Fig. 9*c*, and *d*). The highly conserved carboxylate-rich active site implicates a metal-ion-dependent mechanism of catalysis by these XRNs. It is unclear what makes them specific for RNA degradation and whether XRNs may have endonuclease activities if a proper substrate-binding partner is present. Eukaryotic XRN1, the major 5′–3′ exonuclease of RNAs, shares the conserved catalytic residues of XRN2 (Szankasi & Smith, 1996) and is predicted to have a FEN1-like structure and active site.

6.4.5 PIN domain RNA exonuclease

PIN (PilT N-terminal domain) nuclease is a recent addition to the FEN1 superfamily. It is a component of the exosome for RNA turnover and is also involved in nonsense mediated mRNA decay (Arcus *et al.* 2004; Clissold & Ponting, 2000; Eberle *et al.* 2009). Crystal structures of PIN nucleases reveal a stripped down minimal core of FEN1 (Glavan *et al.* 2006) (Fig. 9*e*). Like many members of this superfamily, PIN has both 5′-exo and endonucleolytic activities (Eberle *et al.* 2009; Schneider *et al.* 2009). Three Asp residues after β1, β3 and β4 are highly conserved among PIN nucleases as well as all FEN1 and XPG superfamily members. The fourth (two residues away from the third) can be Asp, Glu, Asn, or His (Arcus *et al.* 2004; Glavan *et al.* 2006). These four are superimposable with the core catalytic residues of all nucleases in the FEN1 superfamily (Fig. 9).

6.5 RecJ and DHH family

RecJ is a 5′–3′ single-strand exonuclease involved in DNA repair and recombination (Kowalczykowski *et al.* 1994). It contains the DHH motif as does the drosophila prune nuclease (Aravind & Koonin, 1998). Like the FEN1 superfamily, the nuclease core domain of RecJ consists of $\beta\alpha$ repeats with a central parallel β-sheet surrounded by α-helices. However, the order of β-strands is 54 312 in RecJ instead of 54 123 as in FEN1 (Fig. 10*a*, and *b*). The catalytically essential residues are located between the end of central three adjacent parallel β-strands (β1, β3 and β4) and the beginning of the following α-helices (Yamagata *et al.* 2002) (Fig. 10*a*). The consecutive DHH residues, which give rise to the name of this nuclease family (Aravind & Koonin, 1998), are located at the end of the 4th strand just like the last two catalytically essential Asp residues in FEN1 (Figs 9 and 10*b*). Mn^{2+} is found in the active site coordinated by the two conserved His residues. In addition to the DHH, four conserved carboxylates are located in the active site and are likely to be involved in metal-ion binding and catalysis (Fig. 10*b*).

https://doi.org/10.1017/S0033583510000181 Published online by Cambridge University Press

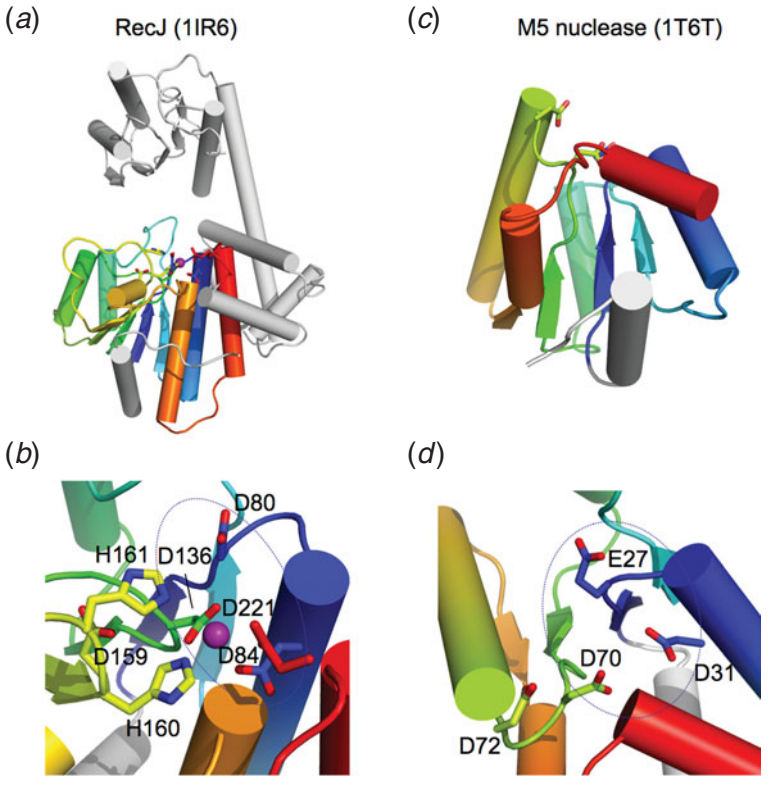


Fig. 10. Two nuclease families related to FEN1. (*a*) RecJ is a representative member of the DHH family. The catalytic and DNA-binding domain of RecJ are shown in ribbon diagrams. The catalytic domain containing the DHH motif is shown in rainbow colors with the gradient of blue N- to red C-terminus. The rest of RecJ is shown in gray. (*b*) A divalent cation is found in the carboxylate-rich active site in the absence of substrate. (*c*) TOPRIM M5 nuclease family has a $\beta\alpha$ fold of a central parallel 4-stranded β-sheet surrounded by α-helices. The catalytic carboxylates are located on the loops linking secondary structures. (*d*) The active site of M5 nuclease. The four carboxylates are shown as sticks.

6.6 TOPRIM nucleases: RNase M5

TOPRIM is a metal-binding module found among TOpoisomerases (type IA and type II) as well as DnaG-like PRIMases (Aravind *et al.* 1998), giving rise to the name of this superfamily. In addition to the topoisomerases and primases, 5S rRNA maturases RNase M5 (Allemand *et al.* 2005), and bacterial ATP-dependent OLD-family nucleases also contain TOPRIM and are thus members of this superfamily (Aravind *et al.* 1998). The TOPRIM module has a Rossmann-like $\beta\alpha$ fold quite similar to the nuclease core domain of RecJ. It consists of a central parallel four-stranded β-sheet in the order of 4312 surrounded by α-helices (Fig. 10*c*, *d*). TOPRIM is also marked by two conserved sequence motifs, E and DXD at the end of 1st and 3rd β-strand, respectively, which are proposed to coordinate divalent cations. Not all TOPRIM domains are involved in phosphoryl transfer reactions. RecR, which is an essential component of RecFOR for recombination, has the TOPRIM structure but is devoid of the metal-binding motifs and nuclease activity (Lee *et al.* 2004).

Bacterial RNase M5 endonucleolytically cleaves precursors of 5S rRNA in the double-stranded region and produces the mature form in the context of ribosome (Condon *et al.* 2001).

https://doi.org/10.1017/S0033583510000181 Published online by Cambridge University Press

The cleavage products are 5′-phosphate and 3′-OH. The crystal structure of RNase M5 has been determined (PDB: 1T6 T) by the Midwest Structure Genomic group (Fig. 10*c*). In addition to the conserved E and DXD common to the TOPRIM, RNase M5 also contains an additional conserved Asp located three residues after the first E (Fig. 10*d*). These four carboxylates are conserved in the catalytic center of the DnaG-like primases (Keck *et al.* 2000). All DNA and RNA polymerases known to date use the two-metal-ion mechanism (Steitz, 1998; Yang *et al.* 2006). Consistent with the two-metal-ion mechanism, three partially occupied metal ion sites are found in the active site of *E. coli* primase in the absence of nucleic acid substrate (Keck *et al.* 2000). Even though RNase M5 is a nuclease and catalyzes the reverse reaction of polymerization, its close relationship to primase and its similarities to RecJ and FEN1 suggest that RNase M5 and related OLD nucleases probably catalyze DNA and RNA cleavage by the two-metal-ion mechanism.

Interestingly, this fourth carboxylate is absent in the topoisomerases containing the TOPRIM module. The missing carboxylate and usage of a Tyr as the nucleophile may lead DNA cleavage by topoisomerases to depend on a single metal ion for catalysis (see section 7.3).

6.7 DNase I-like endo and 3′ exonucleases

Pancreatic DNase I is among the first nucleases discovered and characterized (Hoard & Goad, 1968; Kunitz, 1950; Suck *et al.* 1984). This family of nucleases now encompasses DNase and possibly RNase, and their functions vary greatly from DNA digestion, base excision repair, to RNA processing (Table 1). Most of the members in this superfamily are endonucleases, but the 3′–5′ exonuclease activity of APE1 has also been reported and is essential for the DNA repair functions (Castillo-Acosta *et al.* 2009; Chen *et al.* 1991). The catalytic core of the DNase I superfamily is a four-layered $\alpha\beta\beta\alpha$ structure (Fig. 11*a* and *b*). The two mixed β-sheets in the center share a similar, but permutated folding topology (Suck *et al.* 1984), and the tertiary structures are related by a pseudodyad axis roughly parallel to the β-strands (Mol *et al.* 1995). The active site is composed of conserved Asp, Glu and His residues located at the end of the central β-sheets (Fig. 11*a*).

6.7.1 DNase I

DNase I is most prevalent in mammals and is also found in bacteria, but not in low eukaryotes or plants. DNase I functions in apoptosis and has been implicated in the autoimmune disease SLE (systemic lupus erythematosus) (Martinez Valle *et al.* 2008). The crystal structure of bovine pancreatic DNase I – DNA complex was determined nearly 20 years ago (Weston *et al.* 1992). In the crystal structures of DNase I without DNA, two Ca^{2+} ions were observed at a distance from the active site and thought to play structural and substrate-binding roles (Chen & Liao, 2006). DNase I is most active in the presence of mixed Ca^{2+} and Mg^{2+} (Pan & Lazarus, 1999). All the catalytic residues (four Asp and Glu, two His and one Asn) are located at the end of the central 4 β-strands ($\downarrow\uparrow\uparrow\downarrow$) of both β-sheets (Fig. 11*a–c*). Two conserved His residues surrounding the scissile phosphate have been shown to be important for the general acid-and-base catalysis, and the His mutations can be rescued by imidazole (Chen *et al.* 2007a). The scissile phosphate is distorted and both pro-Rp and pro-Sp oxygens interact with DNase I (Figs 11*c*, 5*c*). Although divalent cation is chelated away by 20 mM EDTA and thus absent in the crystal structure of enzyme–substrate complexes (Weston *et al.* 1992), the requirement of two Asp residues (D168 and D212) and Mg^{2+} for DNA cleavage suggests that metal ions are likely to be essential for catalysis (Jones *et al.* 1996).

https://doi.org/10.1017/S0033583510000181 Published online by Cambridge University Press

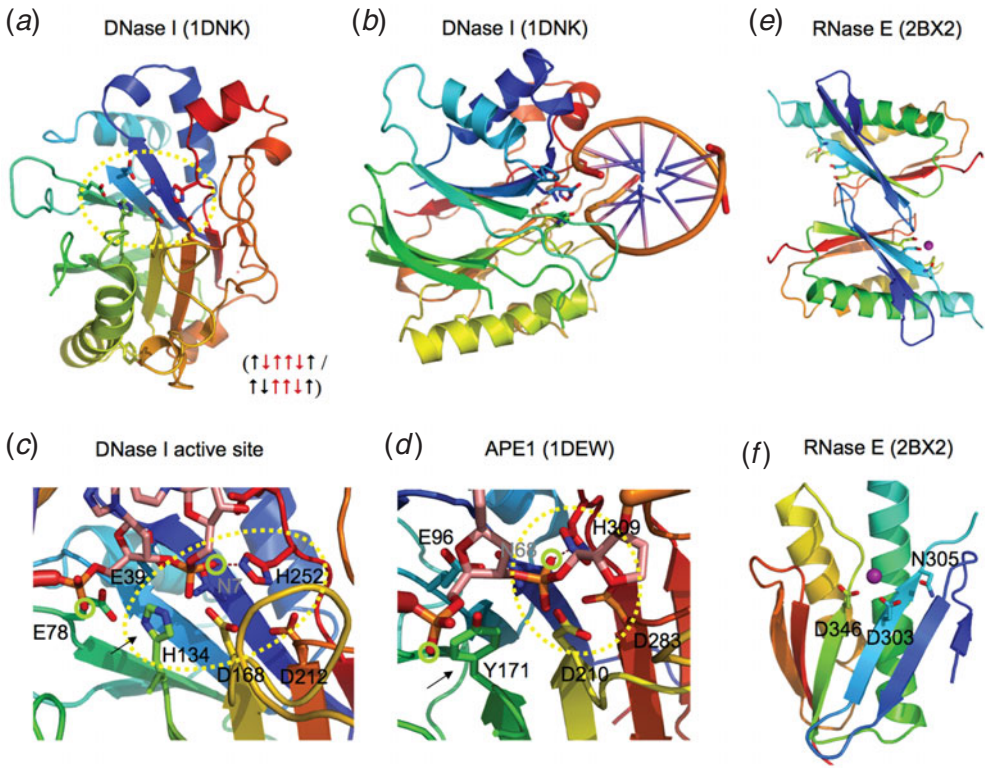


Fig. 11. DNase I family. (*a*) The overall structure of DNase I. Directions of strands are indicated in the parenthesis at the foot of the panel and the strands contributing catalytic residues are highlighted in red. The active site is encircled. (*b*) DNase I with bound substrate. The view is roughly orthogonal to (*a*). The two β-sheets are related by a pseudo-dyad axis lying in the plane of the page and roughly parallel to the strands. (*c*) The active site of DNase I. The pro-Sp oxygens of the scissile phosphate and the neighboring phosphate are encircled in green. Note the distortion of the scissile phosphate. (*d*) Similar distortion of the scissile phosphate is also observed in the APE1–substrate complex. Most of the catalytic residues are conserved between DNase I and APE1 except for the alternative His and Tyr as indicated by the black arrowheads. (*e*) The catalytic domain of RNase E upon dimerization is proposed to be similar to DNase I. Both subunits are shown as rainbow-colored ribbon diagrams from blue N- to red C-terminus. The dyad-axis between the two subunits is perpendicular to the plane of the page. (*f*) The catalytic domain of a single RNase E subunit. The divalent cation is shown as a purple sphere.

6.7.2 AP endonuclease Exo III and APE1

Exonuclease III (Exo III), which is the major apurinic/apyrimidinic endonuclease in *E. coli* and its eukaryotic homologue APE1 share the conserved tertiary structure and active site with DNase I (Gorman *et al.* 1997; Mol *et al.* 1995). These nucleases cleave the phosphodiester bond 5′ to an abasic (apurinic/apyrimidinic) site endonucleolytically and also cleave exonucleolytically to remove a 3′-dRP (dRP = phosphoglycolate, phosphate, or α,β-unsaturated aldehyde) (Demple & Harrison, 1994). Crystal structures of Exo III and APE1 alone (Gorman *et al.* 1997; Mol *et al.* 1995) and APE1 complexed with an abasic DNA substrate without divalent cation and complexed with metal ion and cleavage product have been determined (Mol *et al.* 2000). The active site is highly similar to that of DNase I, except for the replacement of the H134 and E78 by Y171 on the 3′ leaving group side (Fig. 11*c* and *d*). Two Asp and the

https://doi.org/10.1017/S0033583510000181 Published online by Cambridge University Press

C-terminal His surrounding the scissile phosphate are superimposable between DNase I and APE1.

In the APE1–DNA complex structure, the abasic nucleotide is flipped out of the DNA double helix. Concomitantly, the backbone phosphate turns as well and the pro-Sp non-bridging oxygen points inward instead of outward (Fig. 11*d*). The distortion of the scissile phosphate is identical to that in the DNase I complex, where the pro-Sp oxygen rotates toward the minor groove (Fig. 11*c* and *d*). In RNase H and many other two-metal-ion-dependent nucleases, the pro-Sp oxygen coordinates both metal ions (Fig. 5). Here the pro-Sp oxygen is stabilized by the C-terminal His in APE1 and DNase I. Instead, it is likely that the pro-Rp oxygen coordinates two metal ions for the nucleophilic attack (see additional discussion in section 6.16). Consistent with this prediction, sulfur replacement of pro-Sp or pro-Rp oxygen of the scissile phosphate eliminates endonucleolytic cleavage by Exo III (Takeuchi *et al.* 1994).

6.7.3 RNase E and G

RNase E is an endoribonuclease participating in the degradation of messenger and regulatory RNA and the processing of tRNA, rRNA and tmRNA precursors (Worrall & Luisi, 2007). In bacteria, it often functions in a multienzyme assembly known as the RNA degradosome, which contains RNA helicase, enolase and exoribonuclease PNPase. RNase G and RNase E are paralogs and share the conserved active site. RNase E forms a homotetramer with D2 symmetry (Callaghan *et al.* 2003). Each active site is composite and composed of two polypeptide chains, each of which contributes a two-layered $\alpha\beta$ structure (Fig. 11*e*) (Callaghan *et al.* 2005). The catalytic domain of a single RNase E subunit (one $\alpha\beta$ structure) is similar to half of DNase I (Fig. 11*f*). The dyad axis that relates the two RNase E subunits that form a composite active site, however, is approximately perpendicular to the β-sheet instead of parallel to it as in the DNase I structure (Fig. 11*a* and *e*). Dimerization of RNase E actually results in a cluster of conserved carboxylates on either end of the β-sheets and thus two active sites instead of one as in DNase I (Callaghan *et al.* 2005). The catalytic residues of the RNase E and their arrangement bear similarity to DnaQ and RNase H (Figs. 6 and 7). The mechanism for RNase E catalysis is likely two-metal-ion dependent with details yet to be revealed.

6.8 β-CASP nucleases with the metallo-β-lactamase fold

The β-CASP nucleases are named after representative members [CPSF-73 (Cleavage and Polyadenylation Specificity Factor-73), Artemis, Snm1 and Pso2] adopting the metallo-β-lactmase fold (Aravind, 1999; Callebaut *et al.* 2002; Daiyasu *et al.* 2001; Dominski, 2007), which is a four-layer $\alpha\beta\beta\alpha$ structure with a pseudodyad axis relating the two halves. Metallo-β-lactamase is an amidohydrolase and degrades β-lactam in a group of powerful antibiotics that inhibit bacterial cell wall biogenesis (Wang *et al.* 1999), whereas β-CASP nucleases hydrolyze the phosphodiester bond in RNA or DNA. The nuclease activity can be either endo or 5′ exo. The β-lactamase fold is reminiscent of the DNase I fold (Callebaut *et al.* 2002) (Fig. 12*a*), but each β-sheet contains seven strands instead of six and the strand polarities (↓↑↓↑↑↑↑) are different from those in DNase I and APE1 (↑↓↑↑↓↑). The catalytic residues are at one end of the β-sheets (Fig. 12*a*), which is again reminiscent of DNase I and APE1. The β-lactamase family enzymes are unique in their tight binding of two Zn^{2+} ions independent of substrate. The many His residues in the catalytic center may contribute to the selectivity for Zn^{2+} (Baldwin *et al.* 1979).

https://doi.org/10.1017/S0033583510000181 Published online by Cambridge University Press

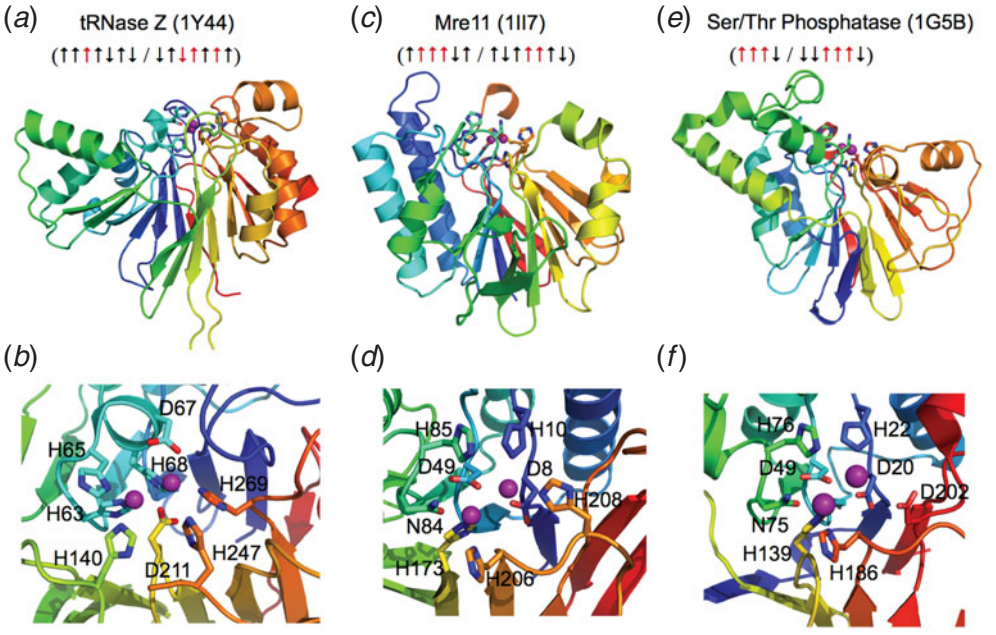


Fig. 12. Nucleases of the metallo-β-lactamase and protein phosphatase (PP2A) families. (*a*) The overall structure of tRNase Z of the metallo-β-lactamase family. Directions of strands in the two β-sheets are indicated by the array of arrows. Strands contributing the catalytic residues are highlighted in red. (*b*) The active site of tRNase Z consists of six His and two Asp residues. Two metal ions are bound independent of substrate. (*c*) The overall structure of Mre11. It bears significant similarity to tRNase Z in the topology, tertiary structure, active site composition and metal-ion binding. However, the composition and locations of the catalytic residues are different. (*d*) The active site of Mre11 consists of five His, one Asn and two Asp. (*e*) A Ser/Thr phosphatase structure is shown for comparison. Its topology has some differences from tRNase Z and Mre11. (*f*) The active site of the protein phosphatase is nearly superimposable with that of Mre11.

6.8.1 RNase Z for tRNA maturation

RNase Z is an endonuclease that processes the 3′ end of tRNA precursors (pre-tRNA) and is also known as the 3′ tRNase. It is widely spread from bacteria, archaea to eukaryotes (Schiffer *et al.* 2002). RNase Z cleaves 3′ to the discriminator base, which is the last in the acceptor stem and primes the CCA addition. If CCA is already present, RNase Z can cleave after CCA, but cleavage before CCA is severely inhibited thereby avoiding futile cycles of CCA addition (Minagawa *et al.* 2004). The crystal structure of RNase Z (de la Sierra-Gallay *et al.* 2005; Ishii *et al.* 2005; Kostelecky *et al.* 2006) confirms the sequence-based prediction of its resemblance to β lactamase (Schiffer *et al.* 2002) and the two Zn^{2+}-based catalytic mechanism (Minagawa *et al.* 2004). Five conserved His and two conserved Asp residues are involved in metal-ion coordination (Fig. 12*b*).

6.8.2 CPSF-73 and RNase J1

Mammalian CPSF-73 was predicted to have the metallo-β-lactamase fold and endonuclease activity (Aravind, 1999). Mutagenesis of the yeast CPSF-73 homolog, Ysh1p, confirms the

https://doi.org/10.1017/S0033583510000181 Published online by Cambridge University Press

predicted catalytic nuclease activity and its *in vivo* function (Ryan *et al.* 2004). CPSF-73 has both an endo and 5′-exo nuclease activity and is essential for processing the 3′ end of mRNA precursors (Chanfreau *et al.* 1996; Jenny *et al.* 1996; Marzluff *et al.* 2008; Yang *et al.* 2009). Crystal structures of the human CPSF-73 (Mandel *et al.* 2006) show that the catalytic domain is essentially identical to RNase Z. Like RNase Z, two Zn^{2+} ions are coordinated by five His and two Asp residues.

Bacillus subtilis RNase J1 is a 5′ exonuclease and functions in pre-rRNA maturation and mRNA decay (Bechhofer, 2009; Mathy *et al.* 2007). RNase J1 also has the metallo-β-lactamase fold and shares the conserved catalytic residues of CPSF-73.

6.8.3 Artemis, Snm1 and Pso2

Artemis, which is required to open DNA hairpins in V(D)J recombination, also belongs to the metallo-β-lactamase nuclease family (Moshous *et al.* 2001). Mutations in Artemis are linked to defective V(D)J recombination and immune deficiency SCID. Like CPSF-73, Artemis has both endonuclease and 5′ exonuclease activities. In addition, the DNA cross-link repair nucleases Snm1 and Pso2 have similar nuclease domains (Callebaut *et al.* 2002; Dominski, 2007). These related RNase and DNase share an additional conserved structural domain, called the β-CASP domain, which is inserted near the C-terminus of the nuclease domain (Mandel *et al.* 2006). Although crystal structures of Artemis, Snm1 and Pso2 are not yet determined, based on the sequence homology these nucleases are likely to bind two Zn^{2+} ions in the active site and catalyze DNA cleavage by the two-metal-ion mechanism.

6.9 Mre11 and protein phosphatase 2B fold

Mre11 is an essential component of Mre11–Rad50–Nbs1 complex (MRN), which detects DSBs and promotes repair (Mimitou & Symington, 2009). Similar to APE1, Mre11 has both the 3′ to 5′ exonuclease activity and endonuclease activity (Paull & Gellert, 1998, 1999). Structurally Mre11 is homologous to protein phosphatases 1, 2A and 2B, for example, calcinurin A (Griffith *et al.* 1995; Hopfner *et al.* 2001; Reiter *et al.* 2002) (Fig. 12*c–f*). Like the Ser/Thr phosphatases, Mre11 binds tightly two Mn^{2+} in its active site even in the absence of a DNA substrate (Hopfner *et al.* 2001).

The crystal structures of archaeal Mre11 alone and in complex with DNA reveal a homodimer with the tertiary structure and active sites not unlike that of β-CASP nucleases (Hopfner *et al.* 2001; Williams *et al.* 2008) (Fig. 12). The core of each β-sheet is composed of six strands with the polarity of (↑↓↑↑↑↑), and the active site consists of multiple conserved His residues in addition to conserved carboxylates. The two manganese ions in the active site are also reminiscent of the Zn^{2+} ions in the β-CASP nucleases. Although the DNA in the co-crystal structure is located outside the active site, structural and mutagenic analyses indicate that one conserved His residue specifically orients DNA substrate for the exonuclease cleavage and the second His residue is involved in either metal-ion binding or catalysis directly (Williams *et al.* 2008).

The similarities in the tertiary structure, active site composition and tight binding of metal ions in addition to the shared exo- and endonuclease activities among Mre11 and the β-CASP family Snm1 and Pso2 may explain why their functions partially overlap (Lam *et al.* 2008).

https://doi.org/10.1017/S0033583510000181 Published online by Cambridge University Press

The high degree of homology between Mre11 and the Ser/Thr phosphatases (Voegtli *et al.* 2000) (Fig. 12*c–f*) raises the possibility that Mre11 may function as a phosphatase in addition to being a nuclease during DSB repair.

6.10 LAGLIDADG homing endonucleases

Homing endonucleases are encoded by introns or inteins and recognize long DNA sequences for specific cleavage (for a comprehensive review, see Stoddard, 2005). They are found in single-cell organisms, fungal and protozoan mitochondria and chroloplasts and cleave dsDNA to enhance the mobility of introns and inteins, to which they belong. LAGLIDADG is one of four families of homing endonucleases, which is named after the conserved sequence motif. Despite the name, the sequence motif has many variations including the last D (Asp) that is critical for coordinating the metal ions (Spiegel *et al.* 2006). The LAGLIDADG motif can occur once per subunit if a homing endonuclease is a homodimer, for example, I-CeuI (Spiegel *et al.* 2006) (Fig. 13*a*). Alternatively, internal sequence duplication allows monomeric LAGLIDADG nucleases to function as a pseudodimer, for example, I-SceI (Duan *et al.* 1997; Moure *et al.* 2008) (Fig. 13*b*). The two active sites of a LAGLIDADG nuclease are fused together. Each contributes a conserved Asp and the two together coordinate three Mg^{2+} ions, which form two pairs. Each Mg^{2+} pair forms the catalytic center to cleave one DNA strand (Stoddard, 2005) (Fig. 13*c*). Yeast mating type switch endonuclease (HO) is also a member of this family (Jin *et al.* 1997).

6.11 RNase II and Rrp44

Bacterial RNase II and its eukaryotic homolog Rrp44 (also called Dis3 and the catalytic subunit of exosome) are 3′ exoribonucleases for ssRNA processing and degradation (Andrade *et al.* 2009; Lykke-Andersen *et al.* 2009). RNase R is a paralog of RNase II capable of degrading dsRNA. The active site of this conserved RNase family is composed of four closely spaced Asp residues situated on the loop (inner end) of an uneven β-hairpin structure (Fig. 14). The β-hairpin structure is reminiscent of the active site of the REases, but the DEK motif of the REase family is located at the outer end of the uneven β hairpin (Fig. 8). The active site of RNase II is invariably embedded near the end of a narrow channel, which may prevent RNA substrate from dissociation and promote processivity (Frazao *et al.* 2006; Lorentzen *et al.* 2008; Zuo *et al.* 2006) (Fig. 14*a*). A divalent metal ion is observed in the active site of RNase II and Rrp44 complexed with a ssRNA substrate (Fig. 14*b*). Its position is close to the leaving group (3′-OH) and thus similar to the metal ion B. RNA cleavage by RNase II is most likely by the two-metal-ion mechanism. The absence of the second metal ion in the crystal structures may be due to the mutations of Asp to Asn, a metal-ion ligand (Frazao *et al.* 2006; Lorentzen *et al.* 2008) (Fig. 14*b*).

6.12 RNase III and Dicer

Bacterial RNase III and eukaryotic Dicer and Drosha are homologous dsRNA endonucleases, and Dicer and Drosha generate guide RNAs in the processes of RNAi (Ji, 2008; MacRae & Doudna, 2007; Nowotny, 2009). These enzymes are either homodimers or pseudodimeric

https://doi.org/10.1017/S0033583510000181 Published online by Cambridge University Press

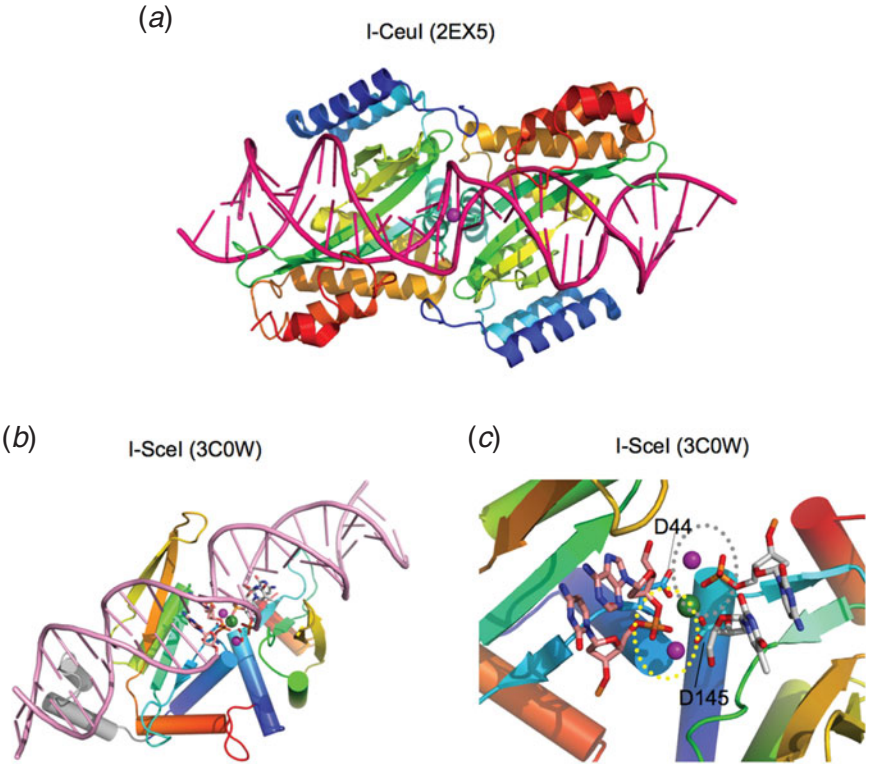


Fig. 13. The LAGLIDADG homing endonucleases. (*a*) The structure of homodimeric I–CeuI in complex with DNA substrate. Each subunit is shown in a rainbow color gradient from blue N- to red C-terminus. The DNA is shown in hot pink ribbon diagrams. The divalent cation bound in the active site is shown as a purple sphere. (*b*) Structure of the monomeric I–SceI with two homologous domains in one polypeptide chain. Each domain is colored in blue to red gradient from N- to C-terminus. The green and purple spheres represent the divalent and monovalent cations, respectively. (*c*) The active site of I–SceI consists of three cations and two overlapping catalytic centers, which are encircled in gray and yellow. The two scissile phosphates and surrounding nucleotides are colored pink (not cleaved) and white (cleaved). The most conserved Asp residues of the LAGLIDA**D**G motif are shown as blue and red sticks.

monomers that have two active sites for dsRNA cleavage. Crystal structures of a bacterial RNase III and eukaryotic dicer have been determined (Gan *et al.* 2006; MacRae & Doudna, 2007). The active sites are situated such that they cleave dsRNA symmetrically and produce a 2-nt 3′ overhang on each cleaved end (Fig. 15*a*, *b*). Each active site is composed of two Asp and Glu pairs located on two closely placed α-helices, one pair of carboxylates a piece (Fig. 15*c*). RNase III has a dsRNA-binding domain C-terminal to the catalytic domain (Fig. 15*a*) to facilitate substrate binding and sequence-non-specific cleavage. Eukaryotic dicers generate dsRNA of defined length, often $\sim$20 bp in length. This is because they contain additional dsRNA and 3′ end binding domains to confer the length and structure specificity (MacRae *et al.* 2006, 2007). Kinetic analysis of RNase III clearly shows that two closely placed metal ions are required for the catalysis of cleavage (Sun *et al.* 2005). The crystal structures of RNase III complexed with dsRNA substrate and product provide atomic details of the binding of two metal ions and a catalytic mechanism similar to that of RNase H (Fig. 15*c*) (Gan *et al.* 2006, 2008).

https://doi.org/10.1017/S0033583510000181 Published online by Cambridge University Press

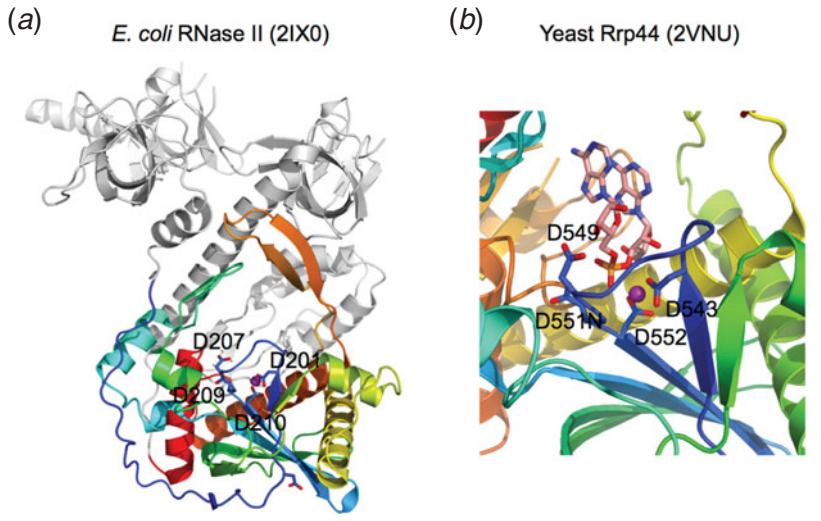


Fig. 14. Bacterial and eukaryotic RNase II. (*a*) *E. coli* RNase II. The catalytic domain is highlighted in rainbow colors and the remaining domains are shown in gray. The active site is marked by four conserved Asp residues and a bound metal ion (purple sphere). (*b*) The active site of Rrp44 in complex with ssRNA. Rrp44 is the yeast homolog of RNase II and is a part of exosome. The four Asp residues are all located on the loop of a β hairpin.

6.13 RNase PH, PNPase and exosome

Bacterial RNase PH is a 3′ phosphorolytic exoribonuclease that carries out RNA processing and degradation (Deutscher & Li, 2001) (Fig. 2*f*). It uses inorganic phosphate as the nucleophile and releases nucleoside-5′-diphosphates as cleavage products. Its functional form is a hexameric ring formed as a trimer of dimers (Fig. 16*a*). Bacterial polynucleotide phosphorylase (PNPase) is a paralog of RNase PH and turns over mRNA and processes tRNA by phosphorolysis. PNPases are ring-shaped homo-trimers. Each subunit containing two RNase PH domains, but only one such domain is catalytically active. Archaeal exosomes are homologous to PNPases and contain six RNase PH-like chains, three Rrp41 and three Rrp42 (Buttner *et al.* 2005; Lorentzen *et al.* 2005). Only Rrp41 subunits have the catalytic activity. Interestingly in eukaryotic exosomes, RNase PH homologues form the hexameric ring-shaped structure as well, but have no catalytic activity for RNA degradation (Dziembowski *et al.* 2007; Liu *et al.* 2006).

A single RNase PH domain is a four-layered $\beta\alpha\beta\alpha$ structure (Fig. 16*b*). The active site, composed of both basic residues and carboxylates, is located at one end of the $\beta\alpha\beta$ sandwich. Two such domains tightly associate to form a dimer and ssRNA substrate is bound at the dimer interface. A Cl^- ion in the co-crystal structure of archaeal exosome–ssRNA complex is suggested to mimic the phosphate for nucleophilic attack (Fig. 16*c*). The locations of two conserved carboxylates resemble many two-metal-ion-dependent nucleases. However, a metal ion is found outside of the active site of the archeal exosome and shown to play a structural role (Lorentzen *et al.* 2007). Although a catalytic metal-ion binding site is not evident in the crystal structures, it was reported that the phosphorolytic activity of RNase PH and PNPase is Mg^{2+} dependent (Deutscher *et al.* 1988; Gorchakova, 1981). Whether and how many Mg^{2+} ions are needed for phosphorolysis by RNase PH and PNPase are yet to be determined.

https://doi.org/10.1017/S0033583510000181 Published online by Cambridge University Press

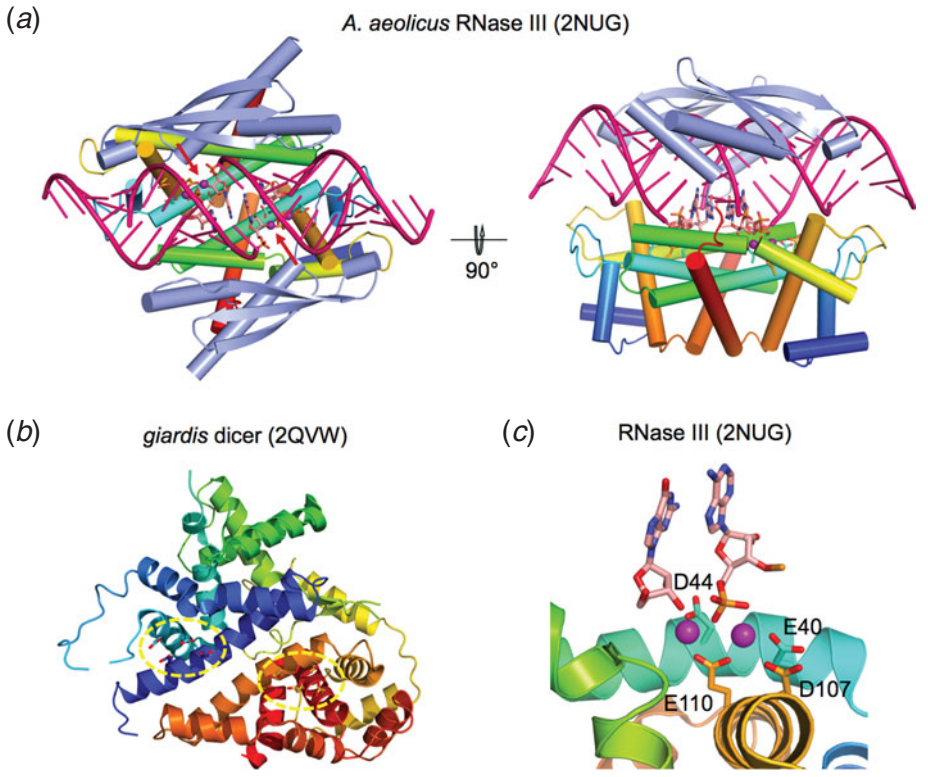


Fig. 15. RNase III and dicers. (*a*) The orthogonal views of a homodimeric RNase III. Each subunit consists of a catalytic domain (rainbow color) and the RNA-binding domain (light blue). The two active sites are marked by the bound divalent cations (purple spheres). The red arrowheads point at the scissile bonds. The catalytic residues and nucleotides flanking the scissile phosphates are shown in sticks. (*b*) A eukaryotic dicer is shown in a similar orientation as in (*a*). It contains two RNase III-like domains. The region of the duplicated catalytic domain is shown in rainbow color from the blue N- to red C-terminus, and the two active sites are encircled in yellow. (*c*) The active site of the bacterial RNase III and the cleaved RNA.

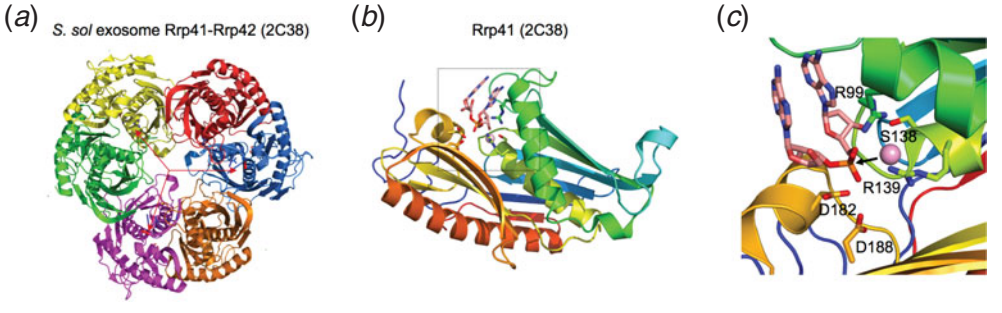


Fig. 16. Archaeal and eukaryotic RNase PH (PNPase). (*a*) The RNase PH core of an archaeal exosome consists of a trimer of Rrp41–Rrp42 heterodimer. The red arrowheads indicate the active sites. (*b*) The catalytically active Rrp41 is shown as rainbow-colored ribbon diagrams. The pink sphere represents the Cl^- observed in the crystal structure. The two 3′ nucleotides of ssRNA and the residues in the active site are shown as sticks. (*c*) A zoom-in view of the catalytic center as boxed in (*b*). The Cl^- mimicking the nucleophile Pi is poised for nucleophilic attack to produce a fresh 3′-OH and NDP.

https://doi.org/10.1017/S0033583510000181 Published online by Cambridge University Press

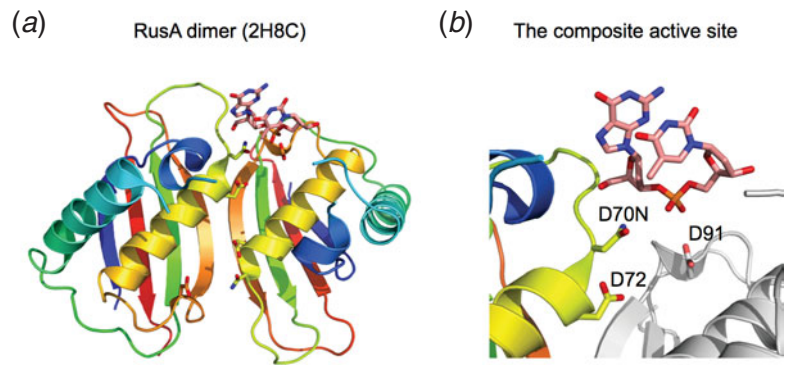


Fig. 17. HJ resolvase RusA. (*a*) An overall view of RusA homodimer. Each subunit is shown in rainbow colors. The active site residues and bound DNA near one active site are depicted in sticks. (*b*) A close-up view of the active site. Each active site consists of residues from both subunits (one in rainbow color and the other in silver). Hence, it is composite. The catalytic side chains and two nucleotides surrounding the scissile phosphate are shown as sticks.

6.14 RusA

RusA is a HJ resolvase encoded by a defective prophage in *E. coli*, and its homologues are found in many bacteria (Sharples *et al.* 1994). RusA is a homodimer in solution and each active site appears to be composite and consists of two Asp from one subunit and a third Asp from the second subunit (Fig. 17) (Macmaster *et al.* 2006). DNA-junction cleavage by RusA is Mg^{2+} dependent (Sharples *et al.* 1994), and the carboxylate-rich active site is suggestive of the two-metal-ion mechanism. The crystal structures of RusA alone and RusA–DNA duplex complex have been determined. However, the required Mg^{2+} has not been located (Macmaster *et al.* 2006; Rafferty *et al.* 2003). One possible reason for the absence of metal ions is that the DNA co-crystallized with RusA is a duplex rather than a four-way junction and hence not a true substrate. The other possible reason is that a RusA mutant D70N was used in DNA co-crystallization and the mutation is likely to reduce Mg^{2+} binding (Fig. 17*b*).

6.15 Ribozymes

To date, two types of ribozymes are confirmed to cleave RNA in a metal-ion-dependent manner. They are self-splicing group I and group II introns (Kruger *et al.* 1982; Peebles *et al.* 1986) and the universal tRNA 5′-processing RNase P (Guerrier-Takada *et al.* 1983; Kirsebom, 2007). These metal-ion-dependent ribozyme nucleases generate 5′-phosphate and 3′-OH cleavage products. In fact, the two-metal-ion mechanism was first proposed to explain how group I and II introns catalyze RNA cleavage (Steitz & Steitz, 1993).

6.15.1 Group I intron

Self-splicing group I introns catalyze two consecutive phosphoryl transfer reactions (Fig. 18*a*) and are the best characterized example of two Mg^{2+}-dependent ribozymes (Stahley & Strobel, 2006). The nucleophile in the first step (cleavage reaction of the 5′ exon–intron juction) is the 3′-OH of a free guanosine (or GMP, GTP), which becomes covalently linked to the 5′-end of

https://doi.org/10.1017/S0033583510000181 Published online by Cambridge University Press

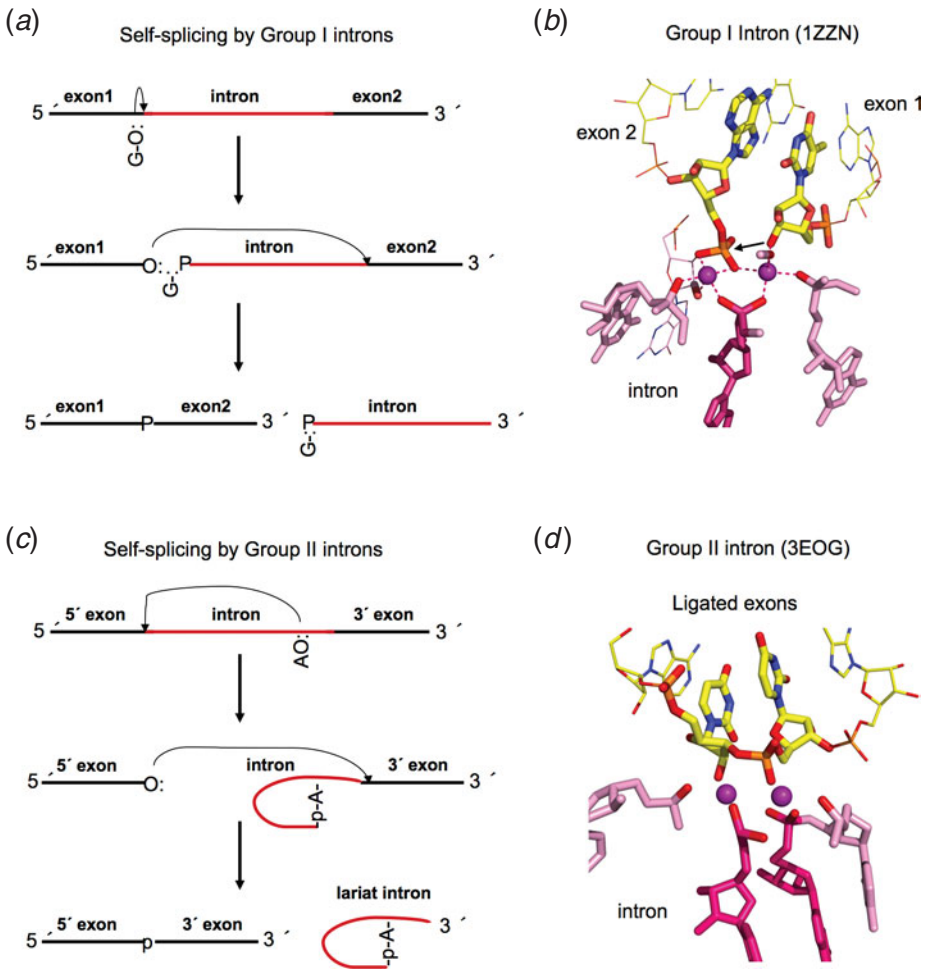


Fig. 18. Self-splicing introns. (*a*) A schematic drawing of phosphoryl transfer reactions catalyzed by group I introns. G–O: represents a free guanosine with its 2′-O serving as the nucleophile. (*b*) The structure of the catalytic center of group I introns. The exons to be ligated are shown in yellow and the nucleotides of the intron involved in catalyses are highlighted in pink and hot pink. Two Mg^{2+} (purple spheres) are jointly coordinated by the scissile phosphate and a backbone phosphate that mimics the side chain of Asp in protein enzymes. (*c*) A schematic drawing of phosphoryl transfer reactions catalyzed by group II introns. A–O: represents an internal adenosine with its 2′-O serving as the nucleophile. (*d*) The structure of the catalytic center of a group II intron in complex with ligated exons as the product of splicing. Two metal ions (purple spheres) again are found in the active site.

the intron. In the second step, the 3′-OH of the cleaved exon (product of the first cleavage reaction) serves as the nucleophile and attacks the 3′ intron–exon junction to produce the ligated exons and a free intron (Vicens & Cech, 2006) (Fig. 18*a*). Cleavage substrates, the intron–exon junctions, are structured and the bases surrounding each scissile phosphate are paired and stacked in a double helix (Fig. 18*b*) (Adams *et al.* 2004). Two divalent cations are coordinated between a non-bridging oxygen (pro-Sp) of the scissile phosphate and a backbone phosphate of the ribozyme, which acts exactly like the most conserved Asp in the active site of many two-metal-ion-dependent protein enzymes (Yang *et al.* 2006). The two metal ions are likely to switch their roles of activating nucleophiles in the consecutive reaction steps, similar to DNA

https://doi.org/10.1017/S0033583510000181 Published online by Cambridge University Press

transposition by retroviral integrase and bacterial transposases (section 6.2.2, Fig. 7*c*) (Nowotny *et al.* 2005; Steitz & Steitz, 1993).

6.15.2 Group II intron

Group II introns also catalyze their own excision and function in retro-transposition in addition (Aizawa *et al.* 2003; Peebles *et al.* 1986). The splicing reaction consists of two steps like group I introns, but group II introns use the 2′-OH of an internal Ade to initiate self-splicing (Doudna & Cech, 2002). The intron is excised in a lariat form of a 2′–5′ cyclic diester bond (Fig. 18*c*), which is similar to mRNA splicing by spliceosomes in eukaryotes (Michel *et al.* 2009). The crystal structure of the product form of a group II intron was recently determined, and two metal ions are found in the catalytic center (Toor *et al.* 2008) (Fig. 18*d*). A two-metal-ion-dependent catalysis mechanism similar to that of group I introns has been postulated for self-splicing group II introns and spliceosomes, in general, for mRNA splicing (Toor *et al.* 2009).

6.15.3 RNase P

RNase P is one of the first ribozymes identified and the universally conserved nuclease that endonucleolytically cleaves pre-tRNA to generate the mature 5′ end (Guerrier-Takada *et al.* 1983). In addition to the catalytic RNA subunit, RNase P also includes a variable number of protein subunits (Kirsebom, 2007). Crystal structures of two types of bacterial RNase P have been determined (Torres-Larios *et al.* 2006). These structures reveal a conserved architecture of the catalytic core. But, in the absence of an RNase P-tRNA ribozyme-substrate complex, details of the active site are uncertain. The catalytic mechanism is likely to be similar to that of group I introns in spite of the uncertainty of which ribonucleotide coordinates the Mg^{2+} ions.

6.16 Three-Zn^{2+}-dependent nucleases

Three metal ions, more specifically three Zn^{2+}, have been found in the active site of two structurally unrelated endonucleases: AP endonuclease IV (Endo IV) and nuclease P1/S1 (Garcin *et al.* 2008; Romier *et al.* 1998). Both result in 5′ phosphate and 3′ hydroxyl cleavage products. Nuclease P1 cleaves ssDNA. Although Endo IV cleaves dsDNA endonucleolytically or as a 3′ exonuclease (Demple & Harrison, 1994), the nucleotide carrying the scissile phosphate (apurine or apyrimidine) is not base-paired and thereby effectively single-stranded with large backbone distortions. The crystal structures of Endo IV complexed with DNA substrate and product reveal that one Zn^{2+} is located in the minor groove of the unpaired scissile phosphate and two remaining Zn^{2+} are coordinated similarly to the two metal ions in RNase H1 and DnaQ (Figs 6, 7 and 19) (Garcin *et al.* 2008). Therefore, two out of the three metal ions are likely to be involved in catalysis. This is reminiscent of the case of three metal ions in alkaline phosphatase with two participating in actual catalysis and the third for alignment of the nucleophile relative to the scissile phosphate (Coleman, 1992; Kim & Wyckoff, 1991; Stec *et al.* 2000; Steitz & Steitz, 1993; Zalatan *et al.* 2008).

6.16.1 *E. coli* Endo IV (AP endonuclease)

Endo IV is the class II and minor AP endonuclease in *E. coli* (second to Exo III, see section 6.7.2) and is known for its EDTA-resistant activity (Demple & Harrison, 1994). Its yeast homologue is

https://doi.org/10.1017/S0033583510000181 Published online by Cambridge University Press

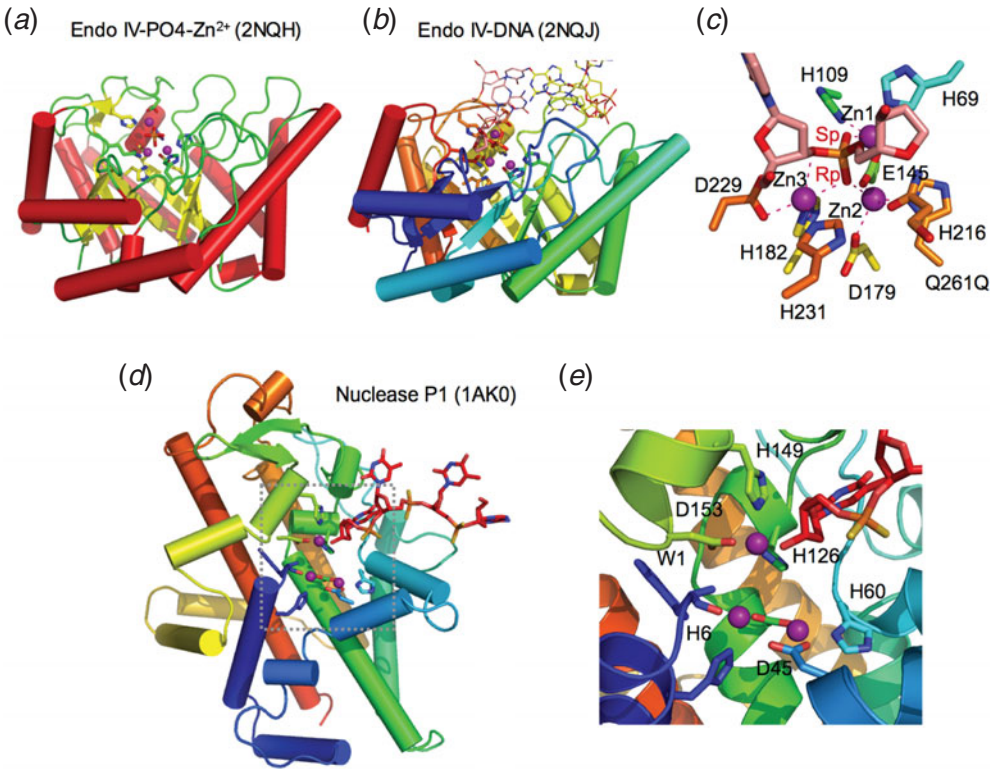


Fig. 19. Nucleases using the three-metal-ion mechanism. (*a*) The structure of AP endonuclease IV (Endo IV) has a TIM barrel fold. The ribbon diagram of Endo IV is colored according to the secondary structures: red α-helices, yellow β-strands and green loops. A bound phosphate ion is shown as sticks and three Zn^{2+} ions are shown as purple spheres. (*b*) The structure of the Endo IV–DNA complex. The protein is shown in rainbow colors from blue N- to red C-terminus. DNA substrate is shown as sticks. The cleavage strand is shown in pink and the other strand in yellow. (*c*) A close-up view of the active site. The scissile phosphate is turned so that both pro-Rp and pro-Sp oxygen atoms are coordinated by metal ions. (*d*) Nuclease P1 consists of mostly α-helices and a β-hairpin. The structure represents an enzyme–ssDNA product complex. (*e*) A close-up view of the nuclease P1 active site as boxed in (*d*). In spite of the unrelated structures, the three Zn^{2+} ions and the coordination ligands are reminiscent of Endo IV.

known as Apn1. Endo IV has the TIM-barrel fold, and the active site is located at one end of the β barrel, where the three Zn^{2+} ions bind (Fig. 19*a*). The crystal structures of the enzyme complexed with substrate and product were also determined at high resolutions (Garcin *et al.* 2008) (Fig. 19*b*). Two out of three metal ions, Zn2 and Zn3, are reminiscent of the metal ions A and B, respectively, in the two-metal-ion mechanism (Fig. 19*c*). However, instead of the pro-Sp nonbridging oxygen of the scissile phosphate jointly coordinating these two metal ions, the scissile phosphate in the Endo IV complex turns toward the minor groove and the pro-Rp oxygen coordinates Zn2 and Zn3. This is very similar to the cases of DNase I and APE1 (Fig. 11*c*, *d*). In Endo IV, Zn1 (instead of a His as in APE1 and DNase I) stabilizes the pro-Sp oxygen and facilitates the distortion of the scissile phosphate (Fig. 19*c*).

In Endo IV, the Zn3 metal ion is coordinated by both the pro-Rp and the 3′ leaving oxygens just like the B site ion in the two-metal-ion mechanism (Fig. 5*a* and *c*). Mutational studies also confirm that coordination of Zn3 is more sensitive to amino acid substitution than the other

https://doi.org/10.1017/S0033583510000181 Published online by Cambridge University Press

two-metal-ion-binding sites and that the Zn3 metal ion plays a more important role in catalysis (Garcin *et al.* 2008). Moreover, for Endo IV to be active, the Zn3 site also has a strong preference for Mn^{2+} over Zn^{2+} (Demple & Harrison, 1994; Garcin *et al.* 2008). Supporting the crystallographic observation, sulfur replacement of the pro-Sp oxygens at the scissile phosphate reduces the Endo IV cleavage activity, but sulfur substitution of the pro-Rp oxygen eliminates the nuclease activity (Takeuchi *et al.* 1994). Five His and four carboxylates contribute to tight binding of the three metal ions (Fig. 19*c*), which may explain why Endo IV is EDTA resistant. E261, which coordinates the Zn2 ion (equivalent to metal ion A), is suggested to be essential for nucleophile activation and cleavage (Garcin *et al.* 2008).

6.16.2 Nuclease P1 and S1

Nuclease P1 and S1 are single-strand-specific nucleases that degrade DNA or RNA either endonucleolytically or as a 3′ exonuclease (Desai & Shankar, 2003). P1 nuclease is all α-helical and resembles bacterial phospholipase C (Hough *et al.* 1989; Romier *et al.* 1998) (Fig. 19*d*). Although P1 nuclease and Endo IV are unrelated in amino acid sequence or tertiary structure, they both use carboxylates and histidines to tightly bind three Zn^{2+} ions even in the absence of substrate (Fig. 19). In P1 nuclease, two Zn^{2+} ions are jointly coordinated by two conserved Asp (Fig. 19*e*). Similar to Endo IV, the pro-Rp rather than the pro-Sp non-bridging oxygen of the scissile phosphate is intolerant of thio-replacement (Romier *et al.* 1998). Although a P1-substrate complex structure is not available, the sulfur replacement experiment is in agreement with the metal ion coordination observed in Endo IV. It is likely that the pro-Rp oxygen of the scissile phosphate together with the two conserved Asp residues coordinates the two catalytic metal ions.

6.17 Nucleases that may use two metal ions for catalysis

6.17.1 Staphylococcal nuclease

Staphylococcal nuclease (SNase) is a Ca^{2+} dependent extracellular phosphodiesterase that cleaves ssRNA and ssDNA to 3′-phospho mono- and di-nucleotides (Tucker *et al.* 1978). The enzyme contains two antiparallel β-sheets and three α-helices (Fig. 20*a*). The active site is composed of four carboxylates at the end of the large β-sheet. High-resolution crystal structures of its complex with nucleotide analog/inhibitor pdTp and metal ions Ca^{2+} or Co^{2+} (inhibitor) reveal a single but mobile metal ion (Loll *et al.* 1995). Because of the lack of a confirmed general base, the metal ion is postulated to deprotonate and to activate the nucleophilic water (Hale *et al.* 1993; Loll *et al.* 1995). In the absence of an enzyme–substrate complex, the catalytic mechanism remains undefined. It is possible that SNase uses a single metal ion as observed in the crystal structure, or the two-metal-ion mechanism given the carboxylate-rich active site, or even three metal ions similar to Endo IV and DNase P1/S1 because SNase prefers ssDNA and ssRNA. Since the cleavage product of SNase is 3′-phosphate, which is radically different from all the confirmed two-metal-ion-dependent nucleases, it is likely that it has a different catalytic mechanism.

6.17.2 MutL

MutL is an essential enzyme for DNA mismatch repair in bacteria and eukaryotes, and inactivation of MutL in humans leads to dramatically increased susceptibility to hereditary colon

https://doi.org/10.1017/S0033583510000181 Published online by Cambridge University Press

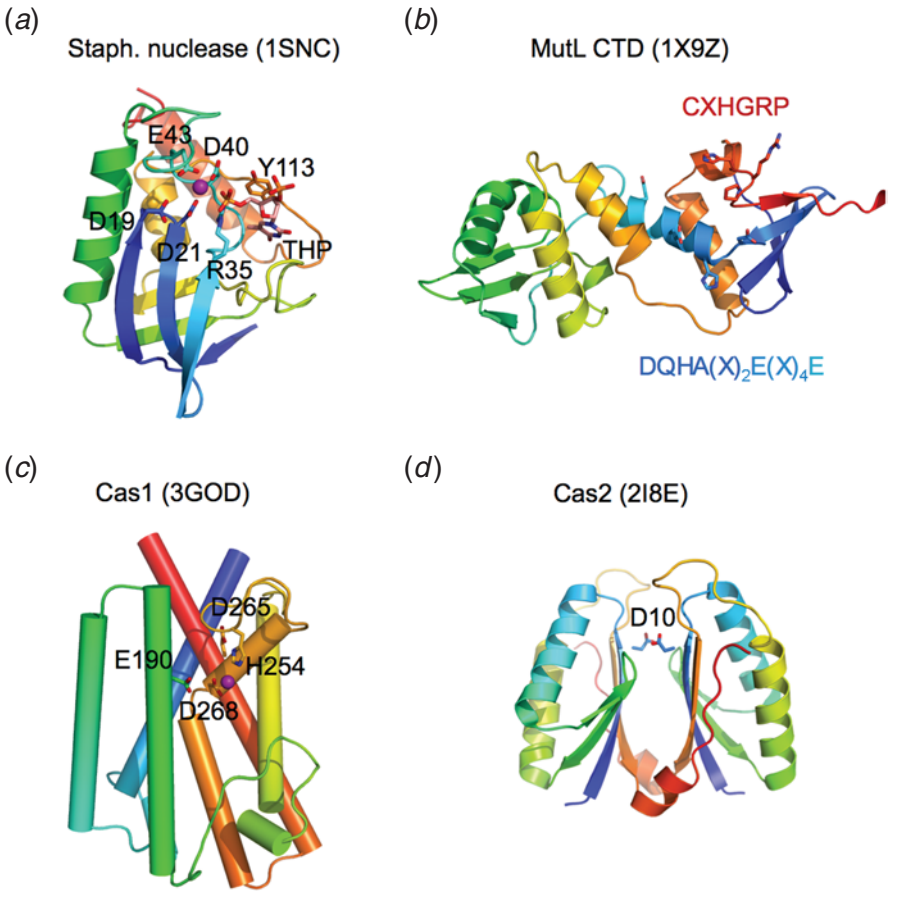


Fig. 20. Nucleases that may use the two-metal-ion mechanism. (*a*) Staphylococcal nuclease (SNase) is shown in a rainbow-colored ribbon diagram. Thymidine diphosphate (pdTp, THP) co-crystallized and the catalytic residues are shown as sticks. A Ca^{2+} ion captured in the structure is shown as a purple sphere. (*b*) The MutL endonuclease activity resides in its C-terminal domain (CTD). The crystal structure of *E. coli* MutL CTD (known as LC20) is shown in a rainbow-colored ribbon diagram. Conserved sequence motifs for the metal-ion-binding site are indicated in matching colors of the ribbon diagram and modeled onto the *E. coli* structure. The potential metal ion ligands are shown as sticks. (*c*) Cas1 is a CRISPR nuclease. One catalytic domain is shown in rainbow-colored ribbon diagrams with helices shown as rods. The active site is composed of three carboxylates and one His. A bound Mn^{2+} is shown as a purple sphere. The dimerization domain is not shown here. (*d*) The structure of Cas2. Cas2 is a CRISPR RNase with the ferredoxin fold. Both subunits of the homodimer Cas2 are shown in rainbow color from the blue N- to the red C-terminus. The active site is located at the dimer interface with the conserved and catalytically essential Asp shown as sticks and labeled.

cancers (Li, 2008). All MutL homologues contain a highly conserved N-terminal ATPase domain (Ban & Yang, 1998a). Four years ago, it was discovered that some MutL homologues also contain metal-ion-dependent weak endonuclease activity in the C-terminal dimerization domain (Kadyrov *et al.*, 2006, 2007). A conserved metal-binding site in the C-terminal domain, which is essential for the MutL endonuclease activity (Duppatla *et al.*, 2009), is modeled based on the crystal structure of *E. coli* MutL (Guarne *et al.*, 2004; Kosinski *et al.*, 2008; Yang, 2007) (Fig. 20*b*). Mutations of the metal ion-coodinating residues lead to the loss of the MutL endonuclease activity *in vitro* and mismatch repair capacity *in vivo* (Fukui *et al.*, 2008).

https://doi.org/10.1017/S0033583510000181 Published online by Cambridge University Press

6.17.3 Cas1

CRISPR (clustered regularly interspaced short palindromic repeats) is a bacterial and archaeal adaptive immune system to resist phage infection (Sorek *et al.* 2008). Phage DNA is cleaved to short oligonucleotides and incorporated into host CRISPR between repetitive DNA sequences and the transcription products are used for target degradation if the same phage infection is encountered again. Cas1 and Cas2 are CRISPR-associated proteins essential for CRISPR (Brouns *et al.* 2008). Cas1 is the universally conserved protein in CRISPRs and is a dimeric metal-dependent DNA endonuclease. The crystal structure reveals a novel fold and a bound Mn^{2+} in the absence of DNA substrate (Wiedenheft *et al.* 2009). The structure contains a helical catalytic domain (Fig. 20*b*) and an $\alpha\beta$ dimerization domain. The helical structure of the Cas1 catalytic domain is reminiscent of DNase P1/S1. With the active site composed of EHDD residues and at least one conserved Asp indispensable for the nuclease activity (Wiedenheft *et al.* 2009), it is possible that DNA cleavage by Cas1 is by the two-metal-ion mechanism.

6.17.4 Cas2

Cas2 is ferredoxin-like and metal-dependent single-strand endoribonuclease (Beloglazova *et al.* 2008). It is dimeric, prefers U-rich regions and produces 3′ -OH and 5′-phosphate oligonucleotides. Given its metal-ion dependence and requirement for a conserved Asp residue, a two-metal-ion-dependent catalysis mechanism has been proposed. Interestingly, in the crystal structure of Cas2 protein, the catalytically essential Asp (D10) is situated at the dimeric interface and two symmetry-related Asp residues are 6·5 Å apart (Beloglazova *et al.* 2008). These two Asp side chains may belong to a single active site (Fig. 20*c*).

7. One-metal-ion-dependent nuclease superfamilies

The one-metal-ion mechanism can be viewed as a variation on the two-metal-ion theme as the location and function of the single metal ion is equivalent to the B-site metal ion in the two-metal-ion mechanism (Yang, 2008) (Fig. 5*b*). The role of this single metal ion appears to be destabilizing the scissile phosphodiester bond and neutralizing the highly negatively charged transition state. A large variety of endonucleases belonging to the $\beta\beta\alpha$-Me and HUH superfamilies (see detailed description below) have been unequivocally shown to cleave DNA or RNA using the one-metal-ion mechanism. The A metal ion in the two-metal-ion mechanism appears to be replaced by positively charged protein side chains. Dependence on the metal ion to activate the nucleophile is alleviated by using His as the general base, or using Tyr as a nucleophile, which is more readily deprotonated than a water molecule at the neutral pH. All nucleases using the one-metal-ion mechanism generate 5′ phosphate and 3′ OH products.

7.1 The $\beta\beta\alpha$-Me superfamily

All nucleases in this superfamily share the conserved structural motif, a β hairpin followed by an α-helix (Fig. 21*a*). Within the consecutive $\beta\beta\alpha$ structures, an invariable His at the end of the first β-strand serves as the general base to deprotonate and activate the nucleophilic water molecule (Fig. 21). Additional conserved His (H) and Asn (N) in the active site are most often involved in coordinating the single metal ion (Me). Nucleases in the $\beta\beta\alpha$-Me family

https://doi.org/10.1017/S0033583510000181 Published online by Cambridge University Press

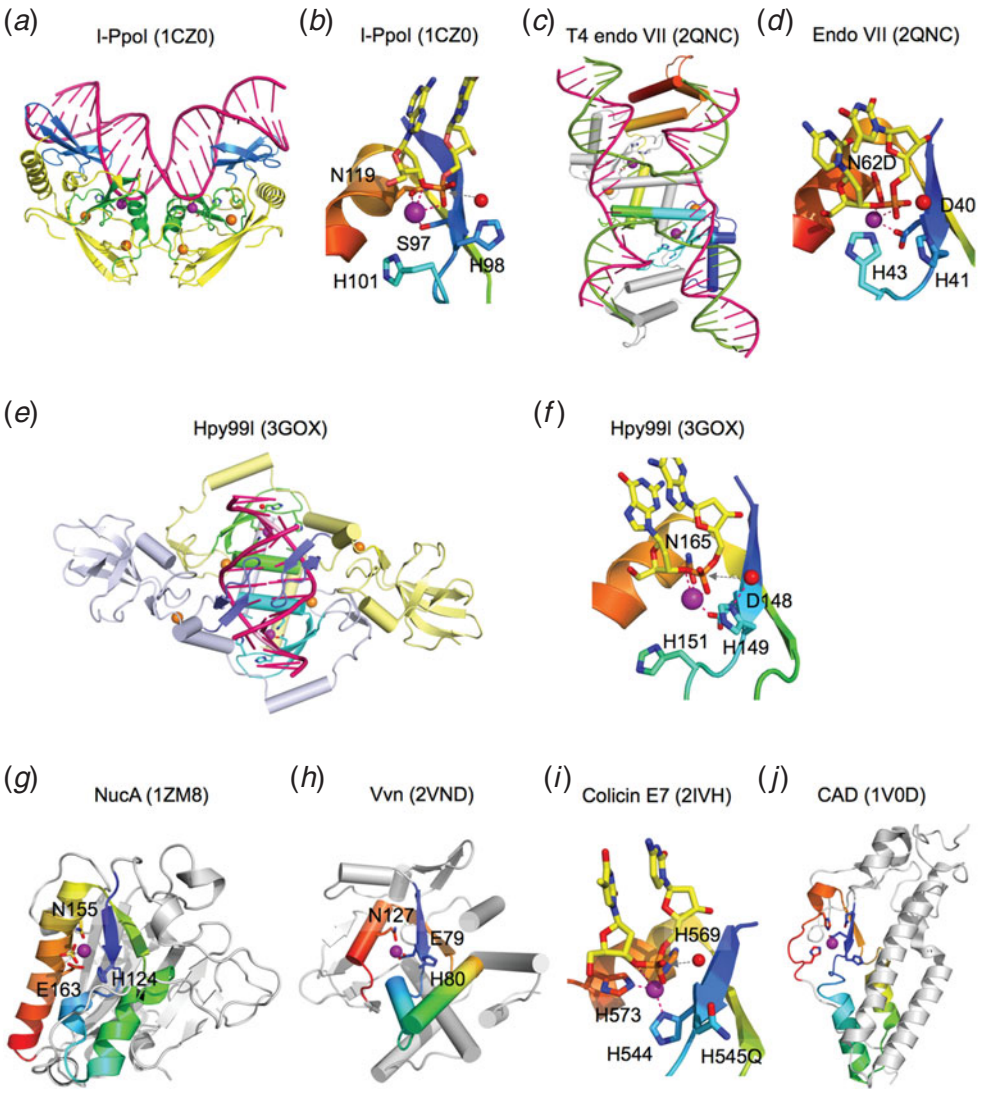


Fig. 21. The $\beta\beta\alpha$-Me nucleases. (*a*) The overall structure of homing endonuclease I–PpoI. It is homodimeric and the identical protein subunits are shown in the same color schemes. The catalytic domain is shown in green, the DNA recognition domain in blue and the connection region in yellow. The cations in the active sites are shown as purple spheres and structurally important Zn^{2+} ions are shown as orange spheres. DNA is shown in hot pink. (*b*) A close-up of the active site. The $\beta\beta\alpha$ structural motif is shown in rainbow colors. The scissile phosphate and surrounding nucleotides are shown as yellow sticks. A Na^{+} mimicking the catalytic divalent cation in this structure is shown in purple. The catalytic residues are shown in sticks and labeled. The potential nucleophilic water is shown as a red sphere. (*c*) T4 endonuclease VII (Endo VII) resolves HJ. One of the two subunits is shown in rainbow color (from blue N- to red C-terminus) and the other in silver. The lime-green DNA strands are to be cleaved. The Mg^{2+} ions in the active site are shown as purple spheres and structural Zn^{2+} ions as orange spheres. One $\beta\beta\alpha$ motif in this panel is colored cyan. (*d*) A close-up view of the active site of Endo VII. The presentation scheme is same as in (*b*). (*e*) The structure of restriction endonuclease Hpy99I in complex with DNA substrate. The two subunits of Hpy99I are shown as pale blue and yellow ribbon diagrams. The DNA-binding modules of both subunits are highlighted in blue and the two $\beta\beta\alpha$-Me motifs in green and cyan. The catalytically essential Mg^{2+} ions are substituted by Na^{+} ions and shown as purple spheres. Zn^{2+} ions (orange spheres) play a

https://doi.org/10.1017/S0033583510000181 Published online by Cambridge University Press

have very diverse functions. The HNH and His-Cys homing endonucleases, DNases involved in cell death, many non-sequence and non-sugar-specific nucleases, colicin E nucleases, certain restriction endonucleases, and a HJ resolvase, all belong to this superfamily (Hsia *et al.* 2005; Stoddard, 2005). Not surprisingly, the overall structures and DNA-binding modes are as varied as the functions. A number of nucleases have large helical insertions between the β and β elements. Nevertheless, the catalytic core structure and the metal-ion-binding sites are superimposable.

7.1.1 HNH and His-Cys homing endonucleases

Although HNH and His-Cys were initially classified into two separate families of homing endonucleases based on conserved sequence motifs, close scrutiny of amino acid sequences has led to the proposal that they derived from a common ancestor and share the same $\beta\beta\alpha$-Me catalytic core (Friedhoff *et al.* 1999; Kuhlmann *et al.* 1999). The HNH motif is involved in the catalytic metal coordination, whereas the His-Cys motif coordinates additional metal ions to stabilize the tertiary structure (Fig. 21 *a*) (Stoddard, 2005). The catalytic metal ion can be Mg^{2+}, Zn^{2+}, Ca^{2+} or other divalent cations, which are often coordinated by His, Asn and Asp (Fig. 21 *b*). Most noticeably, the $\beta\beta\alpha$-Me motif is nearly a stand-alone domain and separate from the DNA sequence-specific binding domains (Fig. 21 *a*). In the His-Cys homing endonuclease I-PpoI, two structural metal ions (Zn) tie the DNA-binding and $\beta\beta\alpha$-Me catalytic domains together in each subunit (Flick *et al.* 1998).

7.1.2 HJ resolvase: phage T4 endonuclease VII

T4 endo VII is the only HJ resolvase that contains the $\beta\beta\alpha$-Me motif for catalysis. It forms a homodimer and recognizes an H-shaped four-way junction (Biertümpfel *et al.* 2007) (Fig. 21 *c* and *d*). The two strands that make a U-turn (aka exchanged strands) in the four-way junction are cleaved. Mg^{2+} is the preferred metal ion for DNA cleavage. Like His-Cys homing endonuclease, a Zn^{2+} is also tightly bound by each T4 endo VII subunit and stabilizes the tertiary structure. Relative to T7 endonuclease I, which has the REase-type active site and uses the two-metal-ion mechanism, T4 endo VII is not as specific for four-way junctions and can cleave 3-way junctions and mismatched DNA heteroduplexes, all of which are characterized by distorted double-helix structures (Jensch & Kemper, 1986; Solaro *et al.* 1993).

7.1.3 Type-II restriction endonucleases

Several type-II restriction endonucleases also contain the $\beta\beta\alpha$-Me motif for DNA cleavage. They include HphI (Cymerman *et al.* 2006), Eco311 (Jakubauskas *et al.* 2007), KpnI (Chatterjee

structural role. DNA is colored pink and the scissile phosphates are indicated in light pink. (*f*) The active site of Hpy99I. (*g*, *h*) The overall structures of NucA/EndoG and Vvn. The $\beta\beta\alpha$-Me motif in each structure is highlighted in rainbow colors and the metal ion shown as a purple sphere. The remaining protein structures are shown in silver grey. (*i*) The active site ($\beta\beta\alpha$-Me motif) of colicin E7 in complex with DNA substrate. The catalytic Zn^{2+} is coordinated by three His side chains and two oxygens of the scissile phosphate. The general base H545 is mutated to Q to stop the cleavage reaction. (*j*) The catalytic domain of CAD. The $\beta\beta\alpha$-Me motif is highlighted as in (*f*, *g*).

https://doi.org/10.1017/S0033583510000181 Published online by Cambridge University Press

et al. 1991; Vasu *et al.* 2008) and Hpy99I (Sokolowska *et al.* 2009). The active site of these sequence-specific endonucleases contains the conserved DH and N residues just like T4 endo VII (Fig. 21*d* and *e*). Additional DNA-binding domains in these restriction enzymes target cleavage to a specific sequence. The crystal structure of Hpy99I complexed with its cognate DNA substrate reveals an interlocked homodimer, which bears remarkable similarity to T4 endo VII (Fig. 21*c* and *e*). In addition to the catalytic motifs approaching the cognate DNA from the minor groove side, Hpy99I embraces the DNA with sequence-specific binding in the major groove. Different from I-PpoI (Fig. 21*a*), the catalytic motifs, DNA-binding modules and the dimeric interface in Hpy99I are rolled into one. Concommitantly, the recognition sequence of Hpy99I is much shorter (5 bp) than I-PpoI (14 bp) and the cleavage sites border the major-groove recognition rather than being at a distance as with I-PpoI (Fig. 21*a* and *e*).

7.1.4 Sugar-non-specific endonucleases

Sugar-non-specific nucleases degrade ssDNA and ssRNA or dsDNA and dsRNA in a sequence-independent manner (Friedhoff *et al.* 1996). Members of this family have very diverse functions and can take part in bacterial defense, invasion, nutrient scavenging and eukaryotic programmed cell death. Periplasmic Vvn (Hsia *et al.* 2005) defends host cells by degrading foreign nucleic acids. The secreted serratia and cyanobacterium NucA (Muro-Pastor *et al.* 1992) nucleases may be regulated depending on growth phases (Chen *et al.* 1992). The other secreted nucleases, colicins E7 and E9 (Hsia *et al.* 2005), kill non-self-target cells and thereby enhance the chance of host cell survival under stress. Eukaryotic mitochondrial endonuclease G also belongs to this family and is a key enzyme in cell death (Buttner *et al.* 2007). These non-specific nucleases are very efficient and non-discriminative in nucleic acid degradation. Host cells often have specific inhibitors, known as immunity proteins, to avoid self-destruction.

7.1.4.1 Serratia, NucA and Endo G

The Serratia family of nucleases includes bacteria nucleases (NucA) and eukaryotic mitochondrial endonuclease G (Endo G), which is also known as Nuc1p in yeast. The nuclease from *Serratia marcescens* encoded by the nucA gene is the first example described in the family (Benedik & Strych, 1998). Its possible role is scavenging for nutrients. Other bacterial NucA may act as virulence factors in invasion or establishment of a colony. Bacterial hosts, which secrete the nuclease, often have an inhibitor to protect themselves. In eukaryotes, mitochondrial Endo G may play a role in mitochondrial DNA metabolism. Endo G, however, can migrate to the nucleus and function in Caspase-independent cell death (Buttner *et al.* 2007).

These nucleases are structurally very similar. The catalytic $\beta\beta\alpha$ motif forms a structural subdomain and is packed against one face of a six-stranded antiparallel β-sheet (Fig. 21*g*). The active site is marked by a conserved sequence motif RG immediately preceding the general base H in the first β-strand of the $\beta\beta\alpha$ motif (Ghosh *et al.* 2007b). They usually prefer Mg^{2+} for catalysis, and the metal ion is coordinated by the conserved N and E on the α-helix. The catalytic metal ion may be directly chelated by an immunity protein and prevented from substrate binding (Ghosh *et al.* 2007b).

7.1.4.2 Vvn and periplasmic nucleases

Vvn (from *Vibrio vulnificus*) represents the bacterial periplasmic endonuclease I family and is likely to serve a defensive role against uptake of foreign DNA (Wu *et al.* 2001). Its tertiary structure is

https://doi.org/10.1017/S0033583510000181 Published online by Cambridge University Press

unique and has long helical insertions between the β-strand of the $\beta\beta$a-Me motif, but the active site is conserved (Hsia *et al.* 2005) (Fig. 21*h*). Homologous proteins are found in bacteria only, which include endonuclease I from *Vibrio cholerae* and *Vibrio Salmonicida* (Altermark *et al.* 2006; Niiranen *et al.* 2008). The residues for Mg^{2+} coordination are (W)EH and N(GDRG)N within the $\beta\beta\alpha$-Me motif.

7.1.4.3 Colicins E7 and E9

Colicins are toxins produced by *E. coli* and other enterobacteriaceae to kill unprotected competitive organisms as part of the SOS response. Colicins E2, E7, E8 and E9 are E-group toxins containing the $\beta\beta\alpha$-Me motif, which kills by the highly efficient and non-specific DNase activity (James *et al.* 1996). *E. coli* and host cells protect themselves using immunity proteins, which bind and inhibit the DNase (Kolade *et al.* 2002). The crystal structures of colicins E7 and E9 in complex with DNA substrate and their respective immunity protein have been determined (Kleanthous *et al.* 1999; Ko *et al.* 1999; Mate & Kleanthous, 2004; Wang *et al.* 2007). The active site of Colicins E7 and E9 consists of four conserved His. Three appear to coordinate a single metal ion, for which Mg^{2+} and Zn^{2+} are preferred (Mate & Kleanthous, 2004; Wang *et al.* 2007). The remaining His (the second in sequence and also most conserved) functions as the general base to deprotonate and activate the nucleophile water (Wang *et al.* 2007) (H545Q in Fig. 21*i*).

7.1.4.4 Cell death and caspase-activated DNase (CAD)

Caspase-activated DNase (CAD), also known as DFF40 (DNA fragmentation factor 40 kDa), is responsible for degradation of genomic DNA in apoptosis when its specific inhibitor ICAD (or DFF45) is removed (Enari *et al.* 1998; Liu *et al.* 1997; Widlak & Garrard, 2005). The crystal structure of the CAD reveals a Zn^{2+}-dependent dimer shaped like a pair of scissors (Woo *et al.* 2004) (Fig. 21*j*). The active site consists of the $\beta\beta\alpha$-Me motif and is very similar to the nuclease domain of colicin E7 and E9. CAD requires Mg^{2+} for the DNase activity (Widlak, 2000). The putative Mg^{2+} in the active site is coordinated by two His and one Asp (Fig. 21*i*).

7.2 GIY-YIG endonucleases

GIY-YIG endonucleases are named after their conserved sequence motifs first found among homing endonucleases (Paquin *et al.* 1995; Van Roey *et al.* 2002). The family also includes the DNA repair endonuclease UvrC (the N-terminal domain), phage T4 EndoII and type-II restriction endonucleases (Kaminska *et al.* 2008; Lagerback *et al.* 2009; Orlowski & Bujnicki, 2008; Truglio *et al.* 2005). Recognition of a specific sequence or DNA lesion is usually accomplished by DNA-binding modules outside of the nuclease core (Stoddard, 2005). To date no nuclease-substrate complex structure has been determined for the GIY-YIG nucleases. The structures of the conserved GIY-YIG catalytic core of a homing endonuclease I-TevI and UvrC have been reported (Truglio *et al.* 2005; Van Roey *et al.* 2002). The catalytic core consists of a three-stranded antiparallel β-sheet, which is surrounded by helices on either side (Fig. 22*a*). The active site is marked by two Tyr residues of the GIY-YIG motif. The GIY-YIG motif is located on a β-hairpin structure, which is followed by an α-helix (Fig. 22*b*). Thus, the structure of GIY-YIG motif is reminiscent of the $\beta\beta\alpha$ module. However, the active site includes residues (Arg, His or Tyr, Glu and Asn) outside of the GIY-YIG motif (Fig. 22*a* and *c*). A divalent metal ion is found

https://doi.org/10.1017/S0033583510000181 Published online by Cambridge University Press

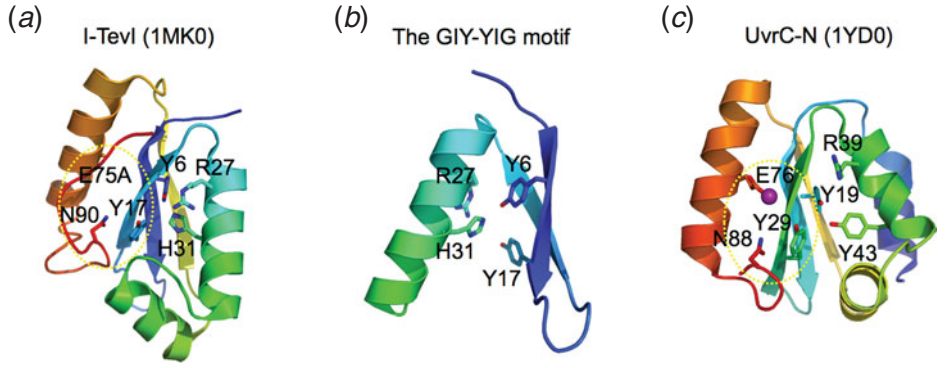


Fig. 22. GIY-YIG nucleases. (*a*) I-TevI homing endonuclease. The catalytic domain is shown in a rainbow-colored ribbon diagram. (*b*) A close-up view of the GIY-YIG motif, which forms a β-hairpin. The conserved Tyr are labeled. With the following α-helix, the structure resembles the $\beta\beta\alpha$-Me motif, but the GIY-YIG motif does not bind metal ion. (*c*) The N-terminal domain of UvrC has the GIY-YIG motif. A divalent cation is coordinated by E76 and probably marks the active site. The catalytic residues Y (of YIG), E and N near the C-terminus are conserved in both and are encircled in yellow.

in the UvrC-N structure and is bound to the conserved Glu (Fig. 22*c*). The catalysis is metal ion dependent and is likely by the one-metal-ion mechanism.

7.3 The HUH superfamily

HUH, which stands for His, hydrophobic residue and His, is the motif shared among endonucleolytic DNases involved in rolling-circle replication. The initiation of rolling-circle replication (RCR) of circular DNA requires a free 3′-OH generated by an endonuclease. HUH endonucleases were initially divided into two families, 'rep' indicating the association with DNA replication and 'mob' indicating the association with DNA mobility via conjugation or transposition (Koonin & Ilyina, 1993). Recently, the HUH motif has been found in ssDNA transposases of the ISHp608 family (Ton-Hoang *et al.* 2005). The two conserved His residues are involved in the metal ion (most often Mg^{2+}) binding. All HUH endonucleases use a Tyr as the nucleophile to catalyze the DNA cleavage and ligation reactions via a 5′-phosphotyrosyl covalent intermediate. DNA cleavage by these nucleases is necessarily rejoined and the phosphotyrosyl bond reverts to a phosphodiester bond after DNA replication or rearrangement. This process of cleavage–religation is similar to the process of topoisomerization and site-specific recombination.

7.3.1 Rep nucleases

Members of the rep family are found in ssDNA and dsDNA bacterial phages, plasmids, plant geminiviruses and animal parvoviruses, such as Adeno-associated virus (Aav) (Hickman *et al.* 2002). By forming 5′-phosphotyrosyl linkage, these nucleases generate a free 3′-OH to initiate DNA synthesis. In addition to the HUH motif for metal-ion coordination, this superfamily also contains the YxxxY motif with two conserved Tyr residues. The crystal structure of Aav5 Rep reveals a nuclease core consisting of a five-stranded antiparallel β-sheet and a number of surrounding α-helices (Hickman *et al.* 2004) (Fig. 23*a*). Most catalytic residues including HUH are located on a pair of adjacent central β-strands, and the nucleophile Tyr is on a nearby α-helix (Fig. 23*a*). As predicted, an Mg^{2+} is coordinated by the two absolutely conserved

https://doi.org/10.1017/S0033583510000181 Published online by Cambridge University Press

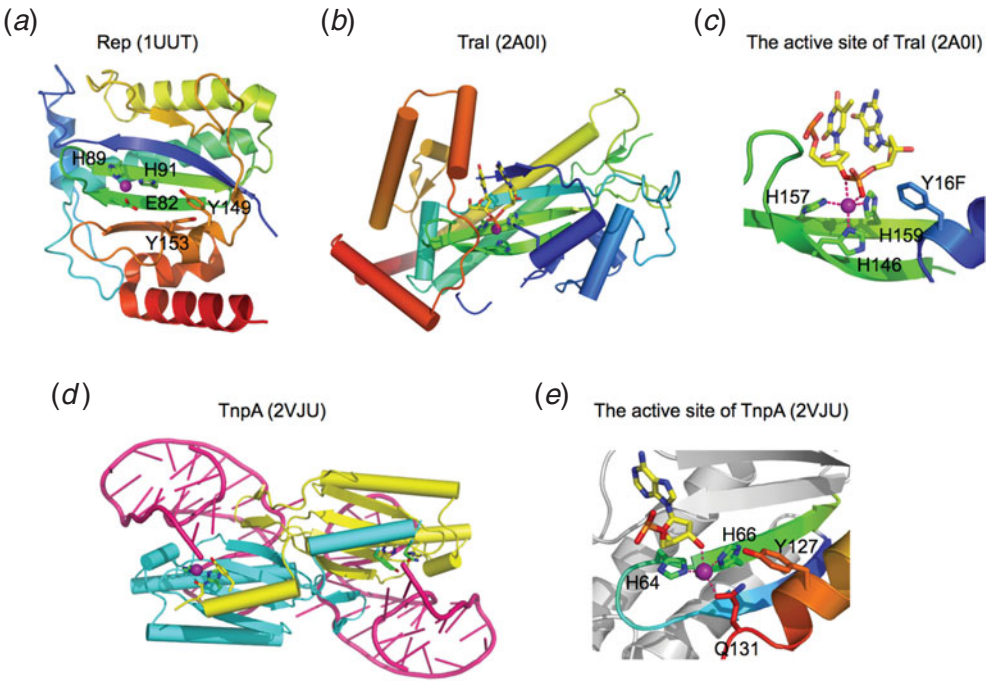


Fig. 23. The HuH nucleases. (*a*) The nuclease domain of Adeno-associated virus 5 (Aav5) Rep shown in rainbow-colored ribbon diagrams. The associated metal ion is shown in purple. (*b*) The structure of TraI relaxase (Y16F mutant) representing the mob family. Only two nucleotides surrounding the scissile phosphate of the ssDNA substrate are shown as sticks. (*c*) A close-up view of the TraI active site. Three His side chains coordinate the Mg^{2+}, which in turn aligns the scissile phosphate for nucleophilic attach by Y16. (*d*) Ribbon diagrams of the DNA transposase (TnpA) of IS608 complexed with a 3′-end cleavage product. TnpA is homodimeric. The two domain-swapped protein subunits are shown in yellow and cyan and the two DNAs in hot pink. (*e*) A close-up view of the composite TnpA active site. The last nucleotide at the 3′ end is also shown. The metal-chelating His residues (of the HUH motif) are from one subunit. The third metal ligand (Q131) and the nucleophile Y127 are from the other subunit.

His and a conserved Glu (Fig. 23*a*). The catalytic mechanism has not been verified by a crystal structure of enzyme-substrate complexes, but the nuclease alone structure resembles that of mob nucleases (see below) and hence the catalysis is likely by the one-metal-ion mechanism.

7.3.2 Mob nucleases (TraI and TrwC)

Mobility of bacterial integrative conjugative elements (ICEs, including conjugative F plasmids and integrative transposons) and ssDNA phage (φx174) depends on DNA nicking by mob nucleases, which are also known as relaxases (Khan, 2005; Llosa *et al.* 2002). Even though some mob nucleases recognize ssDNA and make a single-stranded nick, the DNA substrate is actually folded into a base-paired hairpin structure and the scissile phosphate bond is embedded in the double helix. TraI encoded by *E. coli* F plasmid and TrwC by R388 conjugation plasmid are characterized by two consecutive Tyr residues near the very N-terminus in addition to the HUH motif (Gomis-Ruth & Coll, 2006; Larkin *et al.* 2007). The first Tyr serves as the nucleophile. Because the cleavage–ligation reactions catalyzed by these nucleases relax supercoiled DNA, they are called relaxases, very much like topoisomerases (Fekete & Frost, 2000). In the crystal structure of TraI, the nucleophile Tyr is mutated to Phe and the relaxase is co-crystallized with its

https://doi.org/10.1017/S0033583510000181 Published online by Cambridge University Press

specific DNA substrate (Fig. 23*b*) (Datta *et al.* 2003; Larkin *et al.* 2005). Several positively charged Lys and Arg side chains facilitate substrate DNA binding. The catalytically essential Mg^{2+} is coordinated by the scissile phosphate, the two absolutely conserved His, and a third His only conserved within the mob family (Fig. 23*c*). The active site is superimposable with the metal-ion center in colicin E7 (Yang, 2008), indicating the conserved metal-ion function and catalytic mechanism.

7.3.3 TnpA DNA transposase of IS200/IS605 family

Nucleases with the HUH motif are also involved in DNA transposition of IS elements (Ton-Hoang *et al.* 2005). They differ from rep and mob nucleases by possessing only one instead of two conserved Tyr residues besides the HUH motif. These small and dimeric nucleases (< 200 aa) are represented by the IS200/IS605 family of DNA transposases (Tnp). The ssDNA transposase (TnpA) from transposon ISHp608 is the best-studied example. TnpA recognizes specific ssDNA sequence and utilizes it for substrate recognition by forming base-paired duplex structures for cleavage (Barabas *et al.* 2008). The tertiary structure and catalytic mechanism of TnpA is reminiscent of TraI and TrwC relaxases (Fig. 23), but the nucleophile Tyr is permutated to be near the C-terminus. Each active site is composite with two metal-chelating His residues from one subunit and the nucleophile Tyr from the second subunit by domain swapping (Fig. 23*d* and *e*). A third metal-ion ligand, Gln, is located near the Tyr and supplied in *trans* as well. Interestingly, the domain swapping and subsequent active site formation are entirely dependent on the DNA substrate binding, which induces a gross conformational change (Barabas *et al.* 2008).

8. TOPRIM topoisomerase and Ser recombinase: partial metal-ion dependence

TOPRIM topoisomerases and Ser recombinases both cleave DNA by forming 5′ phosphoprotein covalent bonds (via Tyr and Ser, respectively) and after topological change or rearrangement of DNA they catalyze DNA religation and restore phosphodiester bonds (Grindley *et al.* 2006; Schoeffler & Berger, 2008). In both cases, the strand cleavage step may be metal ion independent but is stimulated by Mg^{2+} ion, whereas the religation step is metal ion dependent (Bhat *et al.* 2009; Domanico & Tse-Dinh, 1991; Reed, 1981; Zhu & Tse-Dinh, 2000). When complexed with either a type-II topoisomerase or Ser recombinase for the cleavage reaction, the DNA substrate is severely bent around the scissile phosphate, suggesting that distortion and stretching of phosphodiester bonds may facilitate the bond breakage. The number, location and mechanism of metal ions involved in the recombination are still unclear. Recent structural analyses suggest that type II topoisomerases use the one-metal-ion mechanism for DNA cleavage and rejoining.

8.1 TOPRIM topoisomerases

Type IA, IIA and IIB topoisomerases are members of the TOPRIM superfamily, an established metal-ion-binding module (Aravind *et al.* 1998). Three conserved carboxylates are found in every member of the TOPRIM family. Two differences divide nucleases containing a TOPRIM domain. The OLD nucleases and RNase M5 (like primases) have an additional carboxylate in the first sequence motif (EGxxD or EGxxE) (see section 6.6), whereas in topoisomerases it is a Lys instead (EK or ESxxK). Secondly, the topoisomerases use a Tyr instead of a water molecule

https://doi.org/10.1017/S0033583510000181 Published online by Cambridge University Press

as the nucleophile for DNA cleavage and form a phosphotyrosyl covalent intermediate. These differences may divide the TOPRIM nucleases and topoisomerases into families that use different numbers of metal ions for the DNA cleavage reaction. Spo11 nucleases, which introduce DSB to initiate meiotic DNA recombination, are highly homologous to type IIB topoisomerases and likewise have three instead of four conserved carboxylates (Keeney, 2001). Mutation of the carboxylates in the TOPRIM domain abolishes the nuclease activity of Spo11 (Diaz *et al.* 2002). The cleavage products of TOPRIM topoisomerases and Spo11 are 5′-phosphate and 3′-OH as for the other TOPRIM nucleases.

8.1.1 Type-II topoisomerases

Type-II topoisomerases are divided into distinct IIA and IIB families, both of which cleave dsDNA (Wang, 2002). Type-II topoisomerases are also Mg^{2+}-dependent ATPases, and Mg^{2+} cannot be omitted from the reaction. These enzymes are dimeric or hetero–tetrameric. Each active site is composite and consists of the nucleophile Tyr on the WHD domain of one subunit and carboxylates on the TOPRIM domain of another subunit (Schoeffler & Berger, 2008). A single Mg^{2+} coordinated by the conserved E and DxD motifs of TOPRIM was first found in the crystal structure of an archaeal type IIB topoisomerase in the absence of DNA substrate (Nichols *et al.* 1999). A Mg^{2+} ion was later found in the active site of yeast Topo II co-crystallized with a nicked DNA substrate (Dong & Berger, 2007) (Fig. 24*a*).

The location of this metal ion is close to the leaving group and is reminiscent of the B metal ion in RNase H1 and the single metal ion in TraI (Figs 7 and 23). The absence of the second metal ion (equivalent to metal ion A on the nucleophile side) is not a proof of a one-metal-ion mechanism, because the second metal ion may have escaped detection due to a crystallographic artifact. The arrangement of the Tyr and the metal ion relative to the DNA substrate in Topo II is rather similar to the mob nucleases, suggesting that the one-metal-ion mechanism may be applicable here. The absence of the fourth carboxylate in the active site and the presence of the Arg adjacent to the nucleophile Tyr to stabilize the scissile phosphate (Fig. 24*a*) also lend support to the one-metal-ion mechanism.

8.1.2 Type-IA topoisomerases

Type IA topoisomerases are monomeric and nick one strand of DNA (Schoeffler & Berger, 2008). In addition, type-IA enzymes are ATP-independent and relax negative supercoils (with the exception of reverse gyrase). Interestingly, the ssDNA co-crystallized with *E. coli* Topo III (type IA) adopts the double-helix-like conformation (Changela *et al.* 2001) (Fig. 24*b*). Similar to Topo II, the active site of monomeric type IA is assembled between two domains and composed of ExxK and DxD from the TOPRIM domain (aka domain I) and the nucleophile Tyr from domain III (equivalent to the WHD of Topo II) (Fig. 24*b* and *c*). It was controversial as to whether metal ion is required for Topo IA. It is now clear that efficient DNA cleavage in addition to the religation by type-IA topoisomerases requires Mg^{2+} (Domanico & Tse-Dinh, 1991). In support of the metal-ion requirement, amino-acid substitutions of the conserved carboxylates in TOPRIM render the mutant topoisomerases defective in DNA supercoil relaxation (Bhat *et al.* 2009; Zhu & Tse-Dinh, 2000).

The crystal structure of a type-IA topoisomerase (Topo III) with the nucleophile Tyr replaced by Phe and in complex with ssDNA substrate provides the highest-resolution view of the active site of TOPRIM topoisomerases (Changela *et al.* 2001). Relative to the scissile phosphate, the

https://doi.org/10.1017/S0033583510000181 Published online by Cambridge University Press

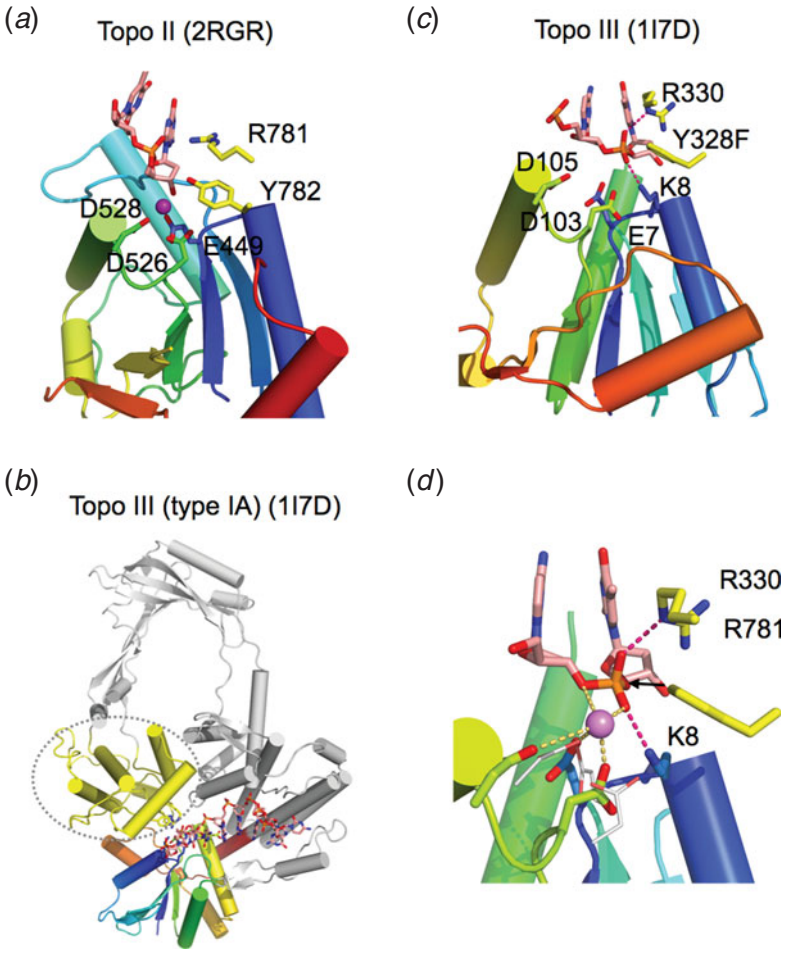


Fig. 24. Topoisomerases containing the TOPRIM motif. (*a*) The active site of *S. cerevisiae* Topo II in complex with dsDNA substrate. The TOPRIM domain is shown in rainbow-colored ribbon diagram. The nucleophile Y782 and its neighbor R781 are supplied in *trans* by the other subunit of the dimeric Topo II and shown as yellow sticks. The scissile phosphate and surrounding nucleotides are shown as pink sticks. Nitrogen and oxygen atoms are colored blue and red, respectively. A Mg^{2+} ion (purple sphere) is coordinated by the conserved carboxylates in the TOPRIM domain. (*b*) Ribbon diagrams of *E. coli* Topo III (Type IA) in complex with ssDNA substrate. The α-helices are represented by cylinders. The TOPRIM domain (aka domain I) is shown in rainbow colors and the catalytic domain (domain III) carrying the Tyr nucleophile is shown in yellow. The ssDNA substrate in shown as sticks. (*c*) A close-up view of the active site of Topo III. The scissile phosphate, the conserved carboxylates and the nucleophile Y328 are nearly superimposable with that of Topo II shown in (*a*). (*d*) A model of the reaction coordinates of DNA cleavage by type IA and type II topoisomerases. The active sites of the two types of TOPRIM topoisomerase are superimposed. The metal ion observed in Topo II is incorporated in the composite active site and shown as a lilac sphere. A Lys (K8) of Topo III approximately occupies the metal ion A position. The Arg next to the nucleophile (R781 of Topo II or R330 of Topo III) in the catalytic domain further stabilizes the scissile phosphate and neutralizes the developing negative charges.

carboxylates and the Tyr of Topo III occupy positions similar to those in Topo II. In addition to the Arg next to the Tyr, a Lys conserved in type IA stabilizes the scissile phosphate (Fig. 24*c*). But due to the high salt concentration in the crystallization buffer (1·3 M $(NH_4)_2SO_4$), soaking in

https://doi.org/10.1017/S0033583510000181 Published online by Cambridge University Press

10 mM $MgCl_2$ was not successful in detecting metal ion binding (Changela *et al.* 2001). The superposition of the catalytic residues of *E. coli* Topo III and yeast Topo II show that the metal ion observed in the Topo II falls right between the conserved carboxylates and scissile phosphate in Topo III (Fig. 24*d*).

The striking similarities of metal ion coordination and nucleophilic attack of the scissile phosphate between TOPRIM topoisomerases and HUH nucleases TraI and TnpA imply a similar catalytic mechanism. The nuclease activity of Topo IA in the absence of Mg^{2+} may be explained by the conserved Lys and Arg in the active site, which can neutralize the developing negative charge on the scissile phosphate (Fig. 24*c*). A divalent cation on the leaving group side may not be necessary, but, in the strand ligation step, the metal ion is on the 3′-OH nucleophile side and may become essential for its deprotonation. It is most likely that type II and type IA topoisomerases with so much in common use the same metal-ion-dependent cleavage mechanisms.

The M5 and OLD family nucleases and type-IA and type-II topoisomerases of the TOPRIM superfamily share the conserved TOPRIM domain yet may use a two- *versus* one-metal-ion-dependent mechanism for DNA cleavage. The divergence appears to originate from different nucleophiles and different environments surrounding the respective scissile phosphate in their cleavage reactions. They may represent an early divergence from a primordial sequence motif and structural domain.

8.2 Ser recombinases

The Ser-recombinase family consists of a large number of bacterial and archaeal resolvases/invertases, transposases and DNA-partitioning enzymes, which use the conserved Ser as a nucleophile to cleave and ligate DNA by forming a 5′-phosphoserine covalent intermediate (Grindley *et al.* 2006). A pair of long DNA recognition sites is required for DNA recombination, and DNA rearrangement takes place between the steps of cleavage and religation of both sites. Although Ser recombinases are usually compared with DNA recombinases rather than topoisomerases, they can relax negative supercoils like topoisomerases if cleavage of four strands (two duplexes) are incomplete and the recombination of DNA is prevented (Falvey *et al.* 1988).

Ser recombinases are bi-lobal and contain an N-terminal catalytic domain and a C-terminal sequence-specific DNA-binding domain (Yang & Steitz, 1995a) (Fig. 25*a*). Dimerization is mandatory for binding to a pseudo-palindromic recognition site and for double strand cleavage (Salvo & Grindley, 1988). For recombination between two specific sites to take place, Ser recombinases have to form a synaptic dimer of dimers (Fig. 25*a* and *b*). After cleavage of both recombination sites, protein and DNA undergo dramatic conformational changes (Li *et al.* 2005). Unlike the Tyr recombinases (see section 10.2.2), the recombination intermediate of Ser recombinases is not a HJ. The DNA rearrangement catalyzed by a Ser recombinase is rather similar to the topological change catalyzed by type-II topoisomerases (Fig. 2*d*) except for that two dsDNA cleavages are required rather than one.

The catalytic domain of Ser recombinases is composed of ~120 N-terminal residues, which form a mixed five-stranded central β-sheet (54 312, ↓↑↑↑↑) surrounded by α-helices (Fig. 25*c*). The nucleophile Ser is at the end of the 1st β-strand. A number of conserved basic residues are essential for DNA cleavage and religation. The catalytic domain of $\gamma\delta$ resolvase was first suggested to be similar to T5-FEN, because they share the first four parallel strands (Artymiuk *et al.* 1997), but $\gamma\delta$ resolvase appears even more similar to RecJ than FEN (Fig. 25*c* and *d*). Structural

https://doi.org/10.1017/S0033583510000181 Published online by Cambridge University Press

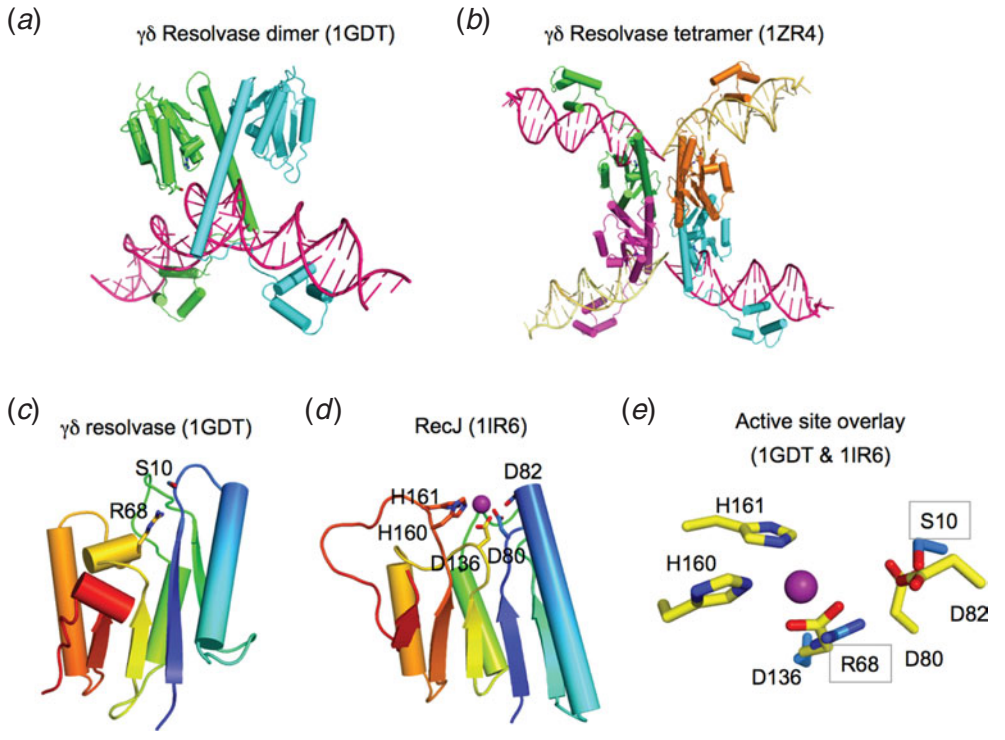


Fig. 25. Metal-independent Ser recombinases. (*a*) The structure of $\gamma\delta$ resolvase dimer complexed with a palindromic DNA cleavage site (site I). Each protein subunit and DNA are shown in different colors. The catalytic residues are shown as sticks. (*b*) The $\gamma\delta$ resolvase tetramer complexed with two cleaved DNA site I. Each protein dimer and DNA site are extensively rearranged. (*c*) The catalytic domain of resolvase is shown in rainbow colors from blue N- to red C-terminus. The catalytic residues S10 and R68 are shown in sticks. (*d*) The catalytic domain of RecJ. The metal coordinating carboxylates and the DHH motif are shown as sticks. (*e*) Superposition of the catalytic residues of resolvase (blue) and RecJ (yellow).

superposition of RecJ and resolvase reveals an uncanny similarity and sheds light on catalytic mechanisms of both nucleases. The Ser nucleophile of resolvase overlays with the two conserved carboxylates in RecJ, which are likely to coordinate a metal ion (A site) in the presence of the DNA substrate for the two-metal-ion-dependent hydrolysis. The metal ion observed in the RecJ structure, which is coordinated by two His residues of the DHH motif, overlays with the catalytically essential Arg (R68) in $\gamma\delta$ resolvase. The overlay suggests that this metal ion may occupy the B site in RecJ and stabilize the transition state. The similarity is consistent with a catalytic mechanism in which Ser attacks the scissile phosphate and Arg68 stabilize the penta-covalent intermediate. How the metal ion comes into play in DNA religation awaits elucidation by future studies.

Interestingly, Ser recombinases bear structural and functional similarity to TOPRIM topoisomerases because of the resemblance between RecJ and TOPRIM OLD nucleases (Fig. 10). The passage of one DNA duplex through another in site-specific recombination by a Ser recombinase is not dissimilar to the dsDNA passing in topological changes by type-II topoisomerases. Ser recombinases may represent the transition from metal-independent to metal-dependent nucleic acid enzymes. Metal-ion-dependent mechanisms have been

https://doi.org/10.1017/S0033583510000181 Published online by Cambridge University Press

associated with (1) high specificity, (2) high efficiency and (3) reversibility of forward and reverse reactions (Yang *et al.* 2006). Ser recombinases achieve their specificity through DNA sequence recognition by the C-terminal domain and reaction efficiency is not a concern as recombination is a rare event in the life of cells. The metal ion is indeed required for the reverse reaction of cleavage (ligation) by Ser recombinases. For topoisomerases, the efficiency of DNA cleavage and religation is in the center of topological change. Correlated with the demands of reaction efficiency and two consecutive phosphoryl transfer reactions, TOPRIM domain, a metal-ion-binding module, comes to being and plays a central role during topoisomerization. In contrast to the metal-independent type IB topoisomerases (see section 10.2), type-IA and type-II topoisomerases have little preferences for specific DNA sequences. The requirement for metal ion may also contribute to the tight coupling of DNA cleavage with topological changes, one (double or single) strand-passage event in each DNA cleavage-and-rejoining cycle.

9. Metal-independent RNase

A large number of RNases catalyze phosphodiester bond breakage without metal ions. This is largely due to the 2′-OH of ribose, which readily makes intramolecular nucleophilic attack on the adjacent 3′-phosphate, thus breaking the RNA backbone (Figs 2*e*, 3*b,* and *c*). RNase A, T1 and T2 are three large RNase families in this class (Deshpande & Shankar, 2002; Raines, 1998; Yoshida, 2001). Endonucleases for tRNA splicing, colicin D and E5, ferredoxin-like Cas6 and CasE and Ire1 are additional metal-independent RNases. Metal-independent RNases, whether protein enzymes or ribozymes, produce 5′-OH and 2′,3′-cyclic phosphate, which are subsequently converted to 3′ phosphate and occasionally to 2′ phosphate as during tRNA splicing (Abelson *et al.* 1998).

These RNases expose and distort the scissile phosphate by splaying the bases surrounding the scissile phosphate far apart (Fig. 3*b* and *c*). Despite secondary structures recognized by some of these RNases, the nucleotides placed in the active site are inevitably single-stranded and unpaired. For example, when bound to barnase the RNA substrate is in an extended conformation with the bases surrounding the scissile phosphate more than 9 Å apart as compared with the 3·2–3·4 Å in a double helix (Fig. 26*a*) (Buckle & Fersht, 1994). The active site residues facilitate the splay of bases in the substrate and distortion of the scissile phosphate for the 2′-O to attack it. An efficient cleavage reaction requires a general base to deprotonate the 2′-OH, positive charges to neutralize the penta-covalent transition state, and a general acid to protonate the 5′-O leaving group. When a general base and acid with pK_a close to neutral pH are absent, such as in ribozymes, the catalytic rate is slow (Cochrane & Strobel, 2008; Zamel *et al.* 2004). In contrast, many protein RNases have excellent general bases and acids and are thus highly active (Deshpande & Shankar, 2002; Raines, 1998; Yoshida, 2001) and usually acquire special inhibitors known as immunity proteins for host protection (Kobe & Deisenhofer, 1996; Kolade *et al.* 2002; Lee *et al.* 1989).

9.1 RNase T1, Barnase and microbial RNases

Members of RNase T1 family are found in bacteria and fungi only. Related are the restrictocin/sarcin and colicins E3, E4 and E6. The active site consists of a Glu-His pair as general base and acid.

https://doi.org/10.1017/S0033583510000181 Published online by Cambridge University Press

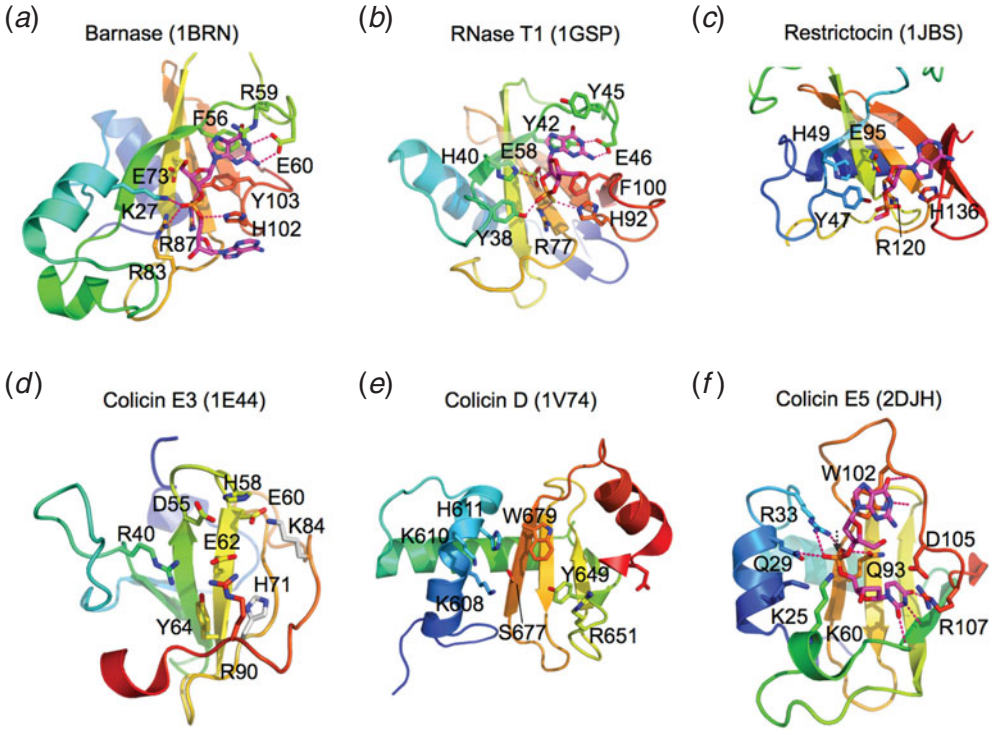


Fig. 26. Metal-independent RNases of T1 family and colicins. (*a*) Barnase in complex with a substrate mimic d(GGAC). The RNase is shown in rainbow-colored ribbon diagrams. The scissile phosphate and surrounding nucleotides are shown as magenta sticks. The active site residues are shown in sticks and labeled. Hydrogen bonds with the scissile phosphate and the surrounding bases are shown as dashed lines. (*b*) RNase T1 complexed with a phosphorothioate cleavage product. The sulfur atom in the 2′,3′ cyclophosphorothioate is shown in light yellow. (*c*) Sarcin homolog restrictocin in complex with the mimic of sarcin/ricin loop. Only the active site is shown. The RNA is not positioned for cleavage. (*d*) The ribonuclease domain of colicin E3. The potential active site residues are shown as sticks in the same colors as their Cα atoms. Those, whose mutations do not decrease the nuclease activity, are shown in silver. (*e*) The nuclease domain of colicin D. The active site residues are shown in sticks. (*f*) Colicin E5 complexed with d(GU). Sequence specificity is determined by the numerous hydrogen bonds between the RNase and the bases surrounding the scissile phosphate. The nucleophilic attack would take place as indicated by the black dashed arrowhead if 2′-OH is present.

9.1.1 Barnase

Barnase, an extracellular ribonuclease of *Bacillus amyloliquefaciens*, has been extensively studied for its folding properties, interaction with its intracellular protein inhibitor barstar and its substrate recognition (Fersht & Daggett, 2002; Urakubo *et al.* 2008). Homologous RNases are found in other bacillus species, e.g. Binase from *Bacillus intermedius* (Schulga *et al.* 1992). Barnase has a characteristically twisted five-stranded contiguous antiparallel β-sheet with long loops surrounding it and short helices covering one side (Fig. 26*a*). The exposed face of the β-sheet binds nucleic acid substrate. Most of the catalytically essential residues are located on the loops except for the central Glu. The crystal structure of Barnase bound to a tetradeoxynucleotide (instead of RNA to prevent cleavage) reveals the mode of substrate recognition and a possible catalytic mechanism (Buckle & Fersht, 1994). Barnase cleaves 3′ to a Gua, which is sandwiched between an Arg and Phe and forms double hydrogen bonds with a Glu (Fig. 26*a*). The scissile phosphate

https://doi.org/10.1017/S0033583510000181 Published online by Cambridge University Press

is neutralized by two Arg and one Lys. The catalytic residues Glu (E73) on the central β-strand and His (H102) on a long loop are on either side of the scissile phosphate and function as the general base and acid, respectively. The conformation of the deoxyribose linked to the scissile phosphate, however, is not in position for the in-line attack in this crystal structure, probably because of the absence of 2′-OH (Buckle & Fersht, 1994). Y103, which stacks against the (deoxy)ribose, together with the Arg and Lys residues, may align and distort the substrate for the nucleophilic attack.

9.1.2 RNase T1

RNase T1, RNase Sa and fungal RNase U2, F1 and Ms belong to RNase T1 family and are homologous to Barnase in sequence and tertiary structures (Yoshida, 2001). They too cleave ssRNA after Gua. The general base and acid pair, Glu and His, are conserved in these RNases. Several crystal structures of RNase T1 bound to various substrate analogs have been reported (Arni *et al.* 1999), and the complex with a cyclic thiophosphate substrate is particularly revealing (Zegers *et al.* 1998). RNase T1 can cleave the cyclic phosphodiester to 3′ phosphate, which is the second half of the normal hydrolysis reaction. The sulfur replacement (thiophosphate) greatly reduces the reaction rate. In the crystal structure, the cyclic phosphate is placed between the conserved Glu (E58) and His (H92) and hydrogen bonded to both (Fig. 26*b*). The ribose is flipped compared to that in Barnase (Fig. 26*a*) and well placed for the general acid–base catalysis. In addition, positively charged H40 and R77 interact and orient the scissile phosphate. The guanine base preceding the scissile phosphate is sandwiched between two Tyr residues and forms bifurcated hydrogen bonds with a glutamate (E46) in addition.

9.1.3 Restrictocin

The homologous restrictocin and sarcin are ribotoxins and specifically cleave 28S ribosome RNA (Olmo *et al.* 2001). Structurally these ribotoxins are related to Barnase and RNase T1 (Yang *et al.* 2001), yet they specifically recognize a well-folded hairpin loop (sarcin/ricin loop) in the 28S rRNA. Because of the modified 2′-groups used in co-crystallization of restrictocin-RNA to prevent cleavage (Yang *et al.* 2001), the RNA substrate is out of register by one nucleotide and the scissile-phosphate mimic is displaced from the catalytic residues. Nevertheless, the structure reveals a dramatically deformed hairpin RNA substrate and the unpaired and flipped-out base 5′ to the scissile phosphate (Correll *et al.* 2004) (Fig. 26*c*). Such distortions are necessary to align the 2′-OH nucleophile for the in-line attack. The bases surrounding the scissile phosphate are thus splayed much like in the cases of Barnase and RNase T1. The catalytic Glu-His pair is E95 and H136 in Ristrictocin. Like RNase T1, restrictocin also depends on aromatic and positively charged residues to bind and orient the scissile phosphate for the cleavage reaction (Fig. 26*c*).

9.1.4 Colicin E3, E4 and E6

Colicin E3, E4 and E6 are homologous and specifically cleave 16S rRNA. Bacteriocin Cloacin DF13 is a ribonuclease homologous to E3 and E6 colicins and it again cleaves 16S rRNA (Akutsu *et al.* 1989). The crystal structure of E3 complexed with its inhibitor reveals the similarity to that of Barnase and RNase T1 (Carr *et al.* 2000) (Fig. 26*d*). The conserved E62 and H71 assume comparable positions as the catalytic Glu-His pair found in the T1 superfamily.

https://doi.org/10.1017/S0033583510000181 Published online by Cambridge University Press

But mutagenic studies show that H58 instead of H71 is critical for catalysis and that E62 and H58 are likely to be the general base and acid pair (Walker *et al.* 2004). Additionally charged residues, Asp, Glu, Lys and Arg, align the active site. Mutagenesis suggests that R40, D55, E60, Y64 and R90 are essential for catalysis (Walker *et al.* 2004). How these RNases recognize their substrate remains unsettled in the absence of a co-crystal structure and additional biochemical studies.

9.2 Colicin D and E5

Colicin D cleaves the anticodon loop of all four Arg tRNA (Kolade *et al.* 2002). The crystal structure of colicin D complexed with its immunity protein has been determined (Graille *et al.* 2004). Although colicin D consists of a contiguous antiparallel β-sheet supported by long α-helix on one side as does RNase T1, the topology is different with the strands (1234) going from right to left instead of left to right (Fig. 26*e*). The crystal structure also reveals that its active site lacks the Glu-His pair. Instead colicin D has a single His (H611), which is suspected to be the general base. In addition, the active site is marked by aromatic residues, which may determine the base specificity, and by positively charged residues, which may orient and neutralize the scissile phosphate (Graille *et al.* 2004).

Colicin E5 is similar to colicin D and is also a tRNase. It recognizes the GU sequence in the anticodon loop of *E. coli* Tyr, His, Asn and Asp tRNA (James *et al.* 1996). The crystal structure of colicin E5 complexed with a substrate mimic (dGpdUp) reveals that GU bases are mainly specified by hydrogen bonds with the backbone atoms of the protein (Yajima *et al.* 2006) (Fig. 26*f*). This structure reveals a near-active reaction coordination, where the scissile phosphate and the preceding (deoxy)ribose (to which the 2′-OH would belong to if present) are perfectly aligned for the nucleophile attack (compared with the reaction product of 2′,3′ cyclic-phosphate shown in Fig. 25*b*). Colicin E5 has no Glu or His in its active site (Fig. 26*f*). Three basic residues (K25, R33 and K60) provide charge neutralization of the scissile phosphate. These positively charged residues may serve as the general acid and base for catalysis at high pH as proposed (Yajima *et al.* 2006). Interestingly, two Gln (Q29 and Q93) are located near the scissile phosphate and are potentially involved in the cleavage reaction.

9.3 RNase A

Bovine pancreatic RNase A is perhaps the most studied ribonuclease, which has culminated in four Nobel prizes (Raines, 1998). It is the protein that Chris Anfinsen used to show that information for disulfide formation and tertiary folding is intrinsically stored in the amino acid sequence (Anfinsen, 1973). Homologs of RNase A are widespread among animals. There are eight versions of RNase A in the human genome, six expressed in pancreas (RNase 1–6) and two in skin (RNase 7 and 8). Genes encoding these RNases tend to be in a cluster on one chromosome. Only homologs of RNase 5 have been reported outside the mammals. The crystal structures of pancreatic RNase A (Avey *et al.* 1967; Kartha *et al.* 1967; Wyckoff *et al.* 1970) and homologous seminal (Mazzarella *et al.* 1993; Merlino *et al.* 2008) and eggwhite ribonucleases (PDB: 2ZPO) have been determined. Like Barnase, RNase A contains a central antiparallel β-sheet, but it is much more extended and twisted (Fig. 27*a*). The catalytic triad, two His (H12 and H119) and one Lys (K41) surround a central substrate-binding groove (Fig. 27*a*).

Pancreatic RNases recognize U or C for endonucleolytic cleavage to produce 3′-Up or 3′-Cp. The apo-protein structure of RNase A was among the first protein crystal structures determined

https://doi.org/10.1017/S0033583510000181 Published online by Cambridge University Press

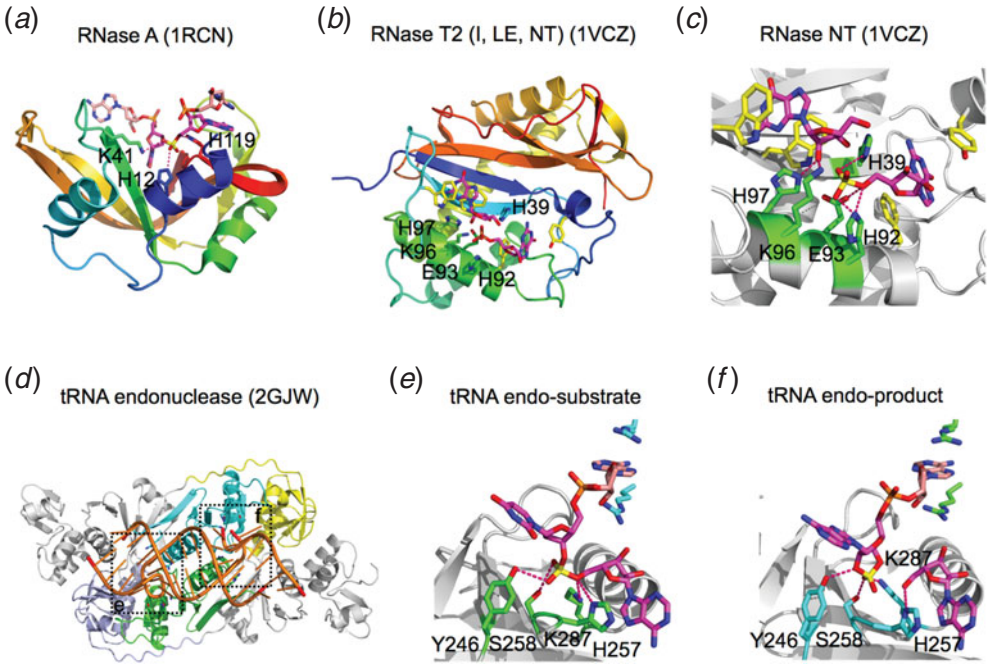


Fig. 27. RNase A and related RNases. (*a*) RNase A in complex with d(ATAAG) substrate mimic. RNase A is shown in rainbow-colored ribbon diagrams with the catalytic triad (HKH) shown as sticks. The scissile phosphate is shown in yellow, the surrounding nucleotides in magenta and other nucleotides in pink sticks. (*b*) An example of RNase T2 family, RNase NT, complexed with two GMP. The structure is shown in the same scheme as in (*a*). (*c*) A close-up view of the substrate recognition by RNase NT. The two bases surrounding the putative scissile phosphate are sandwiched by aromatic side chains (shown in yellow). The HKH catalytic triad (shown in green sticks) appears to be conserved and the two His side chains serve as general acid and base. (*d*) The overall structure of a homodimeric tRNA splicing endonuclease. Each catalytic unit consists of a catalytic domain (shown in green and cyan) and an associated unique domain (shown in yellow and steel blue). Two structural units are shown in silver gray and are homologous to the catalytic units (green + yellow or cyan + light) by gene duplication. The four units can be independent polypeptide chains in other orthologs. The pre-tRNA mimic is shown in orange ribbon diagrams. The uncleaved and cleaved scissile phosphates are boxed and labeled as 'e' and 'f', respectively. (*e*) A close-up view of the active site (green subunit) with uncleaved RNA (substrate). Hydrogen bonds with the scissile phosphate are shown as hot pink dashed lines. RNA substrate is stabilized by cation-π-cation stacking with a neighboring subunit (cyan). (*f*) The active site (cyan subunit) with the cleavage product, 2′,3′-cyclic phosphate.

(Kartha *et al.* 1967; Wyckoff *et al.* 1967), and the RNase complexed with ssDNA substrate mimics were determined in the 1990s (Raines, 1998). The structure of RNase A complexed with d(ATAAG) with the dT mimicking a U is most revealing (Fontecilla-Camps *et al.* 1994). The preference for cleaving after a pyrimidine is due to steric exclusion of purines. The reaction coordinate is rather similar to the other known metal-independent RNases (Figs 26 and 27*a*). The conserved H12 (potentially the general base) is hydrogen bonded with the scissile phosphate on the 3′-O side (2′-OH is replaced by H), and H119 (potentially the general acid) is hydrogen bonded with the leaving group O5′. Studies by chemical perturbation of the catalytic triad and pH profiling indicate that indeed H12 is the general base, H119 the general acid and K41 specifically neutralizes the transition state (Raines, 1998).

https://doi.org/10.1017/S0033583510000181 Published online by Cambridge University Press

9.4 RNase T2

Members of RNase T2 family are widespread from *E. coli* (RNase I), fungi (Rd and DdI), plants (LE and NT) and mammals (Deshpande & Shankar, 2002; Irie & Ohgi, 2001). RNase T2 are sequence non-specific. The structure of RNase T2 consists of a central 4-stranded antiparallel β-sheet surrounded by short strands and long helices on one face. The topology and tertiary structure, however, are different from RNase A and T1 (Fig. 27*b*). The active site is located on the exposed face of the β-sheet. The conserved Glu, Lys and three His residues in the active site are essential for the catalytic activity. Interestingly, mutation of individual amino acids only reduces, but not eliminates, the RNase activity (Tanaka *et al.* 2000). The crystal structure of tobacco RNase T2 (NT) complexed with two 5′ GMP in the active site may mimic the enzyme–substrate complex (Kawano *et al.* 2006). Each guanine bases is sandwiched by two aromatic side chains. The catalytic residues are within hydrogen bonding distance to the scissile phosphate mimics (Fig. 27*c*), a His and Lys coordinating the attacking nucleophile 2′-OH, and the remaining three coordinating the phosphate.

9.5 tRNA-splicing endonuclease

About 5–25% of archaeal and eukaryotic tRNA contain introns, which are recognized and excised by the tRNA-splicing endonuclease (Abelson *et al.* 1998). The tRNA-splicing endonucleases vary from homodimeric (archaea) to hetero-tetrameric (eukarya), but the overall structures are identical. Regardless of the number of peptides, each active molecule contains two catalytic and two structural units, all of which are structurally similar (Calvin & Li, 2008). All tRNA-splicing endonucleases recognize the bulge-helix-bulge (BHB) structure in pre-tRNAs. The crystal structure of an archaeal homodimeric tRNA endonuclease complexed with RNA substrate with two bulges reveals two composite active sites (Xue *et al.* 2006) (Fig. 27*d*). One active site is bound to a non-cleavable 2′-deoxy substrate, and the other is bound to the cleaved product (Fig. 27*e* and *f*).

The pre-tRNA substrate is mostly base-paired except for the cleavage sites in the 3-nt bulges. The bases flanking the scissile phosphate are unpaired and splayed as in substrate complexes of other metal-independent RNases. Each active site is composite. The catalytic residues are from one subunit, while the other subunit donates the Arg residues that sandwich the flipped out base flanking the scissile phosphate by the cation–π interactions (Fig. 27*e*, *f*). The catalytic unit contains a five-stranded mixed β-sheet not unlike metal-independent RNases. The conserved Tyr, His and Lys in the active site are confirmed to play catalytic roles. Double mutation of the Tyr and His eliminates the nuclease activity (Calvin *et al.* 2008). This Tyr–His pair appears to replace the Glu–His in Barnase and the His–His pair in RNase A and acts as the general acid and base in the RNA cleavage reaction. Interestingly, replacing the conserved Lys in the active site by Glu, Gln or Arg abolishes the cleavage activity too, but the K to E mutant enzyme alone can be rescued by a specific divalent cation (Calvin *et al.* 2008). This may be an in-test tube mimic of the evolution from metal-independent to metal-dependent nucleases.

Ligation of the cleavage products 5′-OH and 2′,3′-cyclic phosphate in tRNA splicing is rather baroque (Abelson *et al.* 1998). It requires the 5′ end to be phosphorylated and the 2′,3′ cyclic phosphate to be converted to the 3′-OH and 2′-phosphate by a special phosphodiesterase (Wang & Shuman, 2005). After the standard ligation, the 2′-phosphate needs to be removed by another enzyme. The archaic processing of such metal-ion-independent RNA cleavage

https://doi.org/10.1017/S0033583510000181 Published online by Cambridge University Press

products may suggest an ancient origin. The simpler metal-dependent 3′-OH and 5′-phosphate splicing and cleavage intermediates ready for ligation and replication may arise in parallel to this or after, and they are clearly favored by evolution as shown by their abundance in today's world.

9.6 Ferredoxin-fold Cas6

Cas6 (for CRISPR associated 6) and CasE (Cse3) are related endoribonucleases that specifically recognize and cleave CRISPR RNA repeats to generate guide RNA for antiviral defense in prokaryotes (Brouns *et al.* 2008). The cleavage by Cas6 occurs 21 or 22 nucleotide downstream of the first repeat nucleotide. It is metal ion independent and presumably generates 5′-OH and 2′,3′-cyclic phosphate (Carte *et al.* 2008). Cas6 and CasE belong to one of the repeat-associated mysterious protein (RAMP) families (Makarova *et al.* 2006). The crystal structure of Cas6 reveals that it is composed of two ferredoxin domains in a direct repeat (Fig. 28*a*). Ferredoxin-like domains are often found as RNA-binding modules. In addition to Cas6, Cas2 is also an RNase with a ferredoxin-fold, but Cas2 is metal-ion dependent and generates 5′-phosphate and 3′-OH products (section 6.17.4).

The two Ferredoxin domains in Cas6 are arranged approximately side-by-side and a G(Gly)-rich region fills the gap between the domains (Carte *et al.* 2008) (Fig. 28*a*). The active site of Cas6 consists of highly conserved Tyr, His and Lys in the first ferredoxin domain and a conserved Lys in the G-rich region. The Tyr–His pair is reminiscent of the catalytic residues of tRNA endonucleases. The structure of archaeal protein TTHB192, a homolog of CasE (Cse3), was reported before its function was identified (Ebihara *et al.* 2006). Whether CasE is an RNase has not been confirmed. Interestingly, His, Glu and Arg from the first ferredoxin domain and Lys from the G-rich region of CasE occupy the same positions as the catalytic residues in Cas6 (Fig. 28*a*, *b*). A His–Glu pair may replace the Tyr–His pair for catalysis if CasE is an RNase.

9.7 XendoU

Xenopus laevis RNA endonuclease is involved in the processing of the intron-encoded boxC/D U16 snoRNA for ribosome biogenesis (Laneve *et al.* 2003). Cleavage is poly(U) specific and homologs of XendoU are found in most metazoa (Laneve *et al.* 2008). Although the catalysis was initially thought to be metal ion dependent, metal ions cannot be found in the active site in the crystal structure (Renzi *et al.* 2006). Considering the cleavage products are 3′-phosphate and 5′-OH, the required metal ion was suggested to facilitate RNA substrate binding. The tertiary structure of XendoU is unique. It contains a bunch of α-helices at the N-terminus and a duplication of an α-helix and three-stranded β-sheet unit at the C-terminus (Fig. 28*c*). The catalytic residues are concentrated in the first repeat of the α/β structure and include two His, one Lys and one Arg (Renzi *et al.* 2006).

9.8 Ire1 and RNase L

Ire1 is an ancient transmembrane sensor of ER (endoplasmic reticulum) stress and is conserved in all eukaryotes (Sidrauski & Walter, 1997). In addition to the N-terminal ER luminal domain (receptor of unfolded protein) and a transmembrane segment, Ire1 has both a C-terminal cytoplasmic kinase domain and a kinase-extension nuclease (KEN) domain. Ire1 catalyzes splicing of

https://doi.org/10.1017/S0033583510000181 Published online by Cambridge University Press

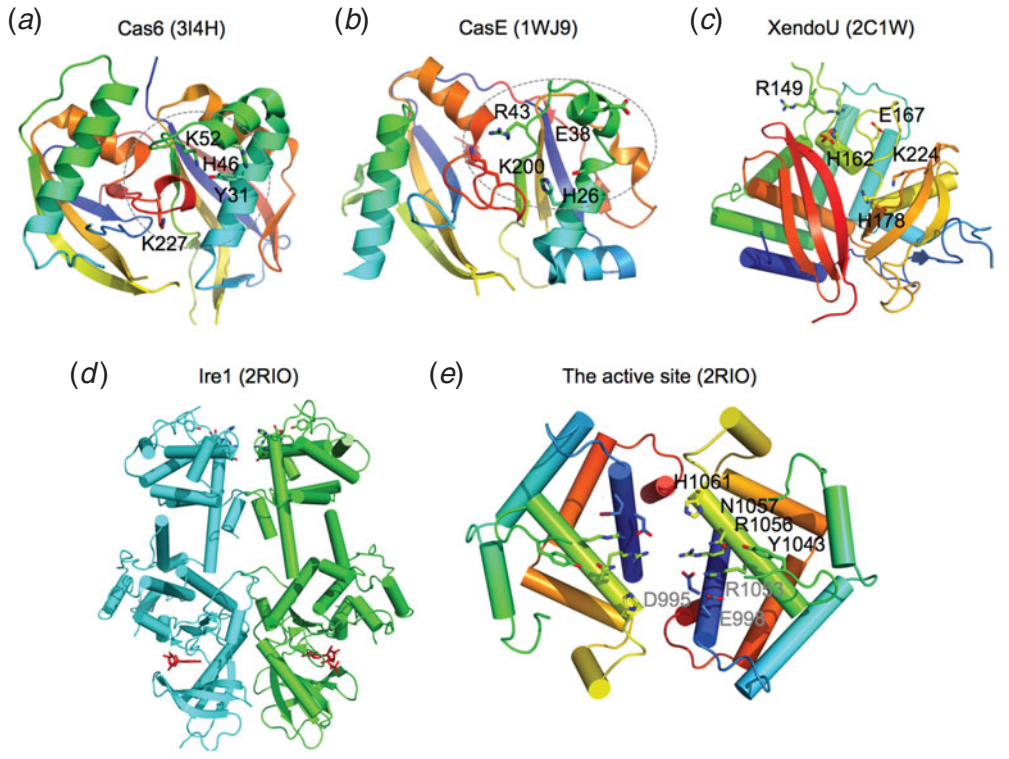


Fig. 28. Other metal-independent RNases. (*a*) *Pyrococcus furiosus* Cas6. The two ferredoxin-like domains arranged in a direct repeat are both shown in rainbow-colored ribbon diagrams, from blue N- to red C-terminus. Putative catalytic residues are shown as sticks. (*b*) *Thermus thermophilus* CasE is related to Cas6 and shown in the same color scheme. Only the Lys near the C-terminal is conserved between Cas6 and CasE. (*c*) Ribbon diagram of XendoU. The protein is in rainbow color from blue N- to red C-terminus. A pseudo-dyad symmetry relates the two 3-stranded β-sheets. A bound phosphate is shown as orange and red sticks. The conserved and catalytic essential residues are also shown and labeled. (*d*) The overall structure of IreI homodimer. The two subunits are shown in green and cyan, and the bound ADP in the kinase domains are shown in red sticks. The nuclease domains (top) are highlighted with the catalytic residues shown in sticks. (*e*) A close-up view of the putative active site of IreI. Each nuclease domain is shown in rainbow colors. The residues (in one subunit) with strong effects on catalysis are labeled in black, and those of with medium effects in gray.

target mRNAs in a spliceosome-independent manner. The cleavage products are 2′,3′ cyclic phosphate and 5′-OH, and the cleavage mechanism is proposed to be similar to RNase A. Dimerization and auto-phosphorylation of Ire1 activate its ribonuclease activity, and binding ADP/ATP in the kinase domain enhances dimerization of the KEN and thereby the nuclease activity (Sidrauski & Walter, 1997). The crystal structure of the kinase and KEN domain has been recently determined (Lee *et al.* 2008) (Fig. 28*d* and *e*). The KEN nuclease is rather unusual and is entirely α-helical without any β-strand. The active site residues are concentrated along an α-helix at the dimer interface, including His, Asn, Tyr and several Arg side chains.

A kinase-like and KEN domains are also found in mammalian RNase L (Bork & Sander, 1993; Dong *et al.* 2001), which contains nine ankarin repeats in addition. In parallel to the nuclease activation of Ire1 by ER stress, RNase L is activated by 2′,5′ oligoadenylates (whose

https://doi.org/10.1017/S0033583510000181 Published online by Cambridge University Press

production is induced by viral infection and mediated by interferon) binding to the ankarin repeats (Silverman, 2007). RNase L cleaves ssRNA at the 3′ of UA or UU sequences and plays an essential role in breaking down viral RNA in innate immune response. Like all other metal-ion-independent RNases, the cleavage products of RNase L are 3′ phosphate and 5′-OH. Reminiscent of the correlated kinase and nuclease activities in Ire1, RNase L activity is dampened by an ATP-binding cassette protein ABCE1 (Silverman, 2007).

9.9 Hammerhead, hairpin, glmS, HDV and VS ribozymes

Metal-independent ribozymes cleave RNA very much like metal-independent protein enzymes by splaying bases surrounding the scissile phosphate and aligning the 2′-OH for in-line nucleophilic attack (see the recent comprehensive review by Cochrane & Strobel, 2008). Because ribozymes lack a general acid and base with pK_a close to neutrality, the fastest ribozyme VS RNA has a turnover rate of $10\ s^{-1}$ (Zamel *et al.* 2004), which is orders of magnitude slower than protein ribonucleases. Three-dimensional structures of the hammerhead, hairpin, glmS, HDV and VS ribozymes, which cleave RNA to generate 2′,3′ cyclic phosphate and 5′-OH, have been determined (Chi *et al.* 2008; Ferre-D'Amare *et al.* 1998; Klein & Ferre-D'Amare, 2006; MacElrevey *et al.* 2008; Rupert *et al.* 2002; Scott *et al.* 1996). In most cases, the unprotonated N1 of a Gua base is placed adjacent to the 2′-OH nucleophile and may serve as a general base. This is evident in the high-resolution structures of hammerhead in the pre- and post-catalytic states and of the hairpin ribozyme along the reaction pathway (Chi *et al.* 2008; Rupert *et al.* 2002) (Fig. 29). The general acid to donate a proton to the 5′ leaving group may also be a nucleobase (Cochrane & Strobel, 2008). Although Mg^{2+} is critical for the folding of ribozymes and may play a role in substrate binding, there is no evidence that Mg^{2+} directly participates in catalysis.

10. Metal-ion-independent DNase

A number of DNases are known to be metal-ion independent. To date, these DNases have been shown to catalyze cleavage reactions in two steps and require a phosphoenzyme covalent intermediate. The classic examples are recombinases and topoisomerases, which use Tyr as a nucleophile and form a 3′-phosphotyrosine covalent intermediate (Grindley *et al.* 2006; Schoeffler & Berger, 2008). In addition, DNase II and BfiI restriction endonuclease represent members of the phospholipase D (PLD) family and cleave DNA via a phosphohistidine intermediate (Sasnauskas *et al.* 2010). The cleavage products of DNase II and BfiI are 5′-phosphate and 3′-OH. The last example of metal-independent DNase is the newly identified halfpipe restriction endonuclease PabI (Miyazono *et al.* 2007). A conserved Tyr is required for catalysis, but a phospho-Tyr intermediate is yet to be confirmed. The metal-ion-independent DNases use positively charged side chains to align the scissile phosphate for nucleophilic attack and to stabilize the penta-covalent intermediate.

10.1 DNase with PLD fold

DNases in the PLD superfamily contain the $HXK(X)_4D$ (or HKD in short) motif and cleave DNA via a two-step mechanism by forming an phosphohistidine intermediate

https://doi.org/10.1017/S0033583510000181 Published online by Cambridge University Press

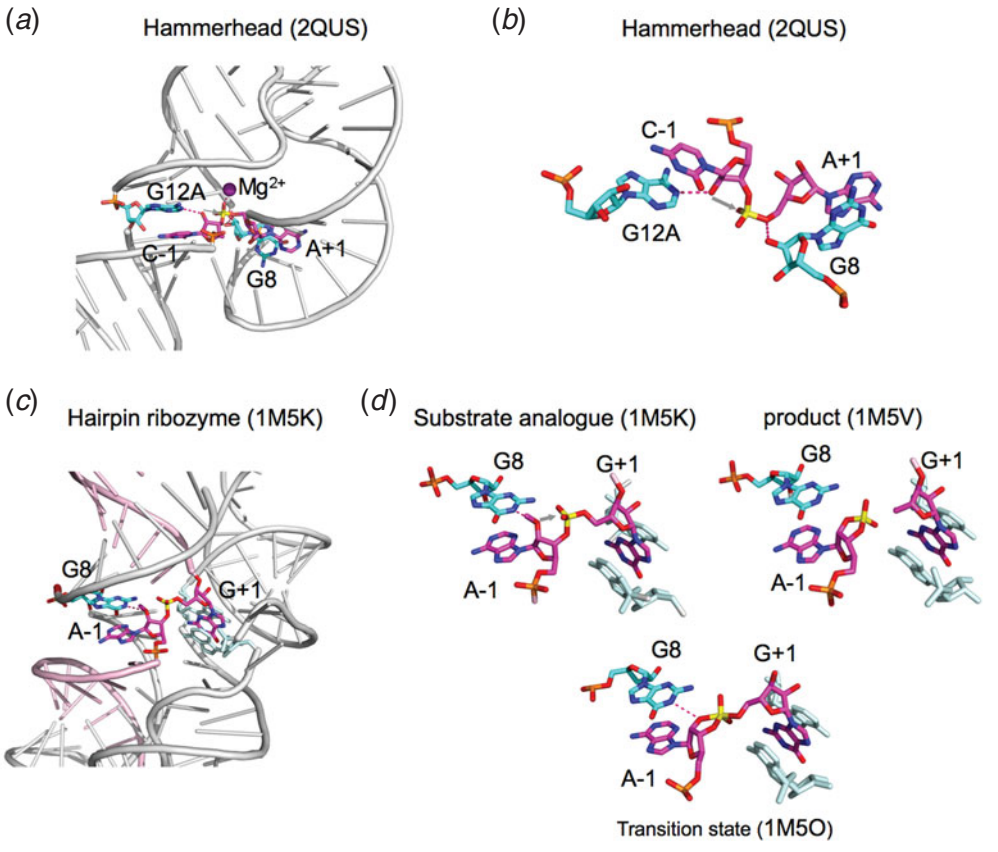


Fig. 29. Metal-independent ribozymes. (*a*) Hammerhead ribozyme. The RNA is shown in silver ribbon diagrams. The scissile phosphate is shown in yellow, the surrounding nucleotides (C−1 and A+1) in magenta, and the catalytic nucleotides in cyan. A Mg^{2+} (purple sphere) happens to be coordinated by the scissile phosphate. (*b*) A close-up view of the catalytic center in the hammerhead. The Mg^{2+} is omitted for clarity. The reaction is stopped because of the G12A mutation, which reduces the effectiveness of the general base. The 2′-OH of G8 is proposed to be the general acid. (*c*) The overall structure of a catalytically active Hairpin ribozyme. The RNA substrate is shown in pink ribbon diagrams, and the others are shown in the same scheme as in (*a*). (*d*) Close-up views of the active site of the hairpin ribozyme complexed with a substrate analog (A-1 is 2′-O-methylated), transition state analog (vanadate) and product (2′,3′-cyclic phosphate).

(Gottlin *et al.* 1998). The conserved HKD motif is present twice in each PLD family member either by homodimerization or an internal duplication (Uesugi & Hatanaka, 2009). The His and Lys of the HKD motif are involved in catalysis, whereas the Asp appears to stabilize the structure by hydrogen bonding with the main chain amides. The catalytic mechanism appears to be highly conserved in the PLD family, whether the substrate is phospholipids, DNA or phosphorylated proteins (Davies *et al.* 2004). The reaction coordinate is examplified by the crystal structure of human tyrosyl-DNA phosphodiesterase (TDP1) complexed with vanadate mimicking the transition state (Davies *et al.* 2004) (Fig. 30*a*). One of the two conserved His residues acts as the nucleophile and the other as the general acid to protonate the leaving group (Fig. 30*b*).

https://doi.org/10.1017/S0033583510000181 Published online by Cambridge University Press

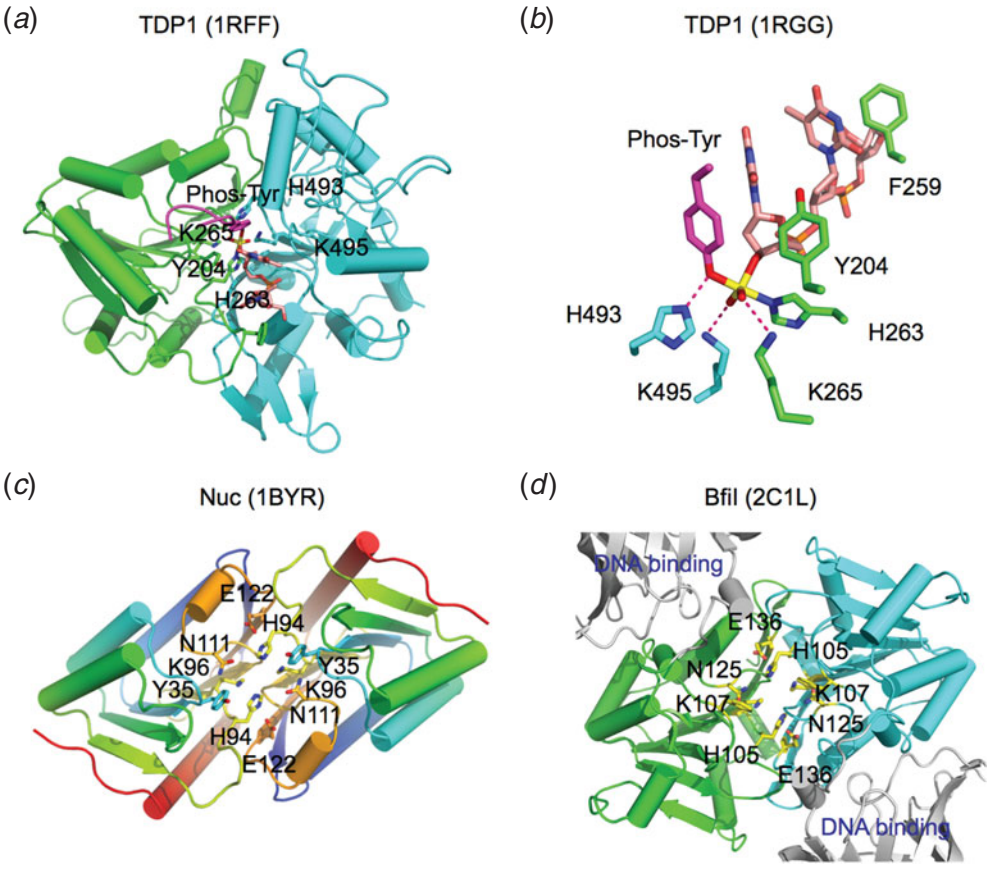


Fig. 30. Metal-independent DNase of the PLD family. (*a*) The overall structure of tyrosine dephosphatase (TDP1). TDP1 serves as a paradigm of phosphoryl transferases using His as the nucleophile. Two gene-duplicated domains are shown in green and cyan. The phosphorylated Tyr is shown in magenta, the scissile phosphate in yellow sticks and the remaining oligonucleotides in pink. The catalytic residues are shown in sticks and colored in green and cyan as the Cα atoms. (*b*) A close-up view of the catalytic center. A mimic of the covalent intermediate (vanadate) is shown in yellow. The duplicated His and Lys are directly involved in catalysis. (*c*) The overall structure of *S. typ* Nuc is shown in the orientation similar to TDP1 in (*a*). The two identical subunits are both shown in rainbow colors. (*d*) The catalytic domains of dimeric restriction endonuclease BfiI. The catalytic domains of two subunits are shown in green and cyan and oriented similarly as TDP1 and Nuc. Sequence-specific DNA-binding domains are shown in silver gray.

10.1.1 Nuc and DNase II

Nuc of *Salmonella typhimurium* provided the first glimpse of a PLD family enzyme. It is a homodimer. The conserved His residues from two subunits (H94) align a narrow groove forming one active site and most probably act as the nucleophile and general acid in the *trans*-esterification reaction (Stuckey & Dixon, 1999) (Fig. 30*c*). The reaction intermediate may be stabilized by the conserved Lys residues (K96) much as in cleavage by RNase A. The structure and metal-ion-independent catalysis indicate that the DNA substrate is recognized in the single-stranded form. Like all PLD-like DNases, Nuc generates 5′-phosphate and 3′-OH. Metazoa DNase II are homologs of bacterial Nuc and belong to the PLD family. DNase II in lysosomes of macrophages plays an essential role in degrading DNA downstream from CAD/DFF40 after

https://doi.org/10.1017/S0033583510000181 Published online by Cambridge University Press

engulfment of apoptotic cells (Nagata, 2007). Without DNase II, residual DNA fragments lead to autoimmune diseases. The Nuc and DNase II are non-sequence specific.

10.1.2 BfiI restriction endonuclease

BfiI restriction endonuclease presents the first crystal structure of Mg^{2+} independent type-II restriction endonucleases (Grazulis *et al.* 2005; Vitkute *et al.* 1998). It is a homodimer in solution and the two PLD-like domains form one active site (Lagunavicius *et al.* 2003) (Fig. 30*d*). Like all PLD-family enzymes, BfiI cleaves DNA via a two-step *trans*-esterification mechanism (Sasnauskas *et al.* 2007). In the first step, it uses the conserved His as a nucleophile to cleave DNA forming a 5′ phosphoenzyme. In the second step, it transfers the phosphodiester bond to a water or alcohol molecule to regenerate the enzyme. The transition intermediate is likely to be stabilized by the conserved Lys residues as in TDP1 (Davies *et al.* 2004). Although BfiI cleaves dsDNA, it cleaves one strand first and then the second (Sasnauskas *et al.* 2010). Sequence-specific recognition is achieved by the DNA-binding domains that are separate from the catalytic domains (Fig. 30*d*) and occurs several base pairs away from the cleavage site (Grazulis *et al.* 2005; Vitkute *et al.* 1998).

10.2 TopIB and Tyr recombinase

TopIB and Tyr recombinases share a conserved catalytic core and similar reaction mechanism (Cheng *et al.* 1998; Hickman *et al.* 1997). These recombinases and topoisomerases contain one or more DNA-binding domains in addition to the catalytic domain and often have a preference for certain DNA sequences. They all have an absolutely conserved Tyr, which serves as the nucleophile and forms a phosphotyrosyl DNA–protein bond. The cleavage reaction produces a 3′-phosphotyrosine and 5′-OH. The DNA–enzyme covalent bond is cleaved by the 5′-OH of DNA in the religation step of recombination or topoisomerization (Grindley *et al.* 2006; Schoeffler & Berger, 2008). If Topo IB fails to religate the DNA, the covalently linked DNA and protein intermediate is the substrate of TDP1 (Fig. 30*a* and *b*) (Pouliot *et al.* 1999). In the absence of a DNA substrate, the Tyr is disordered or in a conformation unsuitable for catalysis (Biswas *et al.* 2005; Cheng *et al.* 1998; Kwon *et al.* 1997; Perry *et al.* 2006b; Yang & Mizuuchi, 1997). In the assembled active site, the Tyr is surrounded by a handful of basic residues which participate in the chemistry of cleavage and religation.

10.2.1 TopIBs

TopIBs relax supercoiled DNA. They can be sequence-specific like viral topoisomerases (Cheng *et al.* 1998) or have weak preference for certain DNA sequences like eukaryotic cellular TopIB (Redinbo *et al.* 1998). Many crystal structures of Topo 1B, from protein alone (Cheng *et al.* 1998), protein–DNA complexes (Perry *et al.* 2006b; Redinbo *et al.* 1998) to a cleavage transition mimic (Davies *et al.* 2006), have been determined. The active site contains two Arg, one Lys, one His and the nucleophile Tyr (Fig. 31*a*). The basic residues orient and neutralize the DNA backbone. One conserved Arg that is hydrogen bonded to both scissile phosphate and the nucleophile Tyr (Fig. 31*b*) is postulated to be the general base to deprotonate the Tyr (Davies *et al.* 2006; Yakovleva *et al.* 2008). The remaining Arg is proposed to work together with the Lys to act as the general acid and protonate the 5′ leaving group (Hwang *et al.* 1998; Yakovleva *et al.* 2008).

https://doi.org/10.1017/S0033583510000181 Published online by Cambridge University Press

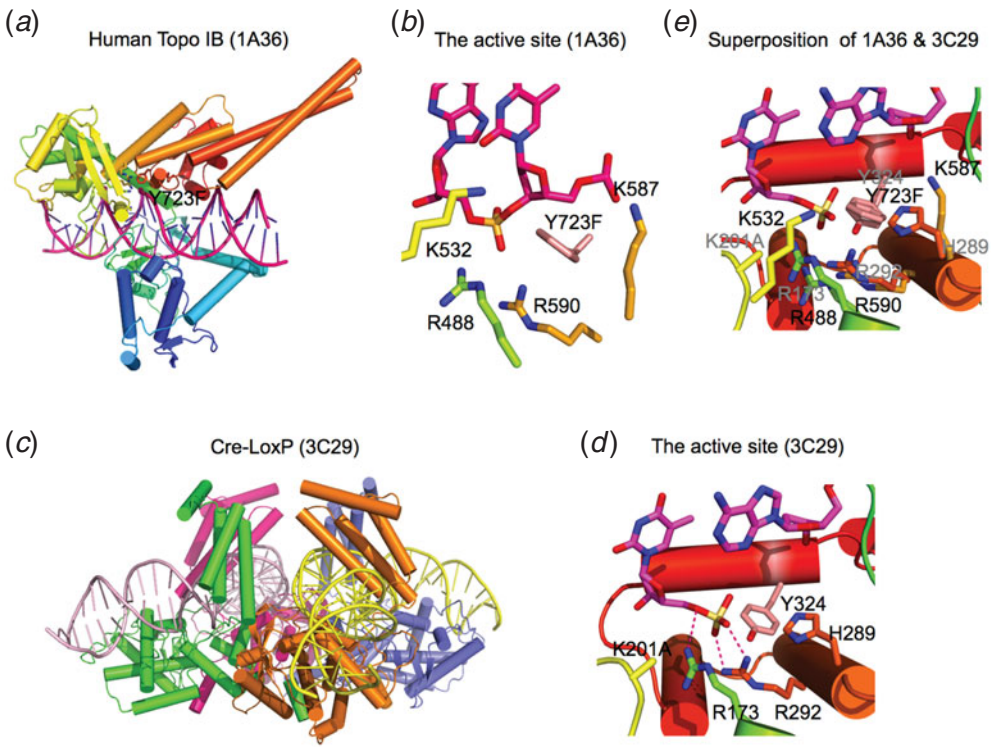


Fig. 31. Metal-independent topoisomerases and Tyr recombinases. (*a*) The overall structure of Human Topo IB. The protein is shown in rainbow-colored ribbon diagrams. The DNA duplex is shown in pink/blue ribbons. The active site is highlighted with the catalytic residues shown in sticks. The nucleophile Y723 (mutated to Phe) is labeled. (*b*) A close-up view of the active site of Topo IB. The reaction is stopped because of the Y723F (shown in pink) mutation. The scissile phosphate is neutralized by Arg and Lys side chains. (*c*) The overall structure of the Cre recombinase complexed with substrate LoxP site. The tetrameric Cre is shown in four colors and the two LoxP in pink and yellow. The DNA-binding domains are above the DNA and the catalytic domains are below. (*d*) A close-up view of the active site of Cre-LoxP. The scissile phosphate is already pre-nicked. (*e*) Superposition of the catalytic residues of Topo IB and Cre.

10.2.2 Tyr recombinases: Cre, Flp, Xer and Phage integrase

The representative members of the Tyr recombinase superfamily include phage integrases (λ and HP1) (Biswas *et al.* 2005; Hickman *et al.* 1997), the Cre–loxP recombination system (Baldwin *et al.* 2003; Guo *et al.* 1997) widely used in the gene knockout techniques, XerC/D for bacterial DNA segregation (Subramanya *et al.* 1997), and yeast Flp recombinase (Chen *et al.* 2000). They are all site-specific recombinases and share the conserved catalytic motif RHR in addition to the Tyr nucleophile. These recombinases are most often bi-lobal with a sequence-specific DNA-binding domain at the N-terminus and catalytic domain at the C-terminus (Fig. 31*c*). Many crystal structures have been determined along the reaction pathway (Grindley *et al.* 2006), and the active site and the surrounding structure of these recombinases can be superimposed with that of Topo IB (Fig. 31*d* and *e*). The Tyr nucleophile is located on the third helix in a three-helix bundle, which resembles a classic HTH domain (Yang & Steitz, 1995a) (Fig. 31*d*). Positioning the Tyr for nucleophilic attack requires the synapsis of four protein subunits and two palindromic DNA recombination sites (Ghosh *et al.* 2007a) (Fig. 31*c*). A HJ is a necessary intermediate in

https://doi.org/10.1017/S0033583510000181 Published online by Cambridge University Press

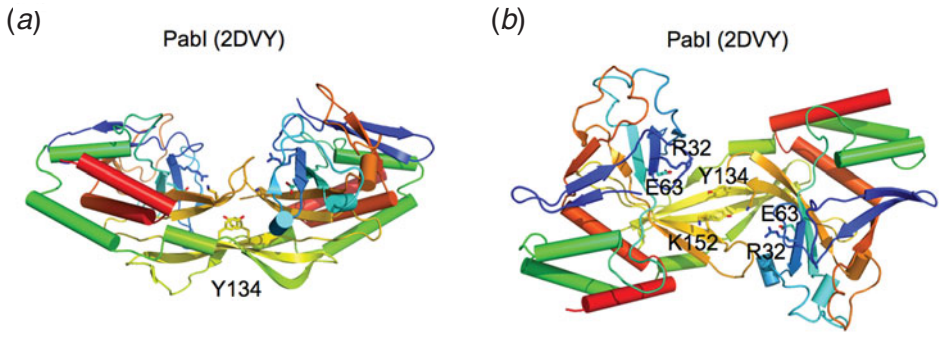


Fig. 32. PabI family of restriction endonuclease. (*a*) The overall structure of homodimeric PabI. Two subunits are both shown in rainbow colors. The shape is likened to a halfpipe. The catalytically essential Y134 from both subunits are close together at the bottom of the central groove. (*b*) An orthogonal view of PabI. The catalytically essential residues are shown in sticks and labeled.

recombination (Voziyanov *et al.* 1999). A catalytically competent active site may consist of residues from two adjacent subunits (so-called *trans*-configuration) (Chen *et al.* 2000). The Tyr nucleophile is likely to be deprotonated by one of the two conserved Arg residues as with human and vaccinia Topo IB (Fig. 31*e*) (Redinbo *et al.* 2000; Yakovleva *et al.* 2008). The other conserved Arg and Lys residues in the active site orient the scissile phosphate, stabilize the transition state, and may also protonate the 5′-O leaving group.

10.3 Halfpipe restriction endonuclease

The last group of metal-ion-independent nucleases is represented by the newly identified restriction endonucleases PabI encoded by transposable elements in archaea (Ishikawa *et al.* 2005). Homologs of PabI possibly exist in bacteria as well. They are called 'halfpipe', because the quaternary structure of the homodimeric enzyme resembles a halfpipe with a deep groove in the center (Fig. 32) (Miyazono *et al.* 2007). The nuclease is highly toxic to cells, presumably because of its nuclease activity. Overexpression was achieved in a cell-free system for the biochemical and structural studies. The crystal structure is determined without DNA substrate, and the catalytic mechanism is unclear. Mutagenesis indicates that the conserved Tyr (Y134), Glu and Arg are indispensable for the catalytic activity (Miyazono *et al.* 2007). It is not known whether a DNA–tyrosyl covalent bond is formed in the process of DNA cleavage.

11. Concluding remarks and future directions

11.1 Metal ions and nucleases

Classification of nucleases by metal-ion dependence highlights the following general properties. Firstly, when metal ions are not directly involved in catalysis, RNase and DNase do not (and perhaps cannot) use water molecules as nucleophiles to attack a phosphodiester bond. The 2′-OH immediately adjacent to the scissile phosphate is universally used by metal-independent RNase for nucleophilic attack, whereas the hydroxyl group of Tyr or Ser or the imidazole of His is used by metal-independent DNase. Each of these ribose and side-chain nucleophiles has a lower pK_a than water and is more readily deprotonated at physiological pH. In these

https://doi.org/10.1017/S0033583510000181 Published online by Cambridge University Press

metal-independent nucleolytic reactions, cleavage requires a second step to hydrolyze the cyclic diphosphate or covalent enzyme–substrate intermediate (Figs 1*b*, 2*d* and *e*). Incorporation of one or two metal ions into an active site, however, allows water to be a nucleophile and cleavage to occur in one step. Interestingly, the metal-ion site in common between the one and two metal-ion-dependent mechanisms is situated on the leaving group side (B site) (Yang, 2008) and is not directly involved in deprotonating and activating the nucleophilic water.

Secondly, metal-ion-dependent nucleases cleave nucleic acid in the base-stacked helical conformation whether single- or double-stranded, whereas metal-independent nucleases prefer a base unpaired and unstacked single-stranded substrate, for example, all metal-independent RNase and PLD-like DNase. TopIBs and Tyr recombinases are exceptional and cleave a scissile phosphate embedded in the double helix with assistances of Arg and Lys side chains reaching into the DNA minor groove (Fig. 31*a*). Interestingly, these DNases cleave one strand only. This is likely because two such active sites cannot be easily configured in the minor groove adjacent to each other.

Thirdly, cleavage products of metal-ion-dependent reactions are a 5′-phosphate and 3′-OH groups, and products of metal-ion-independent reactions are most often a 5′-OH and 3′-phosphate. This division is observed among all RNase, but among DNase there are a couple of exceptions. SNase (section 6.17.1) is metal dependent but produces 3′-phosphate products. Ser recombinases (section 8.2) and DNase II and BfiII of the PLD family (section 10.1) cleave DNA without metal ions and produce 5′-phosphoserine and 5′-phosphohistidine intermediates, respectively.

Fourthly, nucleases that require no or one metal ion for catalysis most often require specific inhibitors to keep their activity in check. This requirement for inhibition is evident for eukaryotic RNase A and homologs (section 9.3), death-associated DNase (Endo G, Nuc, CAD and DNase II, sections 7.1.4 and 10.1.1), and microbial colicins (sections 7.1.4.3, 9.1.4 and 9.2). The process of inhibition can be quite cumbersome, and each nuclease often requires a specific inhibitor (Ghosh *et al.* 2007b; Kolade *et al.* 2002; Rutkoski & Raines, 2008; Widlak & Garrard, 2005). In contrast, two-metal-ion-dependent nucleases rarely require specific inhibitors to regulate their cleavage activity. The most prevalent protection is by DNA methylation in the restriction–modification systems (Bujnicki, 2001). An addition of methyl groups to a DNA recognition sequence is often sufficient to stop nuclease digestion. The reason that restriction–modification systems can work may be a result of the improved coupling between substrate recognition and catalysis of bond cleavage by the two-metal-ion mechanism (Yang *et al.* 2006). Although one-metal- and no-metal-dependent nucleases can be sequence specific, substrate recognition and the cleavage reaction are less tightly coupled for these enzymes than for two-metal-ion-dependent nucleases, and specificity is achieved by the recognition of longer DNA sequences (e.g. homing endonucleases), additional separate DNA-binding domains (KpnI and BfiI), and formation of high-order protein–DNA complexes (e.g. site-specific recombination).

11.2 Diversity and convergence

Two themes emerge from analyzing the diversity and convergence of nucleases and their biological functions. At one end of the spectrum, a wide range of nucleases of different structures and catalytic mechanisms are employed to catalyze a similar biological reaction. At the other end of the spectrum, a conserved structural module and catalytic sequence motif may function in divergent or completely unrelated biological pathways.

https://doi.org/10.1017/S0033583510000181 Published online by Cambridge University Press

11.2.1 Diversity of nucleases in a similar cleavage reaction

In the first category, the divergence of restriction endonucleases, HJ resolvases, site-specific recombinases, homing endonuclease and AP endonucleases stand out. As noted by Darwin, greater variation is found closer to the evolutionary source of a species. This principal is exemplified in the recent genomic sequencing of African Bushmen (Schuster *et al.* 2010), which reveals that the genetic differences between any two Bushmen is greater than that between a European and an Asian. The diversity of nucleases may indicate that repair of an abasic lesion, homologous and site-specific DNA recombination and restrictive digestion of foreign DNA are ancient processes. The different nucleases that result in a shared outcome may also provide hints of a convergent relationship. For example, two AP endonucleases, Endo IV and Exo III (APE1) (sections 6.7.2 and 6.1.6.1), recognize the abasic site in a very similar way and use the pro-Rp oxygen to coordinate the catalytic two metal ions despite their unrelated tertiary structure and catalytic motifs.

Two cases of diverse nucleases for one biological process are worth noting. HJ or four-way DNA junctions are resolved to two duplexes by nucleases with different structure and mechanisms. Even among bacterial and single-cell eukaryotes there are more than four different HJ resolvases (Table 1). In higher eukaryotes, HJ resolvases exhibit additional diversity both in catalytic motifs and nuclease organization (Fekairi *et al.* 2009; Ip *et al.* 2008). HJ resolvases in lower organisms are homodimeric regardless of differences in catalytic mechanisms and symmetrically cleave fully base-paired four-way junctions in antiparallel or square–planar configurations (Biertümpfel *et al.* 2007; Hadden *et al.* 2007; Lilley & White, 2001). Eukaryotic HJ resolvase SLX1–SLX4 and Mus81-Eme1, however, are heterodimeric, and only one subunit contains the active site (Blanco *et al.* 2010; Ciccia *et al.* 2008). Instead of symmetric and fully base-paired junctions, eukaryotic HJ resolvases can recognize and cleave asymmetric ssDNA flaps. In bacteria, HJ often occur due to localized short palindromic sequences, which can be easily arranged in symmetric antiparallel or open-square conformation to be cleaved by homodimeric HJ resolvases. But in eukaryotes, four-way junctions often arise during homologous recombination between two distal sites or sister chromatids, where a symmetric HJ in antiparallel conformation is not easily achievable. The increasing diversity in HJ resolvases may correlate with the increased genomic complexity from bacteria to eukaryotes.

At least four different types of endonucleases are involved in site-specific DNA recombination: two kinds of Tyr recombinases (sections 7.3 and 10.2), Ser recombinases (section 8.2) and many two-metal-ion-dependent transposases (section 6.2.2). The catalytic mechanisms of these nucleases range from no metal, one-metal to two-metal dependent. Ser and Tyr recombinases are rarely found in eukaryotes and are absent in plants and metazoa. In contrast, two-metal-ion-dependent transposases/recombinases are widespread in bacteria, retroviruses and lower and higher eukaryotes. Usage of two-metal-ion catalysis is also associated with the cut-and-paste mechanism and a widened selection of target DNA for recombination.

11.2.2 Adaptation of a catalytic motif in various nucleases

Several catalytic modules of conserved structure and mechanism are found in many DNases and RNases (see sections 6.1–6.4 and 7.1). The wide distribution of a particular catalytic module is likely to reflect its catalytic efficiency. For example, the DEDD motif is associated with a large number of 3′ exonucleases, regardless of whether the substrate is DNA or RNA, and FEN1-like nucleases containing both a 5′ exo and endonuclease activity are found to remove

https://doi.org/10.1017/S0033583510000181 Published online by Cambridge University Press

primers in DNA replication and to cleave nucleic acid in HJ resolution, DNA repair and RNA processing.

Two catalytic motifs have the widest adaptation and are associated with the most diverse functions. They are the REase fold with the DEK motif (section 6.3) and the $\beta\beta\alpha$-Me motif (section 7.1). These two catalytic motifs share the following features, which may allow them to be incorporated into different nucleases and different pathways. Firstly, the conserved catalytic motif is modular and small in size. Both the DEK and $\beta\beta\alpha$-Me motifs are often contained within a stretch of 20–30 residues. The DEK motif occurs in a β-hairpin structure (Fig. 8), and the $\beta\beta\alpha$-Me motif consists of a β-hairpin followed by an α-helix (Fig. 21). Thus, the DEK and $\beta\beta\alpha$-Me motifs are readily incorporated into diverse surrounding tertiary structures and adapted to different nuclease activities and pathways. Secondly, both the DEK and $\beta\beta\alpha$-Me motif are extremely tolerant of amino acid substitutions. Except for the first D in the DEK motif and a His serving as the general base in $\beta\beta\alpha$-Me, other catalytic residues can vary greatly (see sections 6.3 and 7.1). Thirdly, the REase-like nucleases are further aided by the two-metal-ion mechanism in substrate specificity and catalytic efficiency.

It is worth noting that metal-ion-dependent mechanisms appear most adaptable. This observation may be explained by the advantages of specificity, efficiency and diversity endowed by metal ions (Yang *et al.* 2006). Multiple metal-independent mechanisms and varied catalytic motifs are found among RNases, and this is likely due to efficient catalysis using a 2′-OH as the nucleophile. Adaptation of metal-independent mechanisms among DNase is rather limited and with few alterations, e.g. DNase II *versus* BfiI and TopIBs *versus* Tyr recombinases. The small number of metal-independent DNase may be a result of the limited types of reactions catalyzed and additional requirements for regulation and inhibition of cleavage activity.

11.3 Future directions

Although nucleases are the oldest nucleic acid enzymes characterized, new nucleases are being discovered every year and it is safe to predict that this trend will continue. Among the more recently discovered nucleases, several have novel sequence motifs, and their structures cannot be modeled using existing nucleases. For example, Sae2 in meiotic DNA break repair and nucleases in CRISPR pathways have unique catalytic motifs and unknown structures. For the well-studied processes of mRNA splicing and processing, the mechanism of the spliceosome and involvement of exon junction complex and nonsense-mediated decay are still being fleshed out. Furthermore, for many nucleases whose structures are known or are homologous to nucleases of known structure the catalytic mechanism remains unclear without additional atomic structures of functional enzyme–substrate complexes. Last but not the least many nucleases are linked to genetic or infectious diseases and are potential therapeutic targets. It is clear that exciting discoveries will continue to expand our understanding of these diverse and essential enzymes.

12. Acknowledgment

W.Y. is supported by NIH, NIDDK intramural research fund. The author thanks Dr C. Biertuempfel for initially collecting nucleases deposited with PDB database, and Drs R. Craigie and D. Leahy for reading and editing the manuscript.

https://doi.org/10.1017/S0033583510000181 Published online by Cambridge University Press

13. References

Abelson, J., Trotta, C. R. & Li, H. (1998). tRNA splicing. *Journal of Biological Chemistry* **273**, 12685–12688.

Adams, P. L., Stahley, M. R., Kosek, A. B., Wang, J. & Strobel, S. A. (2004). Crystal structure of a self-splicing group I intron with both exons. *Nature* **430**, 45–50.

Aizawa, Y., Xiang, Q., Lambowitz, A. M. & Pyle, A. M. (2003). The pathway for DNA recognition and RNA integration by a group II intron retrotransposon. *Molecular Cell* **11**, 795–805.

Akutsu, A., Masaki, H. & Ohta, T. (1989). Molecular structure and immunity specificity of colicin E6, an evolutionary intermediate between E-group colicins and cloacin DF13. *Journal of Bacteriology* **171**, 6430–6436.

Allemand, F., Mathy, N., Brechemier-Baey, D. & Condon, C. (2005). The 5S rRNA maturase, ribonuclease M5, is a Toprim domain family member. *Nucleic Acids Research* **33**, 4368–4376.

Altermark, B., Smalas, A. O., Willassen, N. P. & Helland, R. (2006). The structure of *Vibrio cholerae* extracellular endonuclease I reveals the presence of a buried chloride ion. *Acta Crystallographica D: Biological Crystallography* **62**, 1387–1391.

Andersen, K. R., Jonstrup, A. T., Van, L. B. & Brodersen, D. E. (2009). The activity and selectivity of fission yeast Pop2p are affected by a high affinity for Zn^{2+} and Mn^{2+} in the active site. *RNA* **15**, 850–861.

Andrade, J. M., Pobre, V., Silva, I. J., Domingues, S. & Arraiano, C. M. (2009). The role of 3′–5′ exoribonucleases in RNA degradation. *Progress in Molecular Biology and Translation Sciences* **85**, 187–229.

Anfinsen, C. B. (1973). Principles that govern the folding of protein chains. *Science* **181**, 223–230.

Aravind, L. (1999). An evolutionary classification of the metallo-beta-lactamase fold proteins. *In Silico Biology* **1**, 69–91.

Aravind, L. & Koonin, E. V. (1998). A novel family of predicted phosphoesterases includes Drosophila prune protein and bacterial RecJ exonuclease. *Trends in Biochemical Sciences* **23**, 17–19.

Aravind, L., Leipe, D. D. & Koonin, E. V. (1998). Toprim – a conserved catalytic domain in type IA and II topoisomerases, DnaG-type primases, OLD family nucleases and RecR proteins. *Nucleic Acids Research* **26**, 4205–4213.

Arcus, V. L., Backbro, K., Roos, A., Daniel, E. L. & Baker, E. N. (2004). Distant structural homology leads to the functional characterization of an archaeal PIN domain as an exonuclease. *Journal of Biological Chemistry* **279**, 16471–16478.

Ariyoshi, M., Vassylyev, D. G., Iwasaki, H., Nakamura, H., Shinagawa, H. & Morikawa, K. (1994). Atomic structure of the RuvC resolvase: a Holliday junction-specific endonuclease from *E. coli*. *Cell* **78**, 1063–1072.

Arni, R. K., Watanabe, L., Ward, R. J., Kreitman, R. J., Kumar, K. & Walz, Jr. F. G. (1999). Three-dimensional structure of ribonuclease T1 complexed with an isosteric phosphonate substrate analogue of GpU: alternate substrate binding modes and catalysis. *Biochemistry* **38**, 2452–2461.

Artymiuk, P. J., Ceska, T. A., Suck, D. & Sayers, J. R. (1997). Prokaryotic 5′–3′ exonucleases share a common core structure with gamma-delta resolvase. *Nucleic Acids Research* **25**, 4224–4229.

Avey, H. P., Boles, M. O., Carlisle, C. H., Evans, S. A., Morris, S. J., Palmer, R. A., Woolhouse, B. A. & Shall, S. (1967). Structure of ribonuclease. *Nature* **213**, 557–562.

Baldwin, E. P., Martin, S. S., Abel, J., Gelato, K. A., Kim, H., Schultz, P. G. & Santoro, S. W. (2003). A specificity switch in selected cre recombinase variants is mediated by macromolecular plasticity and water. *Chemistry and Biology* **10**, 1085–1094.

Baldwin, G. S., Waley, S. G. & Abraham, E. P. (1979). Identification of histidine residues that act as zinc ligands in beta-lactamase II by differential tritium exchange. *Biochemical Journal* **179**, 459–463.

Ban, C. & Yang, W. (1998a). Crystal structure and ATPase activity of MutL: implications for DNA repair and mutagenesis. *Cell* **95**, 541–552.

Ban, C. & Yang, W. (1998b). Structural basis for MutH activation in *E. coli* mismatch repair and relationship of MutH to restriction endonucleases. *EMBO Journal* **17**, 1526–1534.

Barabas, O., Ronning, D. R., Guynet, C., Hickman, A. B., Ton-Hoang, B., Chandler, M. & Dyda, F. (2008). Mechanism of IS200/IS605 family DNA transposases: activation and transposon-directed target site selection. *Cell* **132**, 208–220.

Bechhofer, D. H. (2009). Messenger RNA decay and maturation in *Bacillus subtilis*. *Progress in Molecular Biology and Translation Sciences* **85**, 231–273.

Beese, L. S. & Steitz, T. A. (1991). Structural basis for the 3′–5′ exonuclease activity of *Escherichia coli* DNA polymerase I: a two metal ion mechanism. *EMBO Journal* **10**, 25–33.

Beloglazova, N., Brown, G., Zimmerman, M. D., Proudfoot, M., Makarova, K. S., Kudritska, M., Kochinyan, S., Wang, S., Chruszcz, M., Minor, W., Koonin, E. V., Edwards, A. M., Savchenko, A. & Yakunin, A. F. (2008). A novel family of sequence-specific endoribonucleases associated with the clustered regularly interspaced short palindromic repeats. *Journal of Biological Chemistry* **283**, 20361–20371.

Benedik, M. J. & Strych, U. (1998). Serratia marcescens and its extracellular nuclease. *FEMS Microbiology Letters* **165**, 1–13.

Bennett, R. J., Dunderdale, H. J. & West, S. C. (1993). Resolution of Holliday junctions by RuvC resolvase: cleavage specificity and DNA distortion. *Cell* **74**, 1021–1031.

https://doi.org/10.1017/S0033583510000181 Published online by Cambridge University Press

Bhagwat, M., Hobbs, L. J. & Nossal, N. G. (1997). The 5′-exonuclease activity of bacteriophage T4 RNase H is stimulated by the T4 gene 32 single-stranded DNA-binding protein, but its flap endonuclease is inhibited. *Journal of Biological Chemistry* **272**, 28523–28530.

Bhat, A. G., Leelaram, M. N., Hegde, S. M. & Nagaraja, V. (2009). Deciphering the distinct role for the metal coordination motif in the catalytic activity of *Mycobacterium smegmatis* topoisomerase I. *Journal of Molecular Biology* **393**, 788–802.

Biertümpfel, C., Yang, W. & Suck, D. (2007). Crystal structure of T4 endonuclease VII resolving a Holliday junction. *Nature* **449**, 616–620.

Biswas, T., Aihara, H., Radman-Livaja, M., Filman, D., Landy, A. & Ellenberger, T. (2005). A structural basis for allosteric control of DNA recombination by lambda integrase. *Nature* **435**, 1059–1066.

Bitinaite, J., Wah, D. A., Aggarwal, A. K. & Schildkraut, I. (1998). FokI dimerization is required for DNA cleavage. *Proceedings of the National Academy of Sciences USA* **95**, 10570–10575.

Blanco, M. G., Matos, J., Rass, U., Ip, S. C. & West, S. C. (2010). Functional overlap between the structure-specific nucleases Yen1 and Mus81-Mms4 for DNA-damage repair in S. cerevisiae. *DNA Repair* (*Amsterdam*) **9**, 394–402.

Bork, P. & Sander, C. (1993). A hybrid protein kinase-RNase in an interferon-induced pathway? *FEBS Letters* **334**, 149–152.

Brautigam, C. A. & Steitz, T. A. (1998). Structural principles for the inhibition of the 3′–5′ exonuclease activity of *Escherichia coli* DNA polymerase I by phosphorothioates. *Journal of Molecular Biology* **277**, 363–377.

Brautigam, C. A., Sun, S., Piccirilli, J. A. & Steitz, T. A. (1999). Structures of normal single-stranded DNA and deoxyribo-3′-S-phosphorothiolates bound to the 3′–5′ exonucleolytic active site of DNA polymerase I from *Escherichia coli*. *Biochemistry* **38**, 696–704.

Breyer, W. A. & Matthews, B. W. (2000). Structure of *Escherichia coli* exonuclease I suggests how processivity is achieved. *Nature Structural Biology* **7**, 1125–1128.

Brouns, S. J., Jore, M. M., Lundgren, M., Westra, E. R., Slijkhuis, R. J., Snijders, A. P., Dickman, M. J., Makarova, K. S., Koonin, E. V. & Van Der Oost, J. (2008). Small CRISPR RNAs guide antiviral defense in prokaryotes. *Science* **321**, 960–964.

Brucet, M., Querol-Audi, J., Serra, M., Ramirez-Espain, X., Bertlik, K., Ruiz, L., Lloberas, J., Macias, M. J., Fita, I. & Celada, A. (2007). Structure of the dimeric exonuclease TREX1 in complex with DNA displays a proline-rich binding site for WW domains. *Journal of Biological Chemistry* **282**, 14547–14557.

Buckle, A. M. & Fersht, A. R. (1994). Subsite binding in an RNase: structure of a barnase-tetranucleotide complex at 1·76-A resolution. *Biochemistry* **33**, 1644–1653.

Budd, M. E., Choe, W. & Campbell, J. L. (2000). The nuclease activity of the yeast DNA2 protein, which is related to the RecB-like nucleases, is essential *in vivo*. *Journal of Biological Chemistry* **275**, 16518–16529.

Bujnicki, J. M. (2001). Understanding the evolution of restriction–modification systems: clues from sequence and structure comparisons. *Acta biochimica Polonica* **48**, 935–967.

Bunting, K. A., Roe, S. M., Headley, A., Brown, T., Savva, R. & Pearl, L. H. (2003). Crystal structure of the *Escherichia coli* dcm very-short-patch DNA repair endonuclease bound to its reaction product-site in a DNA superhelix. *Nucleic Acids Research* **31**, 1633–1639.

Buttner, K., Wenig, K. & Hopfner, K. P. (2005). Structural framework for the mechanism of archaeal exosomes in RNA processing. *Molecular Cell* **20**, 461–471.

Buttner, S., Eisenberg, T., Carmona-Gutierrez, D., Ruli, D., Knauer, H., Ruckenstuhl, C., Sigrist, C., Wissing, S., Kollroser, M., Frohlich, K. U., Sigrist, S. & Madeo, F. (2007). Endonuclease G regulates budding yeast life and death. *Molecular Cell* **25**, 233–246.

Callaghan, A. J., Grossmann, J. G., Redko, Y. U., Ilag, L. L., Moncrieffe, M. C., Symmons, M. F., Robinson, C. V., Mcdowall, K. J. & Luisi, B. F. (2003). Quaternary structure and catalytic activity of the *Escherichia coli* ribonuclease E amino-terminal catalytic domain. *Biochemistry* **42**, 13848–13855.

Callaghan, A. J., Marcaida, M. J., Stead, J. A., Mcdowall, K. J., Scott, W. G. & Luisi, B. F. (2005). Structure of *Escherichia coli* RNase E catalytic domain and implications for RNA turnover. *Nature* **437**, 1187–1191.

Callebaut, I., Moshous, D., Mornon, J. P. & De Villartay, J. P. (2002). Metallo-beta-lactamase fold within nucleic acids processing enzymes: the beta-CASP family. *Nucleic Acids Research* **30**, 3592–3601.

Calvin, K. & Li, H. (2008). RNA-splicing endonuclease structure and function. *Cell Mol Life Sci* **65**, 1176–1185.

Calvin, K., Xue, S., Ellis, C., Mitchell, M. H. & Li, H. (2008). Probing the catalytic triad of an archaeal RNA splicing endonuclease. *Biochemistry* **47**, 13659–13665.

Carr, S., Walker, D., James, R., Kleanthous, C. & Hemmings, A. M. (2000). Inhibition of a ribosome-inactivating ribonuclease: the crystal structure of the cytotoxic domain of colicin E3 in complex with its immunity protein. *Structure* **8**, 949–960.

Carte, J., Wang, R., Li, H., Terns, R. M. & Terns, M. P. (2008). Cas6 is an endoribonuclease that generates guide RNAs for invader defense in prokaryotes. *Genes and Development* **22**, 3489–3496.

Castillo-Acosta, V. M., Ruiz-Perez, L. M., Yang, W., Gonzalez-Pacanowska, D. & Vidal, A. E. (2009). Identification of a residue critical for the excision of 3′-blocking ends in apurinic/apyrimidinic endonucleases of the Xth family. *Nucleic Acids Research* **37**, 1829–1842.

https://doi.org/10.1017/S0033583510000181 Published online by Cambridge University Press

Cerritelli, S. M. & Crouch, R. J. (2009). Ribonuclease H: the enzymes in eukaryotes. *FEBS Journal* **276**, 1494–1505.

Ceschini, S., Keeley, A., Mcalister, M. S., Oram, M., Phelan, J., Pearl, L. H., Tsaneva, I. R. & Barrett, T. E. (2001). Crystal structure of the fission yeast mitochondrial Holliday junction resolvase Ydc2. *EMBO Journal* **20**, 6601–6611.

Ceska, T. A., Sayers, J. R., Stier, G. & Suck, D. (1996). A helical arch allowing single-stranded DNA to thread through T5 5′-exonuclease. *Nature* **382**, 90–93.

Champoux, J. J. (2001). DNA topoisomerases: structure, function, and mechanism. *Annual Review of Biochemistry* **70**, 369–413.

Champoux, J. J. & Schultz, S. J. (2009). Ribonuclease H: properties, substrate specificity and roles in retroviral reverse transcription. *FEBS Journal* **276**, 1506–1516.

Chanfreau, G., Noble, S. M. & Guthrie, C. (1996). Essential yeast protein with unexpected similarity to subunits of mammalian cleavage and polyadenylation specificity factor (CPSF). *Science* **274**, 1511–1514.

Chang, J. H., Kim, J. J., Choi, J. M., Lee, J. H. & Cho, Y. (2008). Crystal structure of the Mus81–Eme1 complex. *Genes and Development* **22**, 1093–1106.

Changela, A., Digate, R. J. & Mondragon, A. (2001). Crystal structure of a complex of a type IA DNA topoisomerase with a single-stranded DNA molecule. *Nature* **411**, 1077–1081.

Chapados, B. R., Hosfield, D. J., Han, S., Qiu, J., Yelent, B., Shen, B. & Tainer, J. A. (2004). Structural basis for FEN-1 substrate specificity and PCNA-mediated activation in DNA replication and repair. *Cell* **116**, 39–50.

Chatterjee, D. K., Hammond, A. W., Blakesley, R. W., Adams, S. M. & Gerard, G. F. (1991). Genetic organization of the KpnI restriction–modification system. *Nucleic Acids Research* **19**, 6505–6509.

Chen, D. S., Herman, T. & Demple, B. (1991). Two distinct human DNA diesterases that hydrolyze 3′-blocking deoxyribose fragments from oxidized DNA. *Nucleic Acids Research* **19**, 5907–5914.

Chen, W. J., Lai, P. J., Lai, Y. S., Huang, P. T., Lin, C. C. & Liao, T. H. (2007a). Probing the catalytic mechanism of bovine pancreatic deoxyribonuclease I by chemical rescue. *Biochemical and Biophysical Research Communications* **352**, 689–696.

Chen, W. J. & Liao, T. H. (2006). Structure and function of bovine pancreatic deoxyribonuclease I. *Protein and Peptide Letters* **13**, 447–453.

Chen, X., Li, N. & Ellington, A. D. (2007b). Ribozyme catalysis of metabolism in the RNA world. *Chemistry and Biodiversity* **4**, 633–655.

Chen, Y., Narendra, U., Iype, L. E., Cox, M. M. & Rice, P. A. (2000). Crystal structure of a Flp recombinase-Holliday junction complex: assembly of an active oligomer by helix swapping. *Molecular Cell* **6**, 885–897.

Chen, Y. C., Shipley, G. L., Ball, T. K. & Benedik, M. J. (1992). Regulatory mutants and transcriptional control of the *Serratia marcescens* extracellular nuclease gene. *Molecular Microbiology* **6**, 643–651.

Cheng, C., Kussie, P., Pavletich, N. & Shuman, S. (1998). Conservation of structure and mechanism between eukaryotic topoisomerase I and site-specific recombinases. *Cell* **92**, 841–850.

Cheng, Y. & Patel, D. J. (2004). Crystallographic structure of the nuclease domain of 3′hExo, a DEDDh family member, bound to rAMP. *Journal of Molecular Biology* **343**, 305–312.

Chi, Y. I., Martick, M., Lares, M., Kim, R., Scott, W. G. & Kim, S. H. (2008). Capturing hammerhead ribozyme structures in action by modulating general base catalysis. *PLoS Biology* **6**, e234.

Chowdhury, D., Beresford, P. J., Zhu, P., Zhang, D., Sung, J. S., Demple, B., Perrino, F. W. & Lieberman, J. (2006). The exonuclease TREX1 is in the SET complex and acts in concert with NM23-H1 to degrade DNA during granzyme A-mediated cell death. *Molecular Cell* **23**, 133–142.

Christianson, D. W. (1991). Structural biology of zinc. *Advances in Protein Chemistry* **42**, 281–355.

Chu, C. Y. & Rana, T. M. (2007). Small RNAs: regulators and guardians of the genome. *Journal of Cellular Physiology* **213**, 412–419.

Ciccia, A., Mcdonald, N. & West, S. C. (2008). Structural and functional relationships of the XPF/MUS81 family of proteins. *Annual Review of Biochemistry* **77**, 259–287.

Clissold, P. M. & Ponting, C. P. (2000). PIN domains in nonsense-mediated mRNA decay and RNAi. *Current Biology* **10**, R888–890.

Cochrane, J. C. & Strobel, S. A. (2008). Catalytic strategies of self-cleaving ribozymes. *Accounts of Chemical Research* **41**, 1027–1035.

Coleman, J. E. (1992). Structure and mechanism of alkaline phosphatase. *Annual Review of Biophysics and Biomolecular Structure* **21**, 441–483.

Condon, C., Brechemier-Baey, D., Beltchev, B., Grunberg-Manago, M. & Putzer, H. (2001). Identification of the gene encoding the 5S ribosomal RNA maturase in *Bacillus subtilis*: mature 5S rRNA is dispensable for ribosome function. *RNA* **7**, 242–253.

Correll, C. C., Yang, X., Gerczei, T., Beneken, J. & Plantinga, M. J. (2004). RNA recognition and base flipping by the toxin sarcin. *Journal of Synchrotron Radiation* **11**, 93–96.

Cowan, J. A. (2002). Structural and catalytic chemistry of magnesium-dependent enzymes. *Biometals* **15**, 225–235.

Crow, Y. J., Hayward, B. E., Parmar, R., Robins, P., Leitch, A., Ali, M., Black, D. N., Van Bokhoven, H., Brunner, H. G., Hamel, B. C., Corry, P. C., Cowan, F. M., Frints, S. G., Klepper, J., Livingston, J. H., Lynch, S. A., Massey, R. F., Meritet, J. F., Michaud, J. L., Ponsot, G., Voit, T., Lebon, P., Bonthron, D. T.,

https://doi.org/10.1017/S0033583510000181 Published online by Cambridge University Press

Jackson, A. P., Barnes, D. E. & Lindahl, T. (2006a). Mutations in the gene encoding the 3′–5′ DNA exonuclease TREX1 cause Aicardi–Goutieres syndrome at the AGS1 locus. *Nature Genetics* **38**, 917–920.

Crow, Y. J., Leitch, A., Hayward, B. E., Garner, A., Parmar, R., Griffith, E., Ali, M., Semple, C., Aicardi, J., Babul-Hirji, R., Baumann, C., Baxter, P., Bertini, E., Chandler, K. E., Chitayat, D., Cau, D., Dery, C., Fazzi, E., Goizet, C., King, M. D., Klepper, J., Lacombe, D., Lanzi, G., Lyall, H., Martinez-Frias, M. L., Mathieu, M., Mckeown, C., Monier, A., Oade, Y., Quarrell, O. W., Rittey, C. D., Rogers, R. C., Sanchis, A., Stephenson, J. B., Tacke, U., Till, M., Tolmie, J. L., Tomlin, P., Voit, T., Weschke, B., Woods, C. G., Lebon, P., Bonthron, D. T., Ponting, C. P. & Jackson, A. P. (2006b). Mutations in genes encoding ribonuclease H2 subunits cause Aicardi–Goutieres syndrome and mimic congenital viral brain infection. *Nature Genetics* **38**, 910–916.

Crow, Y. J. & Rehwinkel, J. (2009). Aicardi-Goutieres syndrome and related phenotypes: linking nucleic acid metabolism with autoimmunity. *Human Molecular Genetics* **18**, R130–R136.

Cymerman, I. A., Obarska, A., Skowronek, K. J., Lubys, A. & Bujnicki, J. M. (2006). Identification of a new subfamily of HNH nucleases and experimental characterization of a representative member, HphI restriction endonuclease. *Proteins* **65**, 867–876.

Daiyasu, H., Osaka, K., Ishino, Y. & Toh, H. (2001). Expansion of the zinc metallo-hydrolase family of the beta-lactamase fold. *FEBS Letters* **503**, 1–6.

Datta, S., Larkin, C. & Schildbach, J. F. (2003). Structural insights into single-stranded DNA binding and cleavage by F factor TraI. *Structure* **11**, 1369–1379.

Davies, D. R., Goryshin, I. Y., Reznikoff, W. S. & Rayment, I. (2000). Three-dimensional structure of the Tn5 synaptic complex transposition intermediate. *Science* **289**, 77–85.

Davies, D. R., Interthal, H., Champoux, J. J. & Hol, W. G. (2004). Explorations of peptide and oligonucleotide binding sites of tyrosyl-DNA phosphodiesterase using vanadate complexes. *Journal of Medicinal Chemistry* **47**, 829–837.

Davies, D. R., Mushtaq, A., Interthal, H., Champoux, J. J. & Hol, W. G. (2006). The structure of the transition state of the heterodimeric topoisomerase I of *Leishmania donovani* as a vanadate complex with nicked DNA. *Journal of Molecular Biology* **357**, 1202–1210.

De La Sierra-Gallay, I. L., Pellegrini, O. & Condon, C. (2005). Structural basis for substrate binding, cleavage and allostery in the tRNA maturase RNase Z. *Nature* **433**, 657–661.

De Silva, U., Choudhury, S., Bailey, S. L., Harvey, S., Perrino, F. W. & Hollis, T. (2007). The crystal structure of TREX1 explains the 3′ nucleotide specificity and reveals a polyproline II helix for protein partnering. *Journal of Biological Chemistry* **282**, 10537–10543.

Declais, A. C. & Lilley, D. M. (2008). New insight into the recognition of branched DNA structure by junction-resolving enzymes. *Current Opinion in Structural Biology* **18**, 86–95.

Demple, B. & Harrison, L. (1994). Repair of oxidative damage to DNA: enzymology and biology. *Annual Review of Biochemistry* **63**, 915–948.

Desai, N. A. & Shankar, V. (2003). Single-strand-specific nucleases. *FEMS Microbiology Reviews* **26**, 457–491.

Deshpande, R. A. & Shankar, V. (2002). Ribonucleases from T2 family. *Critical Reviews in Microbiology* **28**, 79–122.

Deutscher, M. P. & Li, Z. (2001). Exoribonucleases and their multiple roles in RNA metabolism. *Progress in Nucleic Acid Research and Molecular Biology* **66**, 67–105.

Deutscher, M. P., Marshall, G. T. & Cudny, H. (1988). RNase PH: an *Escherichia coli* phosphate-dependent nuclease distinct from polynucleotide phosphorylase. *Proceedings of the National Academy of Sciences USA* **85**, 4710–4714.

Devos, J. M., Tomanicek, S. J., Jones, C. E., Nossal, N. G. & Mueser, T. C. (2007). Crystal structure of bacteriophage T4 5′ nuclease in complex with a branched DNA reveals how flap endonuclease-1 family nucleases bind their substrates. *Journal of Biological Chemistry* **282**, 31713–31724.

Diaz, R. L., Alcid, A. D., Berger, J. M. & Keeney, S. (2002). Identification of residues in yeast Spo11p critical for meiotic DNA double-strand break formation. *Molecular and Cellular Biology* **22**, 1106–1115.

Diebler, H., Eigen, M., Ilgenfritz, G., Maass, G. & Winkler, R. (1969). Kinetics and mechanisms of reactions of main group metal ions with biological carriers. *Pure Applied Chemistry* **20**, 93–115.

Dillingham, M. S. & Kowalczykowski, S. C. (2008). RecBCD enzyme and the repair of double-stranded DNA breaks. *Microbiology and Molecular Biology Reviews* **72**, 642–671, Table of Contents.

Domanico, P. L. & Tse-Dinh, Y. C. (1991). Mechanistic studies on E. coli DNA topoisomerase I: divalent ion effects. *Journal of Inorganic Biochemistry* **42**, 87–96.

Dominski, Z. (2007). Nucleases of the metallo-beta-lactamase family and their role in DNA and RNA metabolism. *Critical Reviews in Biochemistry and Molecular Biology* **42**, 67–93.

Dong, B., Niwa, M., Walter, P. & Silverman, R. H. (2001). Basis for regulated RNA cleavage by functional analysis of RNase L and Ire1p. *RNA* **7**, 361–373.

Dong, K. C. & Berger, J. M. (2007). Structural basis for gate-DNA recognition and bending by type IIA topoisomerases. *Nature* **450**, 1201–1205.

Doudna, J. A. & Cech, T. R. (2002). The chemical repertoire of natural ribozymes. *Nature* **418**, 222–228.

https://doi.org/10.1017/S0033583510000181 Published online by Cambridge University Press

Dryden, D. T., Murray, N. E. & Rao, D. N. (2001). Nucleoside triphosphate-dependent restriction enzymes. *Nucleic Acids Research* **29**, 3728–3741.

Duan, X., Gimble, F. S. & Quiocho, F. A. (1997). Crystal structure of PI-SceI, a homing endonuclease with protein splicing activity. *Cell* **89**, 555–564.

Duppatla, V., Bodda, C., Urbanke, C., Friedhoff, P. & Rao, D. N. (2009). The C-terminal domain is sufficient for endonuclease activity of *Neisseria gonorrhoeae* MutL. *Biochemical Journal* **423**, 265–277.

Dyda, F., Hickman, A. B., Jenkins, T. M., Engelman, A., Craigie, R. & Davies, D. R. (1994). Crystal structure of the catalytic domain of HIV-1 integrase: similarity to other polynucleotidyl transferases. *Science* **266**, 1981–1986.

Dziembowski, A., Lorentzen, E., Conti, E. & Seraphin, B. (2007). A single subunit, Dis3, is essentially responsible for yeast exosome core activity. *Nature Structural and Molecular Biology* **14**, 15–22.

Eberle, A. B., Lykke-Andersen, S., Muhlemann, O. & Jensen, T. H. (2009). SMG6 promotes endonucleolytic cleavage of nonsense mRNA in human cells. *Nature Structural and Molecular Biology* **16**, 49–55.

Ebihara, A., Yao, M., Masui, R., Tanaka, I., Yokoyama, S. & Kuramitsu, S. (2006). Crystal structure of hypothetical protein TTHB192 from Thermus thermophilus HB8 reveals a new protein family with an RNA recognition motif-like domain. *Protein Science* **15**, 1494–1499.

Eckstein, F. (1985). Nucleoside phosphorothioates. *Annual Review of Biochemistry* **54**, 367–402.

Enari, M., Sakahira, H., Yokoyama, H., Okawa, K., Iwamatsu, A. & Nagata, S. (1998). A caspase-activated DNase that degrades DNA during apoptosis, and its inhibitor ICAD. *Nature* **391**, 43–50.

Falvey, E., Hatfull, G. F. & Grindley, N. D. (1988). Uncoupling of the recombination and topoisomerase activities of the gamma delta resolvase by a mutation at the crossover point. *Nature* **332**, 861–863.

Farazi, T. A., Juranek, S. A. & Tuschl, T. (2008). The growing catalog of small RNAs and their association with distinct Argonaute/Piwi family members. *Development* **135**, 1201–1214.

Fekairi, S., Scaglione, S., Chahwan, C., Taylor, E. R., Tissier, A., Coulon, S., Dong, M. Q., Ruse, C., Yates, J. R., 3RD, Russell, P., Fuchs, R. P., Mcgowan, C. H. & Gaillard, P. H. (2009). Human SLX4 is a Holliday junction resolvase subunit that binds multiple DNA repair/recombination endonucleases. *Cell* **138**, 78–89.

Fekete, R. A. & Frost, L. S. (2000). Mobilization of chimeric oriT plasmids by F and R100-1: role of relaxosome formation in defining plasmid specificity. *Journal of Bacteriology* **182**, 4022–4027.

Ferre-D'amare, A. R., Zhou, K. & Doudna, J. A. (1998). Crystal structure of a hepatitis delta virus ribozyme. *Nature* **395**, 567–574.

Fersht, A. R. & Daggett, V. (2002). Protein folding and unfolding at atomic resolution. *Cell* **108**, 573–582.

Fiedler, T. J., Vincent, H. A., Zuo, Y., Gavrialov, O. & Malhotra, A. (2004). Purification and crystallization of *Escherichia coli* oligoribonuclease. *Acta Crystallographica D: Biological Crystallography* **60**, 736–739.

Flaherty, K. M., Mckay, D. B., Kabsch, W. & Holmes, K. C. (1991). Similarity of the three-dimensional structures of actin and the ATPase fragment of a 70-kDa heat shock cognate protein. *Proceedings of the National Academy of Sciences USA* **88**, 5041–5045.

Flick, K. E., Jurica, M. S., Monnat, R. J., JR. & Stoddard, B. L. (1998). DNA binding and cleavage by the nuclear intron-encoded homing endonuclease I-PpoI. *Nature* **394**, 96–101.

Fogg, J. M., Kvaratskhelia, M., White, M. F. & Lilley, D. M. (2001). Distortion of DNA junctions imposed by the binding of resolving enzymes: a fluorescence study. *Journal of Molecular Biology* **313**, 751–764.

Fontecilla-Camps, J. C., De Llorens, R., Le Du, M. H. & Cuchillo, C. M. (1994). Crystal structure of ribonuclease A.d(ApTpApApG) complex. Direct evidence for extended substrate recognition. *Journal of Biological Chemistry* **269**, 21526–21531.

Frazao, C., Mcvey, C. E., Amblar, M., Barbas, A., Vonrhein, C., Arraiano, C. M. & Carrondo, M. A. (2006). Unravelling the dynamics of RNA degradation by ribonuclease II and its RNA-bound complex. *Nature* **443**, 110–114.

Freemont, P. S., Friedman, J. M., Beese, L. S., Sanderson, M. R. & Steitz, T. A. (1988). Cocrystal structure of an editing complex of Klenow fragment with DNA. *Proceedings of the National Academy of Sciences USA* **85**, 8924–8928.

Friedhoff, P., Franke, I., Meiss, G., Wende, W., Krause, K. L. & Pingoud, A. (1999). A similar active site for non-specific and specific endonucleases. *Nature Structural Biology* **6**, 112–113.

Friedhoff, P., Kolmes, B., Gimadutdinow, O., Wende, W., Krause, K. L. & Pingoud, A. (1996). Analysis of the mechanism of the Serratia nuclease using site-directed mutagenesis. *Nucleic Acids Research* **24**, 2632–2639.

Fukui, K., Nishida, M., Nakagawa, N., Masui, R. & Kuramitsu, S. (2008). Bound nucleotide controls the endonuclease activity of mismatch repair enzyme MutL. *Journal of Biological Chemistry* **283**, 12136–12145.

Gabel, H. W. & Ruvkun, G. (2008). The exonuclease ERI-1 has a conserved dual role in 5·8S rRNA processing and RNAi. *Nature Structural and Molecular Biology* **15**, 531–533.

Gan, J., Shaw, G., Tropea, J. E., Waugh, D. S., Court, D. L. & Ji, X. (2008). A stepwise model for double-stranded RNA processing by ribonuclease III. *Molecular Microbiology* **67**, 143–154.

Gan, J., Tropea, J. E., Austin, B. P., Court, D. L., Waugh, D. S. & Ji, X. (2006). Structural insight into the

https://doi.org/10.1017/S0033583510000181 Published online by Cambridge University Press

mechanism of double-stranded RNA processing by ribonuclease III. *Cell* **124**, 355–366.

Garcin, E. D., Hosfield, D. J., Desai, S. A., Haas, B. J., Bjoras, M., Cunningham, R. P. & Tainer, J. A. (2008). DNA apurinic–apyrimidinic site binding and excision by endonuclease IV. *Nature Structural and Molecular Biology* **15**, 515–522.

Genschel, J., Bazemore, L. R. & Modrich, P. (2002). Human exonuclease I is required for 5′ and 3′ mismatch repair. *Journal of Biological Chemistry* **277**, 13302–13311.

Gerlt, J. A., Coderre, J. A. & Mehdi, S. (1983). Oxygen chiral phosphate esters. *Advances in Enzymology and Related Areas of Molecular Biology* **55**, 291–380.

Ghosh, K., Guo, F. & Van Duyne, G. D. (2007a). Synapsis of loxP sites by Cre recombinase. *Journal of Biological Chemistry* **282**, 24004–24016.

Ghosh, M., Meiss, G., Pingoud, A. M., London, R. E. & Pedersen, L. C. (2007b). The nuclease a-inhibitor complex is characterized by a novel metal ion bridge. *Journal of Biological Chemistry* **282**, 5682–5690.

Glavan, F., Behm-Ansmant, I., Izaurralde, E. & Conti, E. (2006). Structures of the PIN domains of SMG6 and SMG5 reveal a nuclease within the mRNA surveillance complex. *EMBO Journal* **25**, 5117–5125.

Gomis-Ruth, F. X. & Coll, M. (2006). Cut and move: protein machinery for DNA processing in bacterial conjugation. *Current Opinion in Structural Biology* **16**, 744–752.

Gorchakova, G. A. (1981). [Polynucleotide phosphorylase from rat liver nuclei. Determination of the activity and some properties]. *Biokhimiia* **46**, 797–801.

Gorman, M. A., Morera, S., Rothwell, D. G., De La Fortelle, E., Mol, C. D., Tainer, J. A., Hickson, I. D. & Freemont, P. S. (1997). The crystal structure of the human DNA repair endonuclease HAP1 suggests the recognition of extra-helical deoxyribose at DNA abasic sites. *EMBO Journal* **16**, 6548–6558.

Gottlin, E. B., Rudolph, A. E., Zhao, Y., Matthews, H. R. & Dixon, J. E. (1998). Catalytic mechanism of the phospholipase D superfamily proceeds via a covalent phosphohistidine intermediate. *Proceedings of the National Academy of Sciences USA* **95**, 9202–9207.

Grailles, M., Mora, L., Buckingham, R. H., Van Tilbeurgh, H. & De Zamaroczy, M. (2004). Structural inhibition of the colicin D tRNase by the tRNA-mimicking immunity protein. *EMBO Journal* **23**, 1474–1482.

Grazulis, S., Manakova, E., Roessle, M., Bochtler, M., Tamulaitiene, G., Huber, R. & Siksnys, V. (2005). Structure of the metal-independent restriction enzyme BfiI reveals fusion of a specific DNA-binding domain with a nonspecific nuclease. *Proceedings of the National Academy of Sciences USA* **102**, 15797–15802.

Griffith, J. P., Kim, J. L., Kim, E. E., Sintchak, M. D., Thomson, J. A., Fitzgibbon, M. J., Fleming, M. A., Caron, P. R., Hsiao, K. & Navia, M. A. (1995). X-ray structure of calcineurin inhibited by the immunophilin-immunosuppressant FKBP12–FK506 complex. *Cell* **82**, 507–522.

Grindley, N. D., Whiteson, K. L. & Rice, P. A. (2006). Mechanisms of site-specific recombination. *Annual Review of Biochemistry* **75**, 567–605.

Guarne, A., Ramon-Maiques, S., Wolff, E. M., Ghirlando, R., Hu, X., Miller, J. H. & Yang, W. (2004). Structure of the MutL C-terminal domain: a model of intact MutL and its roles in mismatch repair. *Embo Journal* **23**, 4134–4145.

Guerrier-Takada, C., Gardiner, K., Marsh, T., Pace, N. & Altman, S. (1983). The RNA moiety of ribonuclease P is the catalytic subunit of the enzyme. *Cell* **35**, 849–857.

Guo, F., Gopaul, D. N. & Van Duyne, G. D. (1997). Structure of Cre recombinase complexed with DNA in a site-specific recombination synapse. *Nature* **389**, 40–46.

Habraken, Y., Sung, P., Prakash, L. & Prakash, S. (1993). Yeast excision repair gene RAD2 encodes a single-stranded DNA endonuclease. *Nature* **366**, 365–368.

Habraken, Y., Sung, P., Prakash, L. & Prakash, S. (1994). A conserved 5′ to 3′ exonuclease activity in the yeast and human nucleotide excision repair proteins RAD2 and XPG. *Journal of Biological Chemistry* **269**, 31342–31345.

Hadden, J. M., Déclais, A.-C., Carr, S. B., Lilley, D. M. J. & Phillips, E. V. (2007). The structural basis of Holliday junction resolution. *Nature* **449**, 621–624.

Hale, S. P., Poole, L. B. & Gerlt, J. A. (1993). Mechanism of the reaction catalyzed by staphylococcal nuclease: identification of the rate-determining step. *Biochemistry* **32**, 7479–7487.

Hamdan, S., Carr, P. D., Brown, S. E., Ollis, D. L. & Dixon, N. E. (2002). Structural basis for proofreading during replication of the *Escherichia coli* chromosome. *Structure* **10**, 535–546.

Harding, M. M. (1999). The geometry of metal-ligand interactions relevant to proteins. *Acta Crystallographica D: Biological Crystallography* **55**, 1432–1443.

Hare, S., Gupta, S. S., Valkov, E., Engelman, A. & Cherepanov, P. (2010). Retroviral intasome assembly and inhibition of DNA strand transfer. *Nature* **464**, 232–236.

Harrington, J. J. & Lieber, M. R. (1994). The characterization of a mammalian DNA structure-specific endonuclease. *EMBO Journal* **13**, 1235–1246.

Haruki, M., Tsunaka, Y., Morikawa, M., Iwai, S. & Kanaya, S. (2000). Catalysis by *Escherichia coli* ribonuclease HI is facilitated by a phosphate group of the substrate. *Biochemistry* **39**, 13939–13944.

Hennecke, F., Kolmar, H., Brundl, K. & Fritz, H. J. (1991). The vsr gene product of *E. coli* K-12 is a strand- and sequence-specific DNA mismatch endonuclease. *Nature* **353**, 776–778.

https://doi.org/10.1017/S0033583510000181 Published online by Cambridge University Press

Hernick, M. & Fierke, C. A. (2005). Zinc hydrolases: the mechanisms of zinc-dependent deacetylases. *Archives of Biochemistry and Biophysics* **433**, 71–84.

Hickman, A. B., Perez, Z. N., Zhou, L., Musingarimi, P., Ghirlando, R., Hinshaw, J. E., Craig, N. L. & Dyda, F. (2005). Molecular architecture of a eukaryotic DNA transposase. *Nature Structural and Molecular Biology* **12**, 715–721.

Hickman, A. B., Ronning, D. R., Kotin, R. M. & Dyda, F. (2002). Structural unity among viral origin binding proteins: crystal structure of the nuclease domain of adeno-associated virus Rep. *Molecular Cell* **10**, 327–337.

Hickman, A. B., Ronning, D. R., Perez, Z. N., Kotin, R. M. & Dyda, F. (2004). The nuclease domain of adeno-associated virus rep coordinates replication initiation using two distinct DNA recognition interfaces. *Molecular Cell* **13**, 403–414.

Hickman, A. B., Waninger, S., Scocca, J. J. & Dyda, F. (1997). Molecular organization in site-specific recombination: the catalytic domain of bacteriophage HP1 integrase at 2·7 A resolution. *Cell* **89**, 227–237.

Hoard, D. E. & Goad, W. (1968). Products in the initial stages of digestion of polydeoxynucleotides by pancreatic deoxyribonuclease (DNase I). *Journal of Molecular Biology* **31**, 595–606.

Hopfner, K. P., Karcher, A., Craig, L., Woo, T. T., Carney, J. P. & Tainer, J. A. (2001). Structural biochemistry and interaction architecture of the DNA double-strand break repair Mre11 nuclease and Rad50-ATPase. *Cell* **105**, 473–485.

Horton, N. C. (2008). DNA Nucleases. In *Protein–Nucleic Acid Interactions* (eds. P. A. Rice & C. C. Correll), pp. 333–363. Cambridge: Royal Society of Chemistry Publishing.

Horton, N. C. & Perona, J. J. (2004). DNA cleavage by EcoRV endonuclease: two metal ions in three metal ion binding sites. *Biochemistry* **43**, 6841–6857.

Hough, E., Hansen, L. K., Birknes, B., Jynge, K., Hansen, S., Hordvik, A., Little, C., Dodson, E. & Derewenda, Z. (1989). High-resolution (1·5 A) crystal structure of phospholipase C from *Bacillus cereus*. *Nature* **338**, 357–360.

Houseley, J., Lacava, J. & Tollervey, D. (2006). RNA-quality control by the exosome. *Nature Reviews Molecular Cell Biology* **7**, 529–539.

Hsia, K. C., Li, C. L. & Yuan, H. S. (2005). Structural and functional insight into sugar-nonspecific nucleases in host defense. *Current Opinion in Structural Biology* **15**, 126–134.

Hsiao, Y. Y., Nakagawa, A., Shi, Z., Mitani, S., Xue, D. & Yuan, H. S. (2009). Crystal structure of CRN-4: implications for domain function in apoptotic DNA degradation. *Molecular and Cellular Biology* **29**, 448–457.

Hwang, K. Y., Baek, K., Kim, H. Y. & Cho, Y. (1998). The crystal structure of flap endonuclease-1 from Methanococcus jannaschii. *Nature Structural Biology* **5**, 707–713.

Ip, S. C., Rass, U., Blanco, M. G., Flynn, H. R., Skehel, J. M. & West, S. C. (2008). Identification of Holliday junction resolvases from humans and yeast. *Nature* **456**, 357–361.

Irie, M. & Ohgi, K. (2001). Ribonuclease T2. *Methods in Enzymology* **341**, 42–55.

Ishii, R., Minagawa, A., Takaku, H., Takagi, M., Nashimoto, M. & Yokoyama, S. (2005). Crystal structure of the tRNA 3′ processing endoribonuclease tRNase Z from Thermotoga maritima. *Journal of Biological Chemistry* **280**, 14138–14144.

Ishikawa, K., Watanabe, M., Kuroita, T., Uchiyama, I., Bujnicki, J. M., Kawakami, B., Tanokura, M. & Kobayashi, I. (2005). Discovery of a novel restriction endonuclease by genome comparison and application of a wheat-germ-based cell-free translation assay: PabI (5′-GTA/C) from the hyperthermophilic archaeon *Pyrococcus abyssi*. *Nucleic Acids Research* **33**, e112.

Ivanov, I., Tainer, J. A. & Mccammon, J. A. (2007). Unraveling the three-metal-ion catalytic mechanism of the DNA repair enzyme endonuclease IV. *Proceedings of the National Academy of Sciences USA* **104**, 1465–1470.

Iwasaki, H., Takahagi, M., Shiba, T., Nakata, A. & Shinagawa, H. (1991). *Escherichia coli* RuvC protein is an endonuclease that resolves the Holliday structure. *EMBO Journal* **10**, 4381–4389.

Jabri, E., Carr, M. B., Hausinger, R. P. & Karplus, P. A. (1995). The crystal structure of urease from Klebsiella aerogenes. *Science* **268**, 998–1004.

Jakubauskas, A., Giedriene, J., Bujnicki, J. M. & Janulaitis, A. (2007). Identification of a single HNH active site in type IIS restriction endonuclease Eco31I. *Journal of Molecular Biology* **370**, 157–169.

James, R., Kleanthous, C. & Moore, G. R. (1996). The biology of E colicins: paradigms and paradoxes. *Microbiology* **142**, 1569–1580.

Jenny, A., Minvielle-Sebastia, L., Preker, P. J. & Keller, W. (1996). Sequence similarity between the 73-kilodalton protein of mammalian CPSF and a subunit of yeast polyadenylation factor I. *Science* **274**, 1514–1517.

Jensch, F. & Kemper, B. (1986). Endonuclease VII resolves Y-junctions in branched DNA *in vitro*. *EMBO Journal* **5**, 181–189.

Ji, X. (2008). The mechanism of RNase III action: how dicer dices. *Current Topics in Microbiology and Immunology* **320**, 99–116.

Jin, Y., Binkowski, G., Simon, L. D. & Norris, D. (1997). Ho endonuclease cleaves MAT DNA *in vitro* by an inefficient stoichiometric reaction mechanism. *Journal of Biological Chemistry* **272**, 7352–7359.

Johnson, E. R. & Mckay, D. B. (1999). Mapping the role of active site residues for transducing an ATP-induced conformational change in the bovine 70-kDa heat shock cognate protein. *Biochemistry* **38**, 10823–10830.

https://doi.org/10.1017/S0033583510000181 Published online by Cambridge University Press

Jones, S. J., Worrall, A. F. & Connolly, B. A. (1996). Site-directed mutagenesis of the catalytic residues of bovine pancreatic deoxyribonuclease I. *Journal of Molecular Biology* **264**, 1154–1163.

Jonstrup, A. T., Andersen, K. R., Van, L. B. & Brodersen, D. E. (2007). The 1·4-A crystal structure of the S. pombe Pop2p deadenylase subunit unveils the configuration of an active enzyme. *Nucleic Acids Research* **35**, 3153–3164.

Joshua-Tor, L. (2006). The Argonautes. *Cold Spring Harbor Symposia on Quantitative Biology* **71**, 67–72.

Kadyrov, F. A., Dzantiev, L., Constantin, N. & Modrich, P. (2006). Endonucleolytic function of MutLalpha in human mismatch repair. *Cell* **126**, 297–308.

Kadyrov, F. A., Holmes, S. F., Arana, M. E., Lukianova, O. A., O'Donnell, M., Kunkel, T. A. & Modrich, P. (2007). *Saccharomyces cerevisiae* MutLalpha is a mismatch repair endonuclease. *Journal of Biological Chemistry* **282**, 37181–37190.

Kaminska, K. H., Kawai, M., Boniecki, M., Kobayashi, I. & Bujnicki, J. M. (2008). Type II restriction endonuclease R.Hpy188I belongs to the GIY-YIG nuclease superfamily, but exhibits an unusual active site. *BMC Structural Biology* **8**, 48.

Kao, H. I. & Bambara, R. A. (2003). The protein components and mechanism of eukaryotic Okazaki fragment maturation. *Critical Reviews in Biochemistry and Molecular Biology* **38**, 433–452.

Karakas, E., Truglio, J. J., Croteau, D., Rhau, B., Wang, L., Van Houten, B. & Kisker, C. (2007). Structure of the C-terminal half of UvrC reveals an RNase H endonuclease domain with an Argonaute-like catalytic triad. *EMBO Journal* **26**, 613–622.

Kartha, G., Bello, J. & Harker, D. (1967). Tertiary structure of ribonuclease. *Nature* **213**, 862–865.

Kawano, S., Kakuta, Y., Nakashima, T. & Kimura, M. (2006). Crystal structures of the Nicotiana glutinosa ribonuclease NT in complex with nucleoside monophosphates. *Journal of Biochemistry* **140**, 375–381.

Keck, J. L., Roche, D. D., Lynch, A. S. & Berger, J. M. (2000). Structure of the RNA polymerase domain of *E. coli* primase. *Science* **287**, 2482–2486.

Keeney, S. (2001). Mechanism and control of meiotic recombination initiation. *Current Topics in Developmental Biology* **52**, 1–53.

Kennedy, A. K., Haniford, D. B. & Mizuuchi, K. (2000). Single active site catalysis of the successive phosphoryl transfer steps by DNA transposases: insights from phosphorothioate stereoselectivity. *Cell* **101**, 295–305.

Khan, S. A. (2005). Plasmid rolling-circle replication: highlights of two decades of research. *Plasmid* **53**, 126–136.

Kim, D. H. & Mobashery, S. (2001). Mechanism-based inhibition of zinc proteases. *Current Medicinal Chemistry* **8**, 959–965.

Kim, D. R., Dai, Y., Mundy, C. L., Yang, W. & Oettinger, M. A. (1999). Mutations of acidic residues in RAG1 define the active site of the V(D)J recombinase. *Genes and Development* **13**, 3070–3080.

Kim, E. E. & Wyckoff, H. W. (1991). Reaction mechanism of alkaline phosphatase based on crystal structures. Two-metal ion catalysis. *Journal of Molecular Biology* **218**, 449–464.

Kim, J. H., Kim, H. D., Ryu, G. H., Kim, D. H., Hurwitz, J. & Seo, Y. S. (2006). Isolation of human Dna2 endonuclease and characterization of its enzymatic properties. *Nucleic Acids Research* **34**, 1854–1864.

Kim, Y., Eom, S. H., Wang, J., Lee, D. S., Suh, S. W. & Steitz, T. A. (1995). Crystal structure of *Thermus aquaticus* DNA polymerase. *Nature* **376**, 612–616.

Kirsebom, L. A. (2007). RNase P RNA mediated cleavage: substrate recognition and catalysis. *Biochimie* **89**, 1183–1194.

Kleanthous, C., Kuhlmann, U. C., Pommer, A. J., Ferguson, N., Radford, S. E., Moore, G. R., James, R. & Hemmings, A. M. (1999). Structural and mechanistic basis of immunity toward endonuclease colicins. *Nature Structural Biology* **6**, 243–252.

Klein, D. J. & Ferre-D'amare, A. R. (2006). Structural basis of glmS ribozyme activation by glucosamine-6-phosphate. *Science* **313**, 1752–1756.

Klett, R. P., Cerami, A. & Reich, E. (1968). Exonuclease VI, a new nuclease activity associated with E. coli DNA polymerase. *Proceedings of the National Academy of Sciences USA* **60**, 943–950.

Ko, T. P., Liao, C. C., Ku, W. Y., Chak, K. F. & Yuan, H. S. (1999). The crystal structure of the DNase domain of colicin E7 in complex with its inhibitor Im7 protein. *Structure* **7**, 91–102.

Kobe, B. & Deisenhofer, J. (1996). Mechanism of ribonuclease inhibition by ribonuclease inhibitor protein based on the crystal structure of its complex with ribonuclease A. *Journal of Molecular Biology* **264**, 1028–1043.

Kolade, O. O., Carr, S. B., Kuhlmann, U. C., Pommer, A., Kleanthous, C., Bouchcinsky, C. A. & Hemmings, A. M. (2002). Structural aspects of the inhibition of DNase and rRNase colicins by their immunity proteins. *Biochimie* **84**, 439–446.

Kolodner, R., Hall, S. D. & Luisi-Deluca, C. (1994). Homologous pairing proteins encoded by the *Escherichia coli* recE and recT genes. *Molecular Microbiology* **11**, 23–30.

Koonin, E. V. & Ilyina, T. V. (1993). Computer-assisted dissection of rolling circle DNA replication. *Biosystems* **30**, 241–268.

Kosinski, J., Plotz, G., Guarne, A., Bujnicki, J. M. & Friedhoff, P. (2008). The PMS2 subunit of human MutLalpha contains a metal ion binding domain of the iron-dependent repressor protein family. *Journal of Molecular Biology* **382**, 610–627.

Kostelecky, B., Pohl, E., Vogel, A., Schilling, O. & Meyer-Klaucke, W. (2006). The crystal structure of the

https://doi.org/10.1017/S0033583510000181 Published online by Cambridge University Press

zinc phosphodiesterase from *Escherichia coli* provides insight into function and cooperativity of tRNase Z-family proteins. *Journal of Bacteriology* **188**, 1607–1614.

Kovall, R. & Matthews, B. W. (1997). Toroidal structure of lambda-exonuclease. *Science* **277**, 1824–1827.

Kowalczykowski, S. C., Dixon, D. A., Eggleston, A. K., Lauder, S. D. & Rehrauer, W. M. (1994). Biochemistry of homologous recombination in *Escherichia coli*. *Microbiology Reviews* **58**, 401–465.

Kruger, K., Grabowski, P. J., Zaug, A. J., Sands, J., Gottschling, D. E. & Cech, T. R. (1982). Self-splicing RNA: autoexcision and autocyclization of the ribosomal RNA intervening sequence of Tetrahymena. *Cell* **31**, 147–157.

Kuhlmann, U. C., Moore, G. R., James, R., Kleanthous, C. & Hemmings, A. M. (1999). Structural parsimony in endonuclease active sites: should the number of homing endonuclease families be redefined? *FEBS Letters* **463**, 1–2.

Kunitz, M. (1950). Crystalline desoxyribonuclease; isolation and general properties; spectrophotometric method for the measurement of desoxyribonuclease activity. *Journal of General Physiology* **33**, 349–362.

Kwon, H. J., Tirumalai, R., Landy, A. & Ellenberger, T. (1997). Flexibility in DNA recombination: structure of the lambda integrase catalytic core. *Science* **276**, 126–131.

Lagerback, P., Andersson, E., Malmberg, C. & Carlson, K. (2009). Bacteriophage T4 endonuclease II, a promiscuous GIY-YIG nuclease, binds as a tetramer to two DNA substrates. *Nucleic Acids Research* **37**, 6174–6183.

Lagunavicius, A., Sasnauskas, G., Halford, S. E. & Siksnys, V. (2003). The metal-independent type IIs restriction enzyme BfiI is a dimer that binds two DNA sites but has only one catalytic centre. *Journal of Molecular Biology* **326**, 1051–1064.

Lam, A. F., Krogh, B. O. & Symington, L. S. (2008). Unique and overlapping functions of the Exo1, Mre11 and Pso2 nucleases in DNA repair. *DNA Repair* (*Amsterdam*) 7, 655–662.

Landree, M. A., Wibbenmeyer, J. A. & Roth, D. B. (1999). Mutational analysis of RAG1 and RAG2 identifies three catalytic amino acids in RAG1 critical for both cleavage steps of V(D)J recombination. *Genes and Development* **13**, 3059–3069.

Laneve, P., Altieri, F., Fiori, M. E., Scaloni, A., Bozzoni, I. & Caffarelli, E. (2003). Purification, cloning, and characterization of XendoU, a novel endoribonuclease involved in processing of intron-encoded small nucleolar RNAs in *Xenopus laevis*. *Journal of Biological Chemistry* **278**, 13026–13032.

Laneve, P., Gioia, U., Ragno, R., Altieri, F., Di Franco, C., Santini, T., Arceci, M., Bozzoni, I. & Caffarelli, E. (2008). The tumor marker human placental protein 11 is an endoribonuclease. *Journal of Biological Chemistry* **283**, 34712–34719.

Lange, S. J. & Que, L., JR. (1998). Oxygen activating nonheme iron enzymes. *Current Opinion in Chemical Biology* **2**, 159–172.

Lapkouski, M., Panjikar, S., Janscak, P., Smatanova, I. K., Carey, J., Ettrich, R. & Csefalvay, E. (2009). Structure of the motor subunit of type I restriction–modification complex EcoR124I. *Nature Structural and Molecular Biology* **16**, 94–95.

Larkin, C., Datta, S., Harley, M. J., Anderson, B. J., Ebie, A., Hargreaves, V. & Schildbach, J. F. (2005). Inter- and intramolecular determinants of the specificity of single-stranded DNA binding and cleavage by the F factor relaxase. *Structure* **13**, 1533–1544.

Larkin, C., Haft, R. J., Harley, M. J., Traxler, B. & Schildbach, J. F. (2007). Roles of active site residues and the HUH motif of the F plasmid TraI relaxase. *Journal of Biological Chemistry* **282**, 33707–33713.

Laskowski, M., SR. (1985). Nucleases: historical respectives. In *Nucleases* (eds. S. M. Linn & R. J. Roberts), pp. 1–21. Cold Spring Harbor, NY: Cold Spring Harbor Laboratory Press.

Lee, B. I., Kim, K. H., Park, S. J., Eom, S. H., Song, H. K. & Suh, S. W. (2004). Ring-shaped architecture of RecR: implications for its role in homologous recombinational DNA repair. *EMBO Journal* **23**, 2029–2038.

Lee, B. I. & Wilson, D. M., 3RD. (1999). The RAD2 domain of human exonuclease 1 exhibits 5′ to 3′ exonuclease and flap structure-specific endonuclease activities. *Journal of Biological Chemistry* **274**, 37763–37769.

Lee, F. S., Auld, D. S. & Vallee, B. L. (1989). Tryptophan fluorescence as a probe of placental ribonuclease inhibitor binding to angiogenin. *Biochemistry* **28**, 219–224.

Lee, J. Y., Chang, J., Joseph, N., Ghirlando, R., Rao, D. N. & Yang, W. (2005). MutH complexed with Hemi- and unmethylated DNAs: coupling base recognition and DNA cleavage. *Molecular Cell* **20**, 155–166.

Lee, K. P., Dey, M., Neculai, D., Cao, C., Dever, T. E. & Sicheri, F. (2008). Structure of the dual enzyme Ire1 reveals the basis for catalysis and regulation in nonconventional RNA splicing. *Cell* **132**, 89–100.

Lehman, I. R. & Nussbaum, A. L. (1964). The deoxyribonucleases of *Escherichia coli* V on the specificity of exonuclease I (phosphodiesterase). *Journal of Biological Chemistry* **239**, 2628–2636.

Li, G. M. (2008). Mechanisms and functions of DNA mismatch repair. *Cell Research* **18**, 85–98.

Li, W., Kamtekar, S., Xiong, Y., Sarkis, G. J., Grindley, N. D. & Steitz, T. A. (2005). Structure of a synaptic gammadelta resolvase tetramer covalently linked to two cleaved DNAs. *Science* **309**, 1210–1215.

Lilley, D. M. (2005). Structure, folding and mechanisms of ribozymes. *Current Opinion in Structural Biology* **15**, 313–323.

https://doi.org/10.1017/S0033583510000181 Published online by Cambridge University Press

Lilley, D. M. & White, M. F. (2001). The junction-resolving enzymes. *Nature Reviews Molecular Cell Biology* **2**, 433–443.

Liu, Q., Greimann, J. C. & Lima, C. D. (2006). Reconstitution, activities, and structure of the eukaryotic RNA exosome. *Cell* **127**, 1223–1237.

Liu, X., Zou, H., Slaughter, C. & Wang, X. (1997). DFF, a heterodimeric protein that functions downstream of caspase-3 to trigger DNA fragmentation during apoptosis. *Cell* **89**, 175–184.

Liu, Y., Kao, H. I. & Bambara, R. A. (2004). Flap endonuclease 1: a central component of DNA metabolism. *Annual Review of Biochemistry* **73**, 589–615.

Llosa, M., Gomis-Ruth, F. X., Coll, M. & De La Cruz Fd, F. (2002). Bacterial conjugation: a two-step mechanism for DNA transport. *Molecular Microbiology* **45**, 1–8.

Loll, P. J., Quirk, S., Lattman, E. E. & Garavito, R. M. (1995). X-ray crystal structures of staphylococcal nuclease complexed with the competitive inhibitor cobalt(II) and nucleotide. *Biochemistry* **34**, 4316–4324.

Lorentzen, E., Basquin, J., Tomecki, R., Dziembowski, A. & Conti, E. (2008). Structure of the active subunit of the yeast exosome core, Rrp44: diverse modes of substrate recruitment in the RNase II nuclease family. *Molecular Cell* **29**, 717–728.

Lorentzen, E., Dziembowski, A., Lindner, D., Seraphin, B. & Conti, E. (2007). RNA channelling by the archaeal exosome. *EMBO Reports* **8**, 470–476.

Lorentzen, E., Walter, P., Fribourg, S., Evguenieva-Hackenberg, E., Klug, G. & Conti, E. (2005). The archaeal exosome core is a hexameric ring structure with three catalytic subunits. *Nature Structural and Molecular Biology* **12**, 575–581.

Lyamichev, V., Brow, M. A. & Dahlberg, J. E. (1993). Structure-specific endonucleolytic cleavage of nucleic acids by eubacterial DNA polymerases. *Science* **260**, 778–783.

Lykke-Andersen, S., Brodersen, D. E. & Jensen, T. H. (2009). Origins and activities of the eukaryotic exosome. *Journal of Cell Science* **122**, 1487–1494.

Lyons, T. J. & Eide, D. J. (2006). Transport and storage of metal ions in biology. In *Biological Inorganic Chemistry: Structure and Reactivity* (eds. I. Bertini, H. B. Gray, E. I. Stiefel & J. S. Valentine), pp. 57–77. Herndon, VA: University Science Books.

Macelrevey, C., Salter, J. D., Krucinska, J. & Wedekind, J. E. (2008). Structural effects of nucleobase variations at key active site residue Ade38 in the hairpin ribozyme. *RNA* **14**, 1600–1616.

Macmaster, R., Sedelnikova, S., Baker, P. J., Bolt, E. L., Lloyd, R. G. & Rafferty, J. B. (2006). RusA Holliday junction resolvase: DNA complex structure – insights into selectivity and specificity. *Nucleic Acids Research* **34**, 5577–5584.

Macrae, I. J. & Doudna, J. A. (2007). Ribonuclease revisited: structural insights into ribonuclease III family enzymes. *Current Opinion in Structural Biology* **17**, 138–145.

Macrae, I. J., Zhou, K. & Doudna, J. A. (2007). Structural determinants of RNA recognition and cleavage by Dicer. *Nature Structural and Molecular Biology* **14**, 934–940.

Macrae, I. J., Zhou, K., Li, F., Repic, A., Brooks, A. N., Cande, W. Z., Adams, P. D. & Doudna, J. A. (2006). Structural basis for double-stranded RNA processing by Dicer. *Science* **311**, 195–198.

Maguire, M. E. & Cowan, J. A. (2002). Magnesium chemistry and biochemistry. *Biometals* **15**, 203–210.

Makarova, K. S., Grishin, N. V., Shabalina, S. A., Wolf, Y. I. & Koonin, E. V. (2006). A putative RNA-interference-based immune system in prokaryotes: computational analysis of the predicted enzymatic machinery, functional analogies with eukaryotic RNAi, and hypothetical mechanisms of action. *Biology Direct* **1**, 7.

Mandel, C. R., Kaneko, S., Zhang, H., Gebauer, D., Vethantham, V., Manley, J. L. & Tong, L. (2006). Polyadenylation factor CPSF-73 is the pre-mRNA 3′-end-processing endonuclease. *Nature* **444**, 953–956.

Marti, T. M. & Fleck, O. (2004). DNA repair nucleases. *Cellular and Molecular Life Science* **61**, 336–354.

Martinez Valle, F., Balada, E., Ordi-Ros, J. & Vilardell-Tarres, M. (2008). DNase 1 and systemic lupus erythematosus. *Autoimmunity Reviews* **7**, 359–363.

Marzluff, W. F., Wagner, E. J. & Duronio, R. J. (2008). Metabolism and regulation of canonical histone mRNAs: life without a poly(A) tail. *Nature Reviews Genetics* **9**, 843–854.

Masuda-Sasa, T., Imamura, O. & Campbell, J. L. (2006). Biochemical analysis of human Dna2. *Nucleic Acids Research* **34**, 1865–1875.

Mate, M. J. & Kleanthous, C. (2004). Structure-based analysis of the metal-dependent mechanism of H-N-H endonucleases. *Journal of Biological Chemistry* **279**, 34763–34769.

Mathy, N., Benard, L., Pellegrini, O., Daou, R., Wen, T. & Condon, C. (2007). 5′-to-3′ exoribonuclease activity in bacteria: role of RNase J1 in rRNA maturation and 5′ stability of mRNA. *Cell* **129**, 681–692.

Mazzarella, L., Capasso, S., Demasi, D., Di Lorenzo, G., Mattia, C. A. & Zagari, A. (1993). Bovine seminal ribonuclease: structure at 1·9 A resolution. *Acta Crystallographica D: Biological Crystallography* **49**, 389–402.

Mchenry, C. S. (1985). DNA polymerase III holoenzyme of *Escherichia coli*: components and function of a true replicative complex. *Molecular and Cellular Biochemistry* **66**, 71–85.

Merlino, A., Ercole, C., Picone, D., Pizzo, E., Mazzarella, L. & Sica, F. (2008). The buried diversity of bovine seminal ribonuclease: shape and cytotoxicity of the swapped non-covalent form of the enzyme. *Journal of Molecular Biology* **376**, 427–437.

https://doi.org/10.1017/S0033583510000181 Published online by Cambridge University Press

Michel, F., Costa, M. & Westhof, E. (2009). The ribozyme core of group II introns: a structure in want of partners. *Trends in Biochemical Sciences* **34**, 189–199.

Midtgaard, S. F., Assenholt, J., Jonstrup, A. T., Van, L. B., Jensen, T. H. & Brodersen, D. E. (2006). Structure of the nuclear exosome component Rrp6p reveals an interplay between the active site and the HRDC domain. *Proceedings of the National Academy of Sciences USA* **103**, 11898–11903.

Mildvan, A. S., Xia, Z., Azurmendi, H. F., Saraswat, V., Legler, P. M., Massiah, M. A., Gabelli, S. B., Bianchet, M. A., Kang, L. W. & Amzel, L. M. (2005). Structures and mechanisms of Nudix hydrolases. *Archives of Biochemistry and Biophysics* **433**, 129–143.

Mimitou, E. P. & Symington, L. S. (2009). DNA end resection: many nucleases make light work. *DNA Repair* (*Amsterdam*) **8**, 983–995.

Minagawa, A., Takaku, H., Takagi, M. & Nashimoto, M. (2004). A novel endonucleolytic mechanism to generate the CCA 3′ termini of tRNA molecules in Thermotoga maritima. *Journal of Biological Chemistry* **279**, 15688–15697.

Miyazono, K., Watanabe, M., Kosinski, J., Ishikawa, K., Kamo, M., Sawasaki, T., Nagata, K., Bujnicki, J. M., Endo, Y., Tanokura, M. & Kobayashi, I. (2007). Novel protein fold discovered in the PabI family of restriction enzymes. *Nucleic Acids Research* **35**, 1908–1918.

Mol, C. D., Izumi, T., Mitra, S. & Tainer, J. A. (2000). DNA-bound structures and mutants reveal abasic DNA binding by APE1 and DNA repair coordination [corrected]. *Nature* **403**, 451–456.

Mol, C. D., Kuo, C. F., Thayer, M. M., Cunningham, R. P. & Tainer, J. A. (1995). Structure and function of the multifunctional DNA-repair enzyme exonuclease III. *Nature* **374**, 381–386.

Monzingo, A. F., Ozburn, A., Xia, S., Meyer, R. J. & Robertus, J. D. (2007). The structure of the minimal relaxase domain of MobA at 2·1 A resolution. *Journal of Molecular Biology* **366**, 165–178.

Moore, M. J. & Proudfoot, N. J. (2009). Pre-mRNA processing reaches back to transcription and ahead to translation. *Cell* **136**, 688–700.

Morita, M., Stamp, G., Robins, P., Dulic, A., Rosewell, I., Hrivnak, G., Daly, G., Lindahl, T. & Barnes, D. E. (2004). Gene-targeted mice lacking the Trex1 (DNase III) 3′→5′ DNA exonuclease develop inflammatory myocarditis. *Molecular and Cellular Biology* **24**, 6719–6727.

Moshous, D., Callebaut, I., De Chasseval, R., Corneo, B., Cavazzana-Calvo, M., Le Deist, F., Tezcan, I., Sanal, O., Bertrand, Y., Philippe, N., Fischer, A. & De Villartay, J. P. (2001). Artemis, a novel DNA double-strand break repair/V(D)J recombination protein, is mutated in human severe combined immune deficiency. *Cell* **105**, 177–186.

Moure, C. M., Gimble, F. S. & Quiocho, F. A. (2008). Crystal structures of I-SceI complexed to nicked DNA substrates: snapshots of intermediates along the DNA cleavage reaction pathway. *Nucleic Acids Research* **36**, 3287–3296.

Muftuoglu, M., Oshima, J., Von Kobbe, C., Cheng, W. H., Leistritz, D. F. & Bohr, V. A. (2008). The clinical characteristics of Werner syndrome: molecular and biochemical diagnosis. *Human Genetics* **124**, 369–377.

Muro-Pastor, A. M., Flores, E., Herrero, A. & Wolk, C. P. (1992). Identification, genetic analysis and characterization of a sugar-non-specific nuclease from the cyanobacterium *Anabaena* sp. PCC 7120. *Molecular Microbiology* **6**, 3021–3030.

Murray, N. E. (2000). Type I restriction systems: sophisticated molecular machines (a legacy of Bertani and Weigle). *Microbiology and Molecular Biology Reviews* **64**, 412–434.

Muyrers, J. P., Zhang, Y. & Stewart, A. F. (2000). ET-cloning: think recombination first. *Genetic Engineering* (*New York*) **22**, 77–98.

Nagata, S. (2007). Autoimmune diseases caused by defects in clearing dead cells and nuclei expelled from erythroid precursors. *Immunological Reviews* **220**, 237–250.

Nandakumar, J., Schwer, B., Schaffrath, R. & Shuman, S. (2008). RNA repair: an antidote to cytotoxic eukaryal RNA damage. *Molecular Cell* **31**, 278–286.

Newman, M., Lunnen, K., Wilson, G., Greci, J., Schildkraut, I. & Phillips, S. E. (1998). Crystal structure of restriction endonuclease BglI bound to its interrupted DNA recognition sequence. *EMBO Journal* **17**, 5466–5476.

Newman, M., Murray-Rust, J., Lally, J., Rudolf, J., Fadden, A., Knowles, P. P., White, M. F. & Mcdonald, N. Q. (2005). Structure of an XPF endonuclease with and without DNA suggests a model for substrate recognition. *EMBO Journal* **24**, 895–905.

Nichols, M. D., Deangelis, K., Keck, J. L. & Berger, J. M. (1999). Structure and function of an archaeal topoisomerase VI subunit with homology to the meiotic recombination factor Spo11. *EMBO Journal* **18**, 6177–6188.

Niiranen, L., Altermark, B., Brandsdal, B. O., Leiros, H. K., Helland, R., Smalas, A. O. & Willassen, N. P. (2008). Effects of salt on the kinetics and thermodynamic stability of endonuclease I from *Vibrio salmonicida* and *Vibrio cholerae*. *FEBS Journal* **275**, 1593–1605.

Nishino, T., Komori, K., Ishino, Y. & Morikawa, K. (2003). X-ray and biochemical anatomy of an archaeal XPF/Rad1/Mus81 family nuclease: similarity between its endonuclease domain and restriction enzymes. *Structure* **11**, 445–457.

Niv, M. Y., Ripoll, D. R., Vila, J. A., Liwo, A., Vanamee, E. S., Aggarwal, A. K., Weinstein, H. & Scheraga, H. A. (2007). Topology of Type II REases revisited; structural classes and the common conserved core. *Nucleic Acids Research* **35**, 2227–2237.

https://doi.org/10.1017/S0033583510000181 Published online by Cambridge University Press

Nowotny, M. (2009). Retroviral integrase superfamily: the structural perspective. *EMBO Reports* **10**, 144–151.

Nowotny, M., Cerritelli, S. M., Ghirlando, R., Gaidamakov, S. A., Crouch, R. J. & Yang, W. (2008). Specific recognition of RNA/DNA hybrid and enhancement of human RNase H1 activity by HBD. *EMBO Journal* **27**, 1172–1181.

Nowotny, M., Gaidamakov, S. A., Crouch, R. J. & Yang, W. (2005). Crystal structures of RNase H bound to an RNA/DNA hybrid: substrate specificity and metal-dependent catalysis. *Cell* **121**, 1005–1016.

Nowotny, M., Gaidamakov, S. A., Ghirlando, R., Cerritelli, S. M., Crouch, R. J. & Yang, W. (2007). Structure of human RNase H1 complexed with an RNA/DNA hybrid: insight into HIV reverse transcription. *Molecular Cell* **28**, 264–276.

Nowotny, M. & Yang, W. (2006). Stepwise analyses of metal ions in RNase H catalysis from substrate destabilization to product release. *EMBO Journal* **25**, 1924–1933.

Nowotny, M. & Yang, W. (2009). Structural and functional modules in RNA interference. *Current Opinion in Structural Biology* **19**, 286–293.

O'Donovan, A., Davies, A. A., Moggs, J. G., West, S. C. & Wood, R. D. (1994). XPG endonuclease makes the 3′ incision in human DNA nucleotide excision repair. *Nature* **371**, 432–435.

Obmolova, G., Ban, C., Hsieh, P. & Yang, W. (2000). Crystal structures of mismatch repair protein MutS and its complex with a substrate DNA. *Nature* **407**, 703–710.

Ollis, D. L., Brick, P., Hamlin, R., Xuong, N. G. & Steitz, T. A. (1985). Structure of large fragment of *Escherichia coli* DNA polymerase I complexed with dTMP. *Nature* **313**, 762–766.

Olmo, N., Turnay, J., Gonzalez De Buitrago, G., Lopez De Silanes, I., Gavilanes, J. G. & Lizarbe, M. A. (2001). Cytotoxic mechanism of the ribotoxin alpha-sarcin. Induction of cell death via apoptosis. *European Journal of Biochemistry* **268**, 2113–2123.

Orlowski, J. & Bujnicki, J. M. (2008). Structural and evolutionary classification of type II restriction enzymes based on theoretical and experimental analyses. *Nucleic Acids Research* **36**, 3552–3569.

Pan, C. Q. & Lazarus, R. A. (1999). Ca^{2+}-dependent activity of human DNase I and its hyperactive variants. *Protein Science* **8**, 1780–1788.

Paquin, B., O'Kelly, C. J. & Lang, B. F. (1995). Intron-encoded open reading frame of the GIY-YIG subclass in a plastid gene. *Current Genetics* **28**, 97–99.

Parker, R. & Song, H. (2004). The enzymes and control of eukaryotic mRNA turnover. *Nature Structural and Molecular Biology* **11**, 121–127.

Parrish, J. Z. & Xue, D. (2006). Cuts can kill: the roles of apoptotic nucleases in cell death and animal development. *Chromosoma* **115**, 89–97.

Patel, A. A. & Steitz, J. A. (2003). Splicing double: insights from the second spliceosome. *Nature Reviews Molecular Cell Biology* **4**, 960–970.

Pauling, L. (1961). *The Nature of the Chemical Bond*. Ithaca: Cornell University Press.

Paull, T. T. & Gellert, M. (1998). The 3′ to 5′ exonuclease activity of Mre 11 facilitates repair of DNA double-strand breaks. *Molecular Cell* **1**, 969–979.

Paull, T. T. & Gellert, M. (1999). Nbs1 potentiates ATP-driven DNA unwinding and endonuclease cleavage by the Mre11/Rad50 complex. *Genes and Development* **13**, 1276–1288.

Peebles, C. L., Perlman, P. S., Mecklenburg, K. L., Petrillo, M. L., Tabor, J. H., Jarrell, K. A. & Cheng, H. L. (1986). A self-splicing RNA excises an intron lariat. *Cell* **44**, 213–223.

Pena, V., Rozov, A., Fabrizio, P., Luhrmann, R. & Wahl, M. C. (2008). Structure and function of an RNase H domain at the heart of the spliceosome. *EMBO Journal* **27**, 2929–2940.

Perrino, F. W., Harvey, S., Mcmillin, S. & Hollis, T. (2005). The human TREX2 3′→5′-exonuclease structure suggests a mechanism for efficient nonprocessive DNA catalysis. *Journal of Biological Chemistry* **280**, 15212–15218.

Perry, J. J., Yannone, S. M., Holden, L. G., Hitomi, C., Asaithamby, A., Han, S., Cooper, P. K., Chen, D. J. & Tainer, J. A. (2006a). WRN exonuclease structure and molecular mechanism imply an editing role in DNA end processing. *Nature Structural and Molecular Biology* **13**, 414–422.

Perry, K., Hwang, Y., Bushman, F. D. & Van Duyne, G. D. (2006b). Structural basis for specificity in the poxvirus topoisomerase. *Molecular Cell* **23**, 343–354.

Pidcock, E. & Moore, G. R. (2001). Structural characteristics of protein binding sites for calcium and lanthanide ions. *Journal of Biology and Inorganic Chemistry* **6**, 479–489.

Pingoud, A., Fuxreiter, M., Pingoud, V. & Wende, W. (2005). Type II restriction endonucleases: structure and mechanism. *Cellular and Molecular Life Science* **62**, 685–707.

Pingoud, V., Wende, W., Friedhoff, P., Reuter, M., Alves, J., Jeltsch, A., Mones, L., Fuxreiter, M. & Pingoud, A. (2009). On the divalent metal ion dependence of DNA cleavage by restriction endonucleases of the EcoRI family. *Journal of Molecular Biology* **393**, 140–160.

Pontius, B. W., Lott, W. B. & Von Hippel, P. H. (1997). Observations on catalysis by hammerhead ribozymes are consistent with a two-divalent-metal-ion mechanism. *Proceedings of the National Academy of Sciences USA* **94**, 2290–2294.

Pouliot, J. J., Yao, K. C., Robertson, C. A. & Nash, H. A. (1999). Yeast gene for a Tyr-DNA phosphodiesterase that repairs topoisomerase I complexes. *Science* **286**, 552–555.

https://doi.org/10.1017/S0033583510000181 Published online by Cambridge University Press

Rafferty, J. B., Bolt, E. L., Muranova, T. A., Sedelnikova, S. E., Leonard, P., Pasquo, A., Baker, P. J., Rice, D. W., Sharples, G. J. & Lloyd, R. G. (2003). The structure of *Escherichia coli* RusA endonuclease reveals a new Holliday junction DNA binding fold. *Structure* **11**, 1557–1567.

Raines, R. T. (1998). Ribonuclease A. *Chem Rev* **98**, 1045–1066.

Rangarajan, E. S. & Shankar, V. (2001). Sugar nonspecific endonucleases. *FEMS Microbiology Reviews* **25**, 583–613.

Redinbo, M. R., Champoux, J. J. & Hol, W. G. (2000). Novel insights into catalytic mechanism from a crystal structure of human topoisomerase I in complex with DNA. *Biochemistry* **39**, 6832–6840.

Redinbo, M. R., Stewart, L., Kuhn, P., Champoux, J. J. & Hol, W. G. (1998). Crystal structures of human topoisomerase I in covalent and noncovalent complexes with DNA. *Science* **279**, 1504–1513.

Reed, R. R. (1981). Transposon-mediated site-specific recombination: a defined in vitro system. *Cell* **25**, 713–719.

Reha-Krantz, L. J. (2010). DNA polymerase proofreading: multiple roles maintain genome stability. *Biochimica et Biophysica Acta* **1804**, 1049–1063.

Reiter, T. A., Reiter, N. J. & Rusnak, F. (2002). Mn^{2+} is a native metal ion activator for bacteriophage lambda protein phosphatase. *Biochemistry* **41**, 15404–15409.

Renzi, F., Caffarelli, E., Laneve, P., Bozzoni, I., Brunori, M. & Vallone, B. (2006). The structure of the endoribonuclease XendoU: From small nucleolar RNA processing to severe acute respiratory syndrome coronavirus replication. *Proceedings of the National Academy of Sciences USA* **103**, 12365–12370.

Rice, P. & Mizuuchi, K. (1995). Structure of the bacteriophage Mu transposase core: a common structural motif for DNA transposition and retroviral integration. *Cell* **82**, 209–220.

Richardson, J. M., Colloms, S. D., Finnegan, D. J. & Walkinshaw, M. D. (2009). Molecular architecture of the Mos1 paired-end complex: the structural basis of DNA transposition in a eukaryote. *Cell* **138**, 1096–1108.

Ritchie, D. B., Schellenberg, M. J., Gesner, E. M., Raithatha, S. A., Stuart, D. T. & Macmillan, A. M. (2008). Structural elucidation of a PRP8 core domain from the heart of the spliceosome. *Nature Structural and Molecular Biology* **15**, 1199–1205.

Roberts, R. J., Vincze, T., Posfai, J. & Macelis, D. (2009). REBASE – a database for DNA restriction and modification: enzymes, genes and genomes. *Nucleic Acids Research* **38** (Database Issue), D234–236.

Romani, A. & Scarpa, A. (1992). Regulation of cell magnesium. *Archives of Biochemistry and Biophysics* **298**, 1–12.

Romier, C., Dominguez, R., Lahm, A., Dahl, O. & Suck, D. (1998). Recognition of single-stranded DNA by nuclease P1: high resolution crystal structures of complexes with substrate analogs. *Proteins* **32**, 414–424.

Rupert, P. B., Massey, A. P., Sigurdsson, S. T. & Ferre-D'amare, A. R. (2002). Transition state stabilization by a catalytic RNA. *Science* **298**, 1421–1424.

Rutkoski, T. J. & Raines, R. T. (2008). Evasion of ribonuclease inhibitor as a determinant of ribonuclease cytotoxicity. *Current Pharmaceutical Biotechnology* **9**, 185–189.

Ryan, K., Calvo, O. & Manley, J. L. (2004). Evidence that polyadenylation factor CPSF-73 is the mRNA 3′ processing endonuclease. *RNA* **10**, 565–573.

Saenger, W. (1984). *Principles of Nucleic Acid Structure*, New York, NY: Springer.

Salvo, J. J. & Grindley, N. D. (1988). The gamma delta resolvase bends the res site into a recombinogenic complex. *EMBO Journal* **7**, 3609–3616.

Sam, M. D. & Perona, J. J. (1999). Catalytic roles of divalent metal ions in phosphoryl transfer by EcoRV endonuclease. *Biochemistry* **38**, 6576–6586.

Sasnauskas, G., Connolly, B. A., Halford, S. E. & Siksnys, V. (2007). Site-specific DNA transesterification catalyzed by a restriction enzyme. *Proceedings of the National Academy of Sciences USA* **104**, 2115–2120.

Sasnauskas, G., Zakrys, L., Zaremba, M., Cosstick, R., Gaynor, J. W., Halford, S. E. & Siksnys, V. (2010). A novel mechanism for the scission of double-stranded DNA: BfiI cuts both 3′–5′ and 5′–3′ strands by rotating a single active site. *Nucleic Acids Research* **38**, 2399–2410.

Scherly, D., Nouspikel, T., Corlet, J., Ucla, C., Bairoch, A. & Clarkson, S. G. (1993). Complementation of the DNA repair defect in xeroderma pigmentosum group G cells by a human cDNA related to yeast RAD2. *Nature* **363**, 182–185.

Schiffer, S., Rosch, S. & Marchfelder, A. (2002). Assigning a function to a conserved group of proteins: the tRNA 3′-processing enzymes. *EMBO Journal* **21**, 2769–2777.

Schneider, C., Leung, E., Brown, J. & Tollervey, D. (2009). The N-terminal PIN domain of the exosome subunit Rrp44 harbors endonuclease activity and tethers Rrp44 to the yeast core exosome. *Nucleic Acids Research* **37**, 1127–1140.

Schoeffler, A. J. & Berger, J. M. (2008). DNA topoisomerases: harnessing and constraining energy to govern chromosome topology. *Quarterly Review of Biophysics* **41**, 41–101.

Schulga, A. A., Nurkiyanova, K. M., Zakharyev, V. M., Kirpichnikov, M. P. & Skryabin, K. G. (1992). Cloning of the gene encoding RNase binase from *Bacillus intermedius* 7P. *Nucleic Acids Research* **20**, 2375.

Schuster, S. C., Miller, W., Ratan, A., Tomsho, L. P., Giardine, B., Kasson, L. R., Harris, R. S., Petersen, D. C., Zhao, F., Qi, J., Alkan, C., Kidd, J. M., Sun, Y., Drautz, D. I., Bouffard, P., Muzny, D. M., Reid, J. G., Nazareth, L. V., Wang, Q., Burhans, R., Riemer, C.,

https://doi.org/10.1017/S0033583510000181 Published online by Cambridge University Press

Wittekindt, N. E., Moorjani, P., Tindall, E. A., Danko, C. G., Teo, W. S., Buboltz, A. M., Zhang, Z., Ma, Q., Oosthuysen, A., Steenkamp, A. W., Oostuisen, H., Venter, P., Gajewski, J., Zhang, Y., Pugh, B. F., Makova, K. D., Nekrutenko, A., Mardis, E. R., Patterson, N., Pringle, T. H., Chiaromonte, F., Mullikin, J. C., Eichler, E. E., Hardison, R. C., Gibbs, R. A., Harkins, T. T. & Hayes, V. M. (2010). Complete Khoisan and Bantu genomes from southern Africa. *Nature* **463**, 943–947.

Scott, W. G., Murray, J. B., Arnold, J. R., Stoddard, B. L. & Klug, A. (1996). Capturing the structure of a catalytic RNA intermediate: the hammerhead ribozyme. *Science* **274**, 2065–2069.

Setlow, P. & Kornberg, A. (1972). Deoxyribonucleic acid polymerase: two distinct enzymes in one polypeptide. II. A proteolytic fragment containing the 5′ leads to 3′ exonuclease function. Restoration of intact enzyme functions from the two proteolytic fragments. *Journal of Biological Chemistry* **247**, 232–240.

Sharma, S., Sommers, J. A., Driscoll, H. C., Uzdilla, L., Wilson, T. M. & Brosh, R. M., JR. (2003). The exonucleolytic and endonucleolytic cleavage activities of human exonuclease 1 are stimulated by an interaction with the carboxyl-terminal region of the Werner syndrome protein. *Journal of Biological Chemistry* **278**, 23487–23496.

Sharples, G. J., Chan, S. N., Mahdi, A. A., Whitby, M. C. & Lloyd, R. G. (1994). Processing of intermediates in recombination and DNA repair: identification of a new endonuclease that specifically cleaves Holliday junctions. *EMBO Journal* **13**, 6133–6142.

Shen, B., Singh, P., Liu, R., Qiu, J., Zheng, L., Finger, L. D. & Alas, S. (2005). Multiple but dissectible functions of FEN-1 nucleases in nucleic acid processing, genome stability and diseases. *Bioessays* **27**, 717–729.

Shevelev, I. V., Ramadan, K. & Hubscher, U. (2002). The TREX2 3′→5′ exonuclease physically interacts with DNA polymerase delta and increases its accuracy. *ScientificWorld Journal* **2**, 275–281.

Sidrauski, C. & Walter, P. (1997). The transmembrane kinase Ire1p is a site-specific endonuclease that initiates mRNA splicing in the unfolded protein response. *Cell* **90**, 1031–1039.

Silverman, R. H. (2007). Viral encounters with 2′,5′-oligoadenylate synthetase and RNase L during the interferon antiviral response. *Journal of Virology* **81**, 12720–12729.

Singleton, M. R., Dillingham, M. S., Gaudier, M., Kowalczykowski, S. C. & Wigley, D. B. (2004). Crystal structure of RecBCD enzyme reveals a machine for processing DNA breaks. *Nature* **432**, 187–193.

Sinha, K. M., Unciuleac, M. C., Glickman, M. S. & Shuman, S. (2009). AdnAB: a new DSB-resecting motor-nuclease from mycobacteria. *Genes and Development* **23**, 1423–1437.

Sokolowska, M., Czapinska, H. & Bochtler, M. (2009). Crystal structure of the beta beta alpha-Me type II restriction endonuclease Hpy99I with target DNA. *Nucleic Acids Research* **37**, 3799–3810.

Sokolowska, M., Kaus-Drobek, M., Czapinska, H., Tamulaitis, G., Szczepanowski, R. H., Urbanke, C., Siksnys, V. & Bochtler, M. (2007). Monomeric restriction endonuclease BcnI in the apo form and in an asymmetric complex with target DNA. *Journal of Molecular Biology* **369**, 722–734.

Solaro, P. C., Birkenkamp, K., Pfeiffer, P. & Kemper, B. (1993). Endonuclease VII of phage T4 triggers mismatch correction *in vitro*. *Journal of Molecular Biology* **230**, 868–877.

Sorek, R., Kunin, V. & Hugenholtz, P. (2008). CRISPR – a widespread system that provides acquired resistance against phages in bacteria and archaea. *Nature Reviews Microbiology* **6**, 181–186.

Spiegel, P. C., Chevalier, B., Sussman, D., Turmel, M., Lemieux, C. & Stoddard, B. L. (2006). The structure of I-CeuI homing endonuclease: Evolving asymmetric DNA recognition from a symmetric protein scaffold. *Structure* **14**, 869–880.

Stahl, M. M., Thomason, L., Poteete, A. R., Tarkowski, T., Kuzminov, A. & Stahl, F. W. (1997). Annealing vs. invasion in phage lambda recombination. *Genetics* **147**, 961–977.

Stahley, M. R. & Strobel, S. A. (2005). Structural evidence for a two-metal-ion mechanism of group I intron splicing. *Science* **309**, 1587–1590.

Stahley, M. R. & Strobel, S. A. (2006). RNA splicing: group I intron crystal structures reveal the basis of splice site selection and metal ion catalysis. *Current Opinion in Structural Biology* **16**, 319–326.

Stec, B., Holtz, K. M. & Kantrowitz, E. R. (2000). A revised mechanism for the alkaline phosphatase reaction involving three metal ions. *Journal of Molecular Biology* **299**, 1303–1311.

Steiniger-White, M., Rayment, I. & Reznikoff, W. S. (2004). Structure/function insights into Tn5 transposition. *Current Opinion in Structural Biology* **14**, 50–57.

Steitz, T. A. (1998). A mechanism for all polymerases. *Nature* **391**, 231–232.

Steitz, T. A. & Steitz, J. A. (1993). A general two-metal-ion mechanism for catalytic RNA. *Proceedings of the National Academy of Sciences USA* **90**, 6498–6502.

Stephenson, J. B. (2008). Aicardi–Goutieres syndrome (AGS). *European Journal of Paediatric Neurology* **12**, 355–358.

Stetson, D. B., Ko, J. S., Heidmann, T. & Medzhitov, R. (2008). Trex1 prevents cell-intrinsic initiation of autoimmunity. *Cell* **134**, 587–598.

Stoddard, B. L. (2005). Homing endonuclease structure and function. *Quarterly Reviews of Biophysics* **38**, 49–95.

https://doi.org/10.1017/S0033583510000181 Published online by Cambridge University Press

Stuckey, J. A. & Dixon, J. E. (1999). Crystal structure of a phospholipase D family member. *Nature Structural Biology* **6**, 278–284.

Subramanya, H. S., Arciszewska, L. K., Baker, R. A., Bird, L. E., Sherratt, D. J. & Wigley, D. B. (1997). Crystal structure of the site-specific recombinase, XerD. *EMBO Journal* **16**, 5178–5187.

Suck, D., Oefner, C. & Kabsch, W. (1984). Three-dimensional structure of bovine pancreatic DNase I at 2·5 A resolution. *EMBO Journal* **3**, 2423–2430.

Sun, W., Pertzev, A. & Nicholson, A. W. (2005). Catalytic mechanism of *Escherichia coli* ribonuclease III: kinetic and inhibitor evidence for the involvement of two magnesium ions in RNA phosphodiester hydrolysis. *Nucleic Acids Research* **33**, 807–815.

Syson, K., Tomlinson, C., Chapados, B. R., Sayers, J. R., Tainer, J. A., Williams, N. H. & Grasby, J. A. (2008). Three metal ions participate in the reaction catalyzed by T5 flap endonuclease. *Journal of Biological Chemistry* **283**, 28741–28746.

Szankasi, P. & Smith, G. R. (1995). A role for exonuclease I from *S. pombe* in mutation avoidance and mismatch correction. *Science* **267**, 1166–1169.

Szankasi, P. & Smith, G. R. (1996). Requirement of *S. pombe* exonuclease II, a homologue of S. cerevisiae Sep1, for normal mitotic growth and viability. *Current Genetics* **30**, 284–293.

Tadokoro, T. & Kanaya, S. (2009). Ribonuclease H: molecular diversities, substrate binding domains, and catalytic mechanism of the prokaryotic enzymes. *FEBS Journal* **276**, 1482–1493.

Takeuchi, M., Lillis, R., Demple, B. & Takeshita, M. (1994). Interactions of *Escherichia coli* endonuclease IV and exonuclease III with abasic sites in DNA. *Journal of Biological Chemistry* **269**, 21907–21914.

Tanaka, N., Arai, J., Inokuchi, N., Koyama, T., Ohgi, K., Irie, M. & Nakamura, K. T. (2000). Crystal structure of a plant ribonuclease, RNase LE. *Journal of Molecular Biology* **298**, 859–873.

Thore, S., Mauxion, F., Seraphin, B. & Suck, D. (2003). X-ray structure and activity of the yeast Pop2 protein: a nuclease subunit of the mRNA deadenylase complex. *EMBO Reports* **4**, 1150–1155.

Tock, M. R. & Dryden, D. T. (2005). The biology of restriction and anti-restriction. *Current Opinion in Microbiology* **8**, 466–472.

Tomlinson, C. G., Atack, J. M., Chapados, B., Tainer, J. A. & Grasby, J. A. (2010). Substrate recognition and catalysis by flap endonucleases and related enzymes. *Biochemical Society Transactions* **38**, 433–437.

Ton-Hoang, B., Guynet, C., Ronning, D. R., Cointin-Marty, B., Dyda, F. & Chandler, M. (2005). Transposition of ISHp608, member of an unusual family of bacterial insertion sequences. *EMBO Journal* **24**, 3325–3338.

Toor, N., Keating, K. S. & Pyle, A. M. (2009). Structural insights into RNA splicing. *Current Opinion in Structural Biology* **19**, 260–266.

Toor, N., Rajashankar, K., Keating, K. S. & Pyle, A. M. (2008). Structural basis for exon recognition by a group II intron. *Nature Structural and Molecular Biology* **15**, 1221–1222.

Torres-Larios, A., Swinger, K. K., Pan, T. & Mondragon, A. (2006). Structure of ribonuclease P – a universal ribozyme. *Current Opinion in Structural Biology* **16**, 327–335.

Tran, P. T., Erdeniz, N., Dudley, S. & Liskay, R. M. (2002). Characterization of nuclease-dependent functions of Exo1p in Saccharomyces cerevisiae. *DNA Repair* (*Amsterdam*) **1**, 895–912.

Truglio, J. J., Rhau, B., Croteau, D. L., Wang, L., Skorvaga, M., Karakas, E., Dellavecchia, M. J., Wang, H., Van Houten, B. & Kisker, C. (2005). Structural insights into the first incision reaction during nucleotide excision repair. *EMBO Journal* **24**, 885–894.

Tsutakawa, S. E., Jingami, H. & Morikawa, K. (1999). Recognition of a TG mismatch: the crystal structure of very short patch repair endonuclease in complex with a DNA duplex. *Cell* **99**, 615–623.

Tucker, P. W., Hazen, E. E., JR. & Cotton, F. A. (1978). Staphylococcal nuclease reviewed: a prototypic study in contemporary enzymology. I. Isolation; physical and enzymatic properties. *Molecular and Cellular Biochemistry* **22**, 67–77.

Uesugi, Y. & Hatanaka, T. (2009). Phospholipase D mechanism using Streptomyces PLD. *Biochimica et Biophysica Acta* **1791**, 962–969.

Unciuleac, M. C. & Shuman, S. (2009). Characterization of the mycobacterial AdnAB DNA motor provides insights into the evolution of bacterial motor-nuclease machines. *Journal of Biological Chemistry* **285**, 2632–2641.

Urakubo, Y., Ikura, T. & Ito, N. (2008). Crystal structural analysis of protein–protein interactions drastically destabilized by a single mutation. *Protein Science* **17**, 1055–1065.

Usui, T., Ohta, T., Oshiumi, H., Tomizawa, J., Ogawa, H. & Ogawa, T. (1998). Complex formation and functional versatility of Mre11 of budding yeast in recombination. *Cell* **95**, 705–716.

Van Gent, D. C., Mizuuchi, K. & Gellert, M. (1996). Similarities between initiation of V(D)J recombination and retroviral integration. *Science* **271**, 1592–1594.

Van Roey, P., Meehan, L., Kowalski, J. C., Belfort, M. & Derbyshire, V. (2002). Catalytic domain structure and hypothesis for function of GIY-YIG intron endonuclease I-TevI. *Nature Structural Biology* **9**, 806–811.

Vasu, K., Saravanan, M., Bujnicki, J. M. & Nagaraja, V. (2008). Structural integrity of the beta beta alpha-Metal finger motif is required for DNA binding and stable protein-DNA complex formation in R.KpnI. *Biochimica et Biophysica Acta* **1784**, 269–275.

https://doi.org/10.1017/S0033583510000181 Published online by Cambridge University Press

Verhoeven, E. E., Van Kesteren, M., Moolenaar, G. F., Visse, R. & Goosen, N. (2000). Catalytic sites for 3′ and 5′ incision of *Escherichia coli* nucleotide excision repair are both located in UvrC. *Journal of Biological Chemistry* **275**, 5120–5123.

Viadiu, H. & Aggarwal, A. K. (1998). The role of metals in catalysis by the restriction endonuclease BamHI. *Nature Structural Biology* **5**, 910–916.

Viadiu, H. & Aggarwal, A. K. (2000). Structure of BamHI bound to nonspecific DNA: a model for DNA sliding. *Molecular Cell* **5**, 889–895.

Vicens, Q. & Cech, T. R. (2006). Atomic level architecture of group I introns revealed. *Trends in Biochemical Sciences* **31**, 41–51.

Viswanathan, M. & Lovett, S. T. (1999). Exonuclease X of *Escherichia coli*. A novel 3′–5′ DNase and Dnaq superfamily member involved in DNA repair. *Journal of Biological Chemistry* **274**, 30094–30100.

Vitkute, J., Maneliene, Z., Petrusyte, M. & Janulaitis, A. (1998). BfiI, a restriction endonuclease from *Bacillus firmus* S8120, which recognizes the novel non-palindromic sequence 5′-ACTGGG(N)5/4–3′. *Nucleic Acids Research* **26**, 3348–3349.

Voegtli, W. C., White, D. J., Reiter, N. J., Rusnak, F. & Rosenzweig, A. C. (2000). Structure of the bacteriophage lambda Ser/Thr protein phosphatase with sulfate ion bound in two coordination modes. *Biochemistry* **39**, 15365–15374.

Voet, D. & Voet, J. G. (2004). *Biochemistry*. Hoboken, NJ: Wiley.

Voziyanov, Y., Pathania, S. & Jayaram, M. (1999). A general model for site-specific recombination by the integrase family recombinases. *Nucleic Acids Research* **27**, 930–941.

Walker, D., Lancaster, L., James, R. & Kleanthous, C. (2004). Identification of the catalytic motif of the microbial ribosome inactivating cytotoxin colicin E3. *Protein Sci* **13**, 1603–1611.

Wang, J. C. (2002). Cellular roles of DNA topoisomerases: a molecular perspective. *Nature Reviews Molecular Cell Biology* **3**, 430–440.

Wang, L. K. & Shuman, S. (2005). Structure-function analysis of yeast tRNA ligase. *RNA* **11**, 966–975.

Wang, Y., Juranek, S., Li, H., Sheng, G., Tuschl, T. & Patel, D. J. (2008). Structure of an argonaute silencing complex with a seed-containing guide DNA and target RNA duplex. *Nature* **456**, 921–926.

Wang, Y., Juranek, S., Li, H., Sheng, G., Wardle, G. S., Tuschl, T. & Patel, D. J. (2009). Nucleation, propagation and cleavage of target RNAs in Ago silencing complexes. *Nature* **461**, 754–761.

Wang, Y. T., Yang, W. J., Li, C. L., Doudeva, L. G. & Yuan, H. S. (2007). Structural basis for sequence-dependent DNA cleavage by nonspecific endonucleases. *Nucleic Acids Research* **35**, 584–594.

Wang, Z., Fast, W., Valentine, A. M. & Benkovic, S. J. (1999). Metallo-beta-lactamase: structure and mechanism. *Current Opinion in Chemical Biology* **3**, 614–622.

West, S. C. & Connolly, B. (1992). Biological roles of the *Escherichia coli* RuvA, RuvB and RuvC proteins revealed. *Molecular Microbiology* **6**, 2755–2759.

Weston, S. A., Lahm, A. & Suck, D. (1992). X-ray structure of the DNase I-d(GGTATACC)2 complex at 2·3 A resolution. *Journal of Molecular Biology* **226**, 1237–1256.

White, M. F. & Lilley, D. M. (1997). Characterization of a Holliday junction-resolving enzyme from *Schizosaccharomyces pombe*. *Molecular Cell Biology* **17**, 6465–6471.

Widlak, P. (2000). The DFF40/CAD endonuclease and its role in apoptosis. *Acta Biochimica Polonica* **47**, 1037–1044.

Widlak, P. & Garrard, W. T. (2005). Discovery, regulation, and action of the major apoptotic nucleases DFF40/CAD and endonuclease G. *Journal of Cellular Biochemistry* **94**, 1078–1087.

Wiedenheft, B., Zhou, K., Jinek, M., Coyle, S. M., Ma, W. & Doudna, J. A. (2009). Structural basis for DNase activity of a conserved protein implicated in CRISPR-mediated genome defense. *Structure* **17**, 904–912.

Williams, R. S., Moncalian, G., Williams, J. S., Yamada, Y., Limbo, O., Shin, D. S., Groocock, L. M., Cahill, D., Hitomi, C., Guenther, G., Moiani, D., Carney, J. P., Russell, P. & Tainer, J. A. (2008). Mre11 dimers coordinate DNA end bridging and nuclease processing in double-strand-break repair. *Cell* **135**, 97–109.

Winkler, F. K., Banner, D. W., Oefner, C., Tsernoglou, D., Brown, R. S., Heathman, S. P., Bryan, R. K., Martin, P. D., Petratos, K. & Wilson, K. S. (1993). The crystal structure of EcoRV endonuclease and of its complexes with cognate and non-cognate DNA fragments. *EMBO Journal* **12**, 1781–1795.

Woo, E. J., Kim, Y. G., Kim, M. S., Han, W. D., Shin, S., Robinson, H., Park, S. Y. & Oh, B. H. (2004). Structural mechanism for inactivation and activation of CAD/DFF40 in the apoptotic pathway. *Molecular Cell* **14**, 531–539.

Worrall, J. A. & Luisi, B. F. (2007). Information available at cut rates: structure and mechanism of ribonucleases. *Current Opinion in Structural Biology* **17**, 128–137.

Wu, M., Reuter, M., Lilie, H., Liu, Y., Wahle, E. & Song, H. (2005). Structural insight into poly(A) binding and catalytic mechanism of human PARN. *EMBO Journal* **24**, 4082–4093.

Wu, S. I., Lo, S. K., Shao, C. P., Tsai, H. W. & Hor, L. I. (2001). Cloning and characterization of a periplasmic nuclease of Vibrio vulnificus and its role in preventing uptake of foreign DNA. *Applied and Environmental Microbiology* **67**, 82–88.

Wyckoff, H. W., Hardman, K. D., Allewell, N. M., Inagami, T., Johnson, L. N. & Richards, F. M. (1967).

https://doi.org/10.1017/S0033583510000181 Published online by Cambridge University Press

The structure of ribonuclease-S at 3·5 A resolution. *Journal of Biological Chemistry* **242**, 3984–3988.

Wyckoff, H. W., Tsernoglou, D., Hanson, A. W., Knox, J. R., Lee, B. & Richards, F. M. (1970). The three-dimensional structure of ribonuclease-S. Interpretation of an electron density map at a nominal resolution of 2 A. *Journal of Biological Chemistry* **245**, 305–328.

Xiang, S., Cooper-Morgan, A., Jiao, X., Kiledjian, M., Manley, J. L. & Tong, L. (2009). Structure and function of the 5′→3′ exoribonuclease Rat1 and its activating partner Rai1. *Nature* **458**, 784–788.

Xu, Q. S., Roberts, R. J. & Guo, H. C. (2005). Two crystal forms of the restriction enzyme MspI–DNA complex show the same novel structure. *Protein Science* **14**, 2590–2600.

Xue, S., Calvin, K. & Li, H. (2006). RNA recognition and cleavage by a splicing endonuclease. *Science* **312**, 906–910.

Xue, Y., Bai, X., Lee, I., Kallstrom, G., Ho, J., Brown, J., Stevens, A. & Johnson, A. W. (2000). *Saccharomyces cerevisiae* RAI1 (YGL246c) is homologous to human DOM3Z and encodes a protein that binds the nuclear exoribonuclease Rat1p. *Molecular and Cellular Biology* **20**, 4006–4015.

Yajima, S., Inoue, S., Ogawa, T., Nonaka, T., Ohsawa, K. & Masaki, H. (2006). Structural basis for sequence-dependent recognition of colicin E5 tRNase by mimicking the mRNA-tRNA interaction. *Nucleic Acids Research* **34**, 6074–6082.

Yakovleva, L., Chen, S., Hecht, S. M. & Shuman, S. (2008). Chemical and traditional mutagenesis of vaccinia DNA topoisomerase provides insights to cleavage site recognition and transesterification chemistry. *Journal of Biological Chemistry* **283**, 16093–16103.

Yamagata, A., Kakuta, Y., Masui, R. & Fukuyama, K. (2002). The crystal structure of exonuclease RecJ bound to Mn^{2+} ion suggests how its characteristic motifs are involved in exonuclease activity. *Proceedings of the National Academy of Sciences USA* **99**, 5908–5912.

Yang, K., Zhang, L., Xu, T., Heroux, A. & Zhao, R. (2008). Crystal structure of the beta-finger domain of Prp8 reveals analogy to ribosomal proteins. *Proceedings of the National Academy of Sciences USA* **105**, 13817–13822.

Yang, W. (2007). Human MutLalpha: the jack of all trades in MMR is also an endonuclease. *DNA Repair* (*Amsterdam*) **6**, 135–139.

Yang, W. (2008). An equivalent metal ion in one- and two-metal-ion catalysis. *Nature Structural and Molecular Biology* **15**, 1228–1231.

Yang, W., Lee, J. Y. & Nowotny, M. (2006). Making and breaking nucleic acids: two-Mg^{2+}-ion catalysis and substrate specificity. *Molecular Cell* **22**, 5–13.

Yang, W. & Mizuuchi, K. (1997). Site-specific recombination in plane view. *Structure* **5**, 1401–1406.

Yang, W. & Steitz, T. A. (1995a). Crystal structure of the site-specific recombinase gamma delta resolvase complexed with a 34 bp cleavage site. *Cell* **82**, 193–207.

Yang, W. & Steitz, T. A. (1995b). Recombining the structures of HIV integrase, RuvC and RNase H. *Structure* **3**, 131–134.

Yang, X., Gerczei, T., Glover, L. T. & Correll, C. C. (2001). Crystal structures of restrictocin-inhibitor complexes with implications for RNA recognition and base flipping. *Nature Structural Biology* **8**, 968–973.

Yang, X. C., Sullivan, K. D., Marzluff, W. F. & Dominski, Z. (2009). Studies of the 5′ exonuclease and endonuclease activities of CPSF-73 in histone pre-mRNA processing. *Molecular and Cellular Biology* **29**, 31–42.

Yarus, M. (2002). Primordial genetics: phenotype of the ribocyte. *Annual Review of Genetics* **36**, 125–151.

Yoshida, H. (2001). The ribonuclease T1 family. *Methods in Enzymology* **341**, 28–41.

Yoshikawa, M., Iwasaki, H. & Shinagawa, H. (2001). Evidence that phenylalanine 69 in *Escherichia coli* RuvC resolvase forms a stacking interaction during binding and destabilization of a Holliday junction DNA substrate. *Journal of Biological Chemistry* **276**, 10432–10436.

Yu, M., Souaya, J. & Julin, D. A. (1998). The 30-kDa C-terminal domain of the RecB protein is critical for the nuclease activity, but not the helicase activity, of the RecBCD enzyme from *Escherichia coli*. *Proceedings of the National Academy of Sciences USA* **95**, 981–986.

Zalatan, J. G., Fenn, T. D. & Herschlag, D. (2008). Comparative enzymology in the alkaline phosphatase superfamily to determine the catalytic role of an active-site metal ion. *Journal of Molecular Biology* **384**, 1174–1189.

Zamel, R., Poon, A., Jaikaran, D., Andersen, A., Olive, J., De Abreu, D. & Collins, R. A. (2004). Exceptionally fast self-cleavage by a Neurospora Varkud satellite ribozyme. *Proceedings of the National Academy of Sciences USA* **101**, 1467–1472.

Zegers, I., Loris, R., Dehollander, G., Fattah Haikal, A., Poortmans, F., Steyaert, J. & Wyns, L. (1998). Hydrolysis of a slow cyclic thiophosphate substrate of RNase T1 analyzed by time-resolved crystallography. *Nature Structural Biology* **5**, 280–283.

Zhang, J., Xing, X., Herr, A. B. & Bell, C. E. (2009). Crystal structure of *E. coli* RecE protein reveals a toroidal tetramer for processing double-stranded DNA breaks. *Structure* **17**, 690–702.

Zhang, Y., Buchholz, F., Muyrers, J. P. & Stewart, A. F. (1998). A new logic for DNA engineering using recombination in *Escherichia coli*. *Nature Genetics* **20**, 123–128.

Zhu, C. X. & Tse-Dinh, Y. C. (2000). The acidic triad conserved in type IA DNA topoisomerases is required for binding of Mg(II) and subsequent conformational change. *Journal of Biological Chemistry* **275**, 5318–5322.

https://doi.org/10.1017/S0033583510000181 Published online by Cambridge University Press

Zuo, Y., Vincent, H. A., Zhang, J., Wang, Y., Deutscher, M. P. & Malhotra, A. (2006). Structural basis for processivity and single-strand specificity of RNase II. *Molecular Cell* **24**, 149–156.

Zuo, Y., Wang, Y. & Malhotra, A. (2005). Crystal structure of *Escherichia coli* RNase D, an exoribonuclease involved in structured RNA processing. *Structure* **13**, 973–984.

Zuo, Y., Zheng, H., Wang, Y., Chruszcz, M., Cymborowski, M., Skarina, T., Savchenko, A., Malhotra, A. & Minor, W. (2007). Crystal structure of RNase T, an exoribonuclease involved in tRNA maturation and end turnover. *Structure* **15**, 417–428.

https://doi.org/10.1017/S0033583510000181 Published online by Cambridge University Press